FABRICATION OF MICROENGINEERED POLYMERIC FILMS AND INVESTIGATION OF BIORESPONSES TO THE SUBSTRATA

By

LIWEN JIN

A DISSERTATION PRESENTED TO THE GRADUATE SCHOOL
OF THE UNIVERSITY OF FLORIDA IN PARTIAL FULFILLMENT
OF THE REQUIREMENTS FOR THE DEGREE OF
DOCTOR OF PHILOSOPHY

UNIVERSITY OF FLORIDA

2010

This work is dedicated to the three most important ladies in my life:
my mother Zhou, Yun
my wife Wei, Yuying
my daughter Jin, Abbie Siyun

ACKNOWLEDGMENTS

I must express my sincere gratitude to my advisor, Dr Ronald Baney, and my co-advisor, Dr. Anthony Brennan. Not only their rich knowledge in their own fields, but also their keen interest toward all aspects of science as well as life have great positive influence on my attitude to the research and life. I appreciate the advice and guidance provided by my doctoral committee consisting of Dr. Laurie Gower, Dr. Christopher Batich, and Dr. Joanna Peris. I must acknowledge and thank my research collaborators Dr. John Finley, Dr. Maureen Callow, Dr. James Callow, Dr. Patrick Antonelli, Dr. Carol Ojano-Dirain, Ms. Qingping Yang, and Ms. Edith Sampson. I also acknowledge Ms. Jennifer Wrighton, Ms. Doris Hallow, Ms. Jennifer Holton, and Ms. Alice Holt for their administrative assistance throughout my graduate studies.

Graduate students, past and present, have been vital for my progression and success throughout this entire process. First, I must thank my mentors, Dr. Soroya Benetez, Dr. Yun Mi Kim and Dr. Le Song, for getting me started with my research and teaching me the culture of Baney group. I would like to thank former and current group members, Dr. Jiwei Wang, Abby Queale, Timothy Gehret, Edward McKenna, Ting Cheng, ChungHao Shih, Ravi Kumar Vasudevan, and Sung Hwan Yeo. I must also acknowledge the senior members of the ONR team, Dr.s Leslie Wilson, Cliff Wilson, Michelle Carman, and James Schumacher, who provided their suggestion and support when I started the ONR project. During this time, I have had the pleasure of working with two great colleagues, Kenneth Chung and Christopher Long, who have both been vital in providing experimental assistance and discussion during the completion of my dissertation research. ONR group members, Chelsea Magin, Angel Ejiesi, Jun-Jiung Chen (Jack), Scott Cooper, Julian Sheats, and David Jackson, helped me with my

experiments and discussion. I'd like to thank them for their support and friendship. I also sincerely thank the many undergraduate research assistants and technicians that have aided in the preparation of samples for assay analysis, including Felicia Svedlund, Andrew Rophie, and Sean Royston. I'd like to thank all my friends here at UF for their friendship and support.

Special thanks to my wife, Yuying Wei. Without her encouragement, support, and endless love, there would not be this work. I want to thank all my family members for their love and support.

TABLE OF CONTENTS

LIST OF TABLES

LIST OF FIGURES

LIST OF ABBREVIATIONS

AF	Antifouling
AFM	Atomic force microscopy
APTES	3-aminopropyltriethoxysilane
BTM	BioTimer medium
CPC	Cetylpyridinium chloride
E	Elastic modulus (or Young's modulus)
ECMs	Extracellular matrices
E. coli	*Escherichia coli*
EPSs	Extracellular polymeric substances or extracellular polysaccharides
ERI	Engineered roughness index
f	The fraction of the rough surface that is in contact with liquid
FR	Foul release
G1650M	Kraton SEBS triblock copolymer with styrene block ~30 wt%
G1657M	Kraton SEBS triblock copolymer with styrene block ~13 wt%
HAIs	Healthcare-associated infections
HMDS	Hexamethyldisilazane
MIC	Minimum inhibitory concentration
MW	Molecular weight
MRSA	Methicillin-resistant *S. aureus*
MS	Mechanosensitive
MSDS	Material safety data sheets
n	The discrete number of the surface features on a micro-engineered surface
P. aeruginosa	*Pseudomonas aeruginosa*
PBS	Phosphate buffered saline

PCA	Principal component analysis
PDMS-5K	Short-chain poly(dimethylsiloxane) with molecular mass ~5 kg/mol
PDMSe	Poly(dimethylsiloxane) elastomer
PEG	Poly(ethylene glycol)
PET	poly(ethylene terephthalate)
PMMA	Poly(methyl methacrylate)
PS	Polystyrene
QS	Quorum sensing
r	Wenzel roughness ratio (total surface area divided by the projected planar surface area)
SEBS	Styrene-ethylene/butadiene-styrene triblock copolymer
S. aureus	*Staphylococcus aureus*
S. epidermidis	*Staphylococcus epidermidis*
TSB	Tryptic soy broth
XPS	X-ray photoelectron spectroscopy
XRR	X-ray reflectometry

Abstract of Dissertation Presented to the Graduate School
of the University of Florida in Partial Fulfillment of the
Requirements for the Degree of Doctor of Philosophy

FABRICATION OF MICROENGINEERED POLYMERIC FILMS AND INVESITGATION OF BIORESPONSES TO THE SUBSTRATA

By

Liwen Jin

August 2010

Chair: Ronald H. Baney
Major: Materials Science and Engineering

Biofouling is the undesired attachment, accumulation and proliferation of biomass (biopolymers and organisms) on various surfaces. This process imparts adverse influences on many aspects of human life. Without introducing any biocidal agents into the materials, a biomimetic micro-topographical structure replicated onto poly(dimethysiloxane) elastomer (PDMSe) has shown antifouling characteristics against marine and medical microorganisms. The purpose of this work was to investigate the efficacy of this pattern on antifouling when it was replicated onto various polymeric substrata with a wide range of mechanical and energetic properties.

A method was developed to covalently graft a demolding/antisticking layer, short-chain poly(dimethylsiloxane), onto a silicon wafer. A series of polymeric materials were chosen with varied mechanical properties (Young's modulus ranging from 1.4 to 3,300 MPa) and surface free energies (ranging from 21.5 to 42.4 mJ/m^2). Polymer films with the micro-engineered patterns were then readily fabricated from the treated wafer using solution casting method. The treated silicon wafer was versatile and robust in replication of topographical features onto those polymeric materials with high fidelity (>99%).

The resulting films were tested against one marine microorganism, *Ulva linza* zoospore. The Sharklet textured surfaces with feature heights of 2.1 and 3.0 microns were tested and corresponding smooth surfaces served as controls. The polymeric films were attached to glass slides with an epoxy glue, which was found to be strongly attractive to the spores. Assuming the influence of the epoxy glue was the same among all the samples, data were analyzed and statistical analyses were performed. Two groups of the surface properties were important for establishing predictive attachment models. However, the results should be interpreted with caution because of the unknown magnitude of the epoxy glue problem.

One bacterium, *Staphylococcus aureus*, was used to test the antifouling capability for the topographical surfaces. The bioactivity measured by the metabolic rate (BioTimer assay) showed that there were more bioactive cells on the Sharklet textured surface than on the smooth one, regardless of the chemical nature of the substrate. SEM imaging showed the opposite: mature biofilms were formed on the smooth surfaces, while disrupted microcolonies were prevailing on the Sharklet textured surfaces. High-dose antibiotic treatments suggested that the bacterial cells on the Sharklet surface were more easily killed after a 12-hr culturing. A new strategy of treating bacteria-associated infections for implanted medical devices was proposed.

New undercut surface topographical structures were proposed and fabricated. It is estimated that the new surface structures may exhibit higher underwater stability and higher reduction of *Ulva* spore attachment.

CHAPTER 1
INTRODUCTION

Bioadhesion of microfoulers/macrofoulers has attracted much interest in current research due to environmental and economic concerns. For example, the biomass accumulated on a ship's hull not only causes higher drag force (and thus higher fuel cost) [1-3], but also provides a means for spreading invasive species [4]. The chronic infections caused by bacterial biofilms in clinical situations, on the other hand, greatly increase risks during recovery and the cost of treatment [5-7]. Therefore, anti-fouling with minimal side-effects has gained more interest during the last two decades.

All surfaces in contact with aqueous environments, wheather marine or physiological, will be conditioned by organic matter within a short period of time [8]. This conditioning will form a layer which attracts certain microorganisms to the surface. When these microorganisms establish colonies in the natural environment, other species (usually larger in size) will be attracted. Gradually a complex biolayer consisting of multiple species (bacteria, plants and animals) will be formed; this process is biofouling.

To prevent biofouling, the traditional strategy is to kill the organisms. That means any microorganism attached to or in proximity of the surface will be killed by toxic surface-bound chemicals or leaching agents blended in the substrate. This strategy has limitations due to stringent environmental regulations and requirements on an effective time period.

Recently a strategy of repelling the microorganisms has been developed and tested for anti-adhesion/antifouling purposes. This strategy, loosely speaking, depends on "disguising" the surface or causing the microorganisms to "dislike" the surface. This

is often realized through manipulation of the structures and/or surface properties of polymer based coatings [9-11]. To effectively protect the surface during its designed lifespan, the surface should first be resistant to organic matter (such as proteins and polysaccharides). So far, such perfectly resistant surfaces have yet to be disgned. Thus the effectiveness of such surfaces against biofouling can be significantly reduced once an organic layer is adsorbed onto them.

After billions of years of evolution, organisms have already developed various ways to avoid undesired attachment from other species. One example is a chemical defense, in which secreted chemicals (e.g. zosteric acid from some sea weeds) interfere the attachment of microorganisms [12]. Another approach is a physical defense. For example, some slowmoving creatures like shell fish can avoid bioadhesion of foulants on their shells with micro-topographical features [13, 14]. These findings encouraged researchers to explore biomimetic strategies for the antifouling applications.

Scope of Research

Biomimetic design for antifouling applications can also borrow ideas from other creatures. The body of a shark is covered by scales with unique microstructures, which not only help the sharks maintain their superb hydrodynamic characteristic [15], but also effectively resist adhesion of microorganisms. Based on the characteristics of shark skin, the Brennan research group at the University of Florida came up with the engineered surface topographical design called Sharklet AF^{TM} [16-20]. These surface topographical features were effective in antifouling against marine organisms [16-19] and bacteria [21].

Based on the current understanding of the interactions between organisms and surfaces, the factors that control the sensing, settling, adhering, and proliferating of

microorganisms may include the surface topography, chemistry, mechanics, torturosity, feature dimension, and surface energetics [22]. Many previous investigations revealed that surface chemistry, wettability, and energy can affect biofouling process on flat surfaces. Systematic control of surface chemistry through self-assembled monolayers (SAMs) showed that the marine microorganism *Ulva* zoospore can select its settling location on a surface [23-25]. Though there was no detectable difference in spore attachment density in a narrow range of stiffness (Young's modulus ranging from 0.2 to 9.8 MPa) [26] on a flat substrate, mechanical force (interaction between the surface feature and the microorganism) may still play a role in spore sensing and settling on a rough surface [20].

A predictive model was proposed to correlate *Ulva* zoospore attachment density with the surface topographical features [18]. The parameter in this model, the engineered roughness index (ERI), was further modified to better correlate and predict *Ulva* spore attachment behavior [27].The biofouling investigations were performed on various topographical features replicated on a poly(dimethyl siloxane) (PDMSe) material (Silastic T2^{TM}). Although the concept of a nanoforce gradient was introduced and explained how that mechanical force may influence spore attachment (Figure 1-1) [20], the influence of factors such as surface chemistry, mechanics, and energetics were not fully explored. One objective of this work was to explore the influence of the various surface properties on the attachment of *Ulva* spores, to help further understanding of the biofouling process. This understanding is hoped to lead to the development of more efficient surface designs for antifouling applications.

In the field of bacterial adhesion to various substrata, surface properties also affect the quantity and pattern of the adhered cells. Short period (usually within several hours) of bacterial adhesion studies showed that the difference of surface chemistry/energy can influence the initial adhesion of the bacterial cells [28-31]. Surface roughness in the nanometer to submicrometer range is another factor found to affect a bacterial cell's adhesion and attachment pattern on various substrata [32, 33]. However, the surface properties, including surface chemistry, energy, wettability, charge, mechanics, and nano-/micro-structure have not been fully explored in the long-term biofilm development. Micro-sized Sharklet AF^{TM} surface features blocked the connection of the bacterial colonies on the surfaces, deterring the formation of biofilms for up to 21 days [21]. This type of micro-sized surface topographical features may thus provide physical defense against bacterial biofilm formation for more general applications.

Based on the application of inhibiting biofilm formation, another objective of this research was to try to answer the following questions regarding bacteria attaching to a surface:

- Does the Sharklet topographical feature have the same effectiveness against bacterial biofilm formation on other polymeric materials than PDMSe? In other words, do other surface properties such as mechanical stiffness and surface energy affect the ability of inhibiting the biofilm formation on a topographical surface?
- In a long-term (7-day) cell culture, does the surface topography affect the morphology of the microcolonies? Are the bacterial cells attached to the topographical surface affected in terms of metabolic rate and defense mechanism?

For these two objectives, an engineered topography was replicated onto the surface of non-toxic polymeric materials with systematically varied elastic moduli and surface energy. Simple and cost-effective processes were explored to fabricate the micro-engineered polymer films. Statistical methods (e.g., principal component

analysis) were employed to determine the influence of various surface properties on the marine biofouling process. Optimized surface design could then be performed for potential marine antifouling applications. The marine biological assays were carried out by Dr John Finley, Dr. Maureen Callow and Professor James Callow at the University of Birmingham, UK; all three are biologists specializing in ship fouling species such as algae and diatoms. Bioassays for biofilm formation and characterization were developed in collaboration with Ms. Qingping Yang, Ms. Edith Simpson, and Dr. Patrick Antonelli of the Department of Otolaryngology at the University of Florida.

Research Goals and Specific Aims

The overall goals of this research were (1) to determine the influence of various surface properties (i.e., surface mechanics, chemistry/energy, and topography) on the attachment behavior of one marine biofouling species *Ulva linza* zoospore, and (2) to understand the effect surface microstructures have on the inhibition of bacterial biofilm formation. Completion of these goals required the successful fabrication of microtopographical polymeric films while maintaining the fidelity of the surface topography. These properties, correlated with the bioresponse data, could allow for the further development of the predictive ERI model. Novel engineered topographies were designed based on this model. At the start of the project, the specific aims listed below were chosen with special emphasis on the use of the Sharklet AF^{TM} topography for biofouling applications.

Specific Aim 1: Fabrication of Micro-engineered Polymeric Films with High Fidelity.

The objective of this aim was to replicate high fidelity (> 95% feature replication), micrometer-scale structures onto the surface of various polymers; the polymers tested

include PDMSe, styrene-ethlyene/butadiene-stryene (SEBS) tri-block copolymer, poly (methyl methacrylate) (PMMA), and polystyrene (PS). These materials have a large span of elastic muduli (from ~1 MPa to ~3 GPa) and low to medium surface energy. Thus the micro-patterned polymer films can be tested against fouling species.

A solution casting method was chosen for these thermoplastic polymers. An anti-sticking layer was covalently grafted onto the silicon wafer patterns and fabrication processes were developed for each polymer. Pattern fidelity was evaluated by light microscopy and scanning electron microscopy (SEM) of the finished, micro-engineered polymer surfaces. Successful completion of this aim was essential to the following bioassay tests.

Specific Aim 2: Investigate the Effects of Mechanics and Surface Chemistry/Energy of Substrata on Algal Spore Attachment on the Sharklet AF^{TM} Surfaces Fabricated with Various Polymeric Materials

The objective of this aim was to determine the effect of mechanical property and surface chemistry/energetics of a substrate on the attachment of a model marine microfouler, *Ulva* zoospores. The polymer films fabricated while researching Specific Aim 1 were tested using *Ulva* spores. It was assumed that the unique Sharklet AF^{TM} pattern was the primary factor in prohibiting the attachment of *Ulva* spores based on current research carried out using PDMSe material. Thus the hypothesis was that the spore attachment reduction would be the same for all tested materials with the same micropattern using the corresponding smooth films as controls, after taking into account other factors such as surface chemistry and energy.

The spore attachment assay protocol and collection of the raw data of these tests were performed by Dr. Maureen Callow and Dr. John Finlay at the University of Birmingham, UK. Statistical analyses of the spore attachment data were carried out to

determine the influence of the mechanics, surface chemistry, surface energetics and topography of the base materials on the marine biofouling process.

Those spores successfully settling on Sharklet surfaces usually squeeze between the features, as can be seen in previous work [17, 22]. The nanoforce gradient on various surface patterns shows significant variation on different base materials (see Table 1-1). If the spore attachment data showed any difference among various substrata, a comprehensive model may be proposed to include contributions from other factors, such as mechanical properties and surface energy.

Specific Aim 3: Investigate the Mechanism of Inhibiting Bacterial Biofilm Formation on the Micro-engineered Topography

There were two objectives for this aim: (1) to test the effect of mechanical and chemical properties of polymeric substrata on long-term bacterial biofilm formation on the topographical surfaces, and (2) to test the effect of antibiotic treatments on the bioactivity of the bacterial cells in the microcolonies formed on the topographical surfaces.

It was hypothesized that the Sharklet AF^{TM} topography replicated on the surfaces of PDMSe, SEBS, and PMMA will show the same inhibition of bacteria attachment and biofilm formation for *Staphylococcus aureus* (*S. aureus*).

An analytical technique utilizing metabolic products (carbon dioxide in this case) to trigger the color change of a pH indicator in the culture medium was used to quantify and statistically compare the amount of active bacterial cells attached on the tested samples. The biofilms were cultured with help from Ms. Qingping Yang in Professor Patrick Antonelli's lab in the Department of Otolaryngology at the University of Florida. An engineered topography originally designed for algal spores (*Ulva*) was shown to

have a significant inhibitory effect on the formation and growth of biofilm from *Staphylococcus aureus* up to 7 days.

Specific Aim 4: Prepare Undercut Surface Topographical Features on Various Substrata, with Estimated Higher Reduction Targeted at Spore Attachment

There were two objectives for this aim: (1) to explore the process of fabricating new surface features, and (2) to predict the improvement of the antifouling properties of the new design based on the predictive model.

A thermal pressing method was used to flatten the top of the protruding features to increase the size of the feature top. Suitable processing temperatures and pressures were found for various materials and new surface features were characterized by SEM imaging to obtain the feature size data. Water contact angle measurements were taken to verify that the novel surface structure could help maintain a stable air pocket underneath the water layer, and thus higher underwater stability than that on the normal protruding features. The new design resulted in higher ERI value, and therefore a higher antifouling capability was expected.

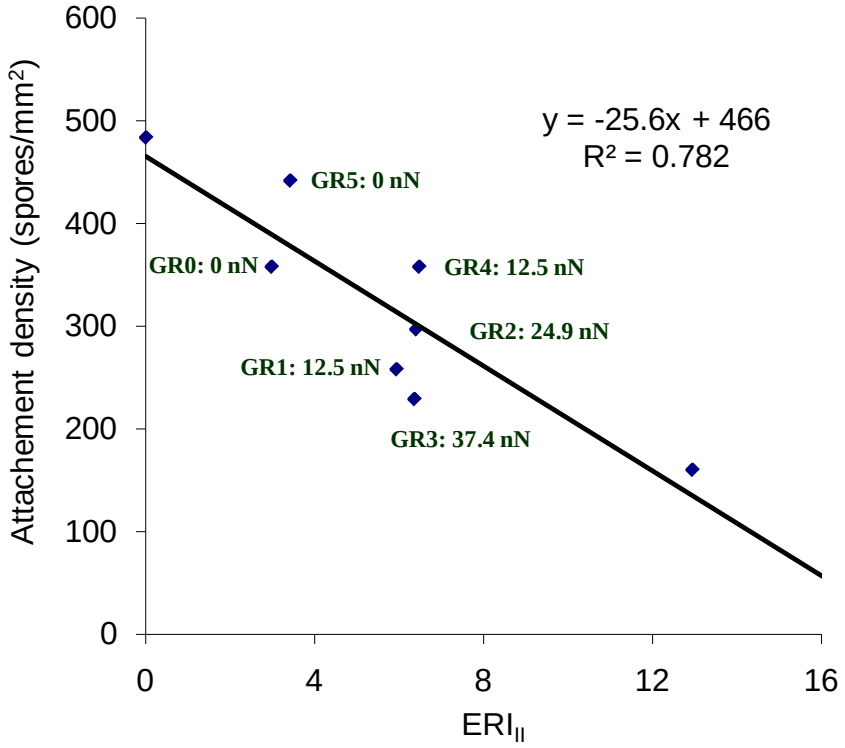

Figure 1-1. Correlation of spore attachment density with ERI values. (Data adapted from Schumacher's work [20, 22].)

Table 1-1. Force gradient between the adjacent feature elements, assuming 1% bending of the features.

Material	Young's Modulus, MPa	+2SK2x2 *, nN	+3SK2x2 **, nN
DMSe	1.4	28	12.5
Kraton G1657M	6.3	126	56
Kraton G1650M	34	680	300
G1650M/PS blend	2.4×10^{2}	4.8×10^{3}	2.1×10^{3}
PMMA	3.3×10^{3}	6.6×10^{4}	2.9×10^{4}

*: +2SK2x2 means Sharklet AF^{TM} pattern with feature height 2 µm, feature spacing 2 µm, and feature width 2 µm;

**: +3SK2x2 means Sharklet AF^{TM} pattern with feature height 3 µm, feature spacing 2 µm, and feature width 2 µm.

CHAPTER 2
BACKGROUND

Introduction

Biofouling is the undesired attachment and development of cell layers on a substrate [34]. This phenomenon can be observed almost everywhere: from bath tubs to kitchen sinks, from our teeth [35] to various medical devices [36], from pipelines and reservoirs to ship hulls. Biofouling most easily occurs at the interfaces of a solid and an aqueous solution, or a solid and humid air [8, 34]. Many consequences are associated with biofouling in various forms. Examples are the plaques and corrosion caused by bacterial biofilms [35], the chronic release of pathogens from bacterial biofilms [37], the blockage of water intakes by biomass accumulation [38], and the increased drag imposed to ship hulls by the multiple layers of marine biofoulants [2, 3]. These examples show that biofouling not only causes large economic losses but also threatens human health.

As biofouling has had these negative impacts, antifouling strategies and technologies have been developed to battle those unwanted effects. Previous strategies have focused on damaging or killing the adhered fouling organisms with toxic agents. However, there are two main drawbacks to this approach. First, the toxic agents can be accumulated and passed on through the food chain, eventually threatening human lives. Second, the target organisms may develop various resistance to the toxic agents; this evolutionary process is thus accelerated by repeated biocide application. Thus, different and more environmentally friendly strategies are called for.

Biomimetics is an interdisciplinary field which employs the chemical and physical methods and concepts of living organisms in the design of devices and

systems [39, 40]. As a result of evolution, organisms have developed superior properties relative to the peer man-made products when dealing with biological environments. In the field of antifouling, these biomimetic principles can also be discovered and employed effectively. In this chapter, marine biofouling and medical biofouling will be reviewed; the current state of antifouling technologies will also be summarized.

Marine Biofouling and Prevention

Marine biofouling is a complex process, which in most cases can be described by a basic sequence of events: biochemical conditioning, bacterial attachment and colonization, and unicellular and then multicellular eukaryotic adhesion and proliferation [8]. When any solid substance is immersed in seawater, the surface will adsorb dissolved chemicals (usually macromolecules) in a short period of time. This process, biochemical conditioning, starts immediately after immersion and reaches equilibrium in a few hours [8]. Then, following chemical cues from the surface, bacteria, unicellular algae, cyanobacteria (blue-green algae), protozoa and fungi, attach and begin to colonize on the conditioned surface within hours [41]. These colonies, or biofilms, are often referred to as “microfouling” or “slime” and provide an anchoring layer for the so-called “macrofouling” species such as higher algae, soft-bodied invertebrates (sponges and tunicates) and calcified invertebrates (barnacles and tubeworms) [8, 41, 42]. The time scale of the fouling stages is shown in Figure 2-1 [8].

Biofouling is undesirable for many reasons. Microbial biofilm can cause local fluctuations in the concentration of various chemical species such as oxygen and metal ions, therefore accelerating corrosion of the metal substrata [42]. The metabolic process or products (e.g. sulfides) may also be corrosive to steel surface [43, 44]. Biofouling can

increase the roughness on ship hulls, resulting in an increased hydrodynamic drag [1, 2]. The increased fuel consumption, together with maintenance costs (such as dry dock cleaning, paint removal and repainting), may cost the US Navy more than one billion dollars annually [3]. In addition to economic losses, a more urgent threat associated with marine biofouling is that it can spread invasive species globally, endangering local biodiversity [4].

The strategies in marine biofouling control include antifouling (AF), in which the surface is capable of killing or repelling the fouling species, and foul release (FR), where, due to the “non-stick” property of the coatings, accumulated foulers are removed by gravity or shearing forces from the water. Various biocides have been used for antifouling, with the most effective being tributyltin (TBT) compounds. Due to the adverse effects on the food chain [45, 46], TBT based coatings were banned by the International Maritime Organization [41] and was supposed to be phased out by the year 2008. Meanwhile, other metal containing antifouling coatings, e.g. Cu_2O, have also raised concern of environmental impacts. Foul release measures, on the other hand, depend on the coating materials (e.g. polydimethylsiloxane) with a low surface energy and a low elastic modulus [47]. The macrofoulers could be removed under normal operating speed, but the slime layer is difficult to detach. Thus, environmental-friendly coating materials and strategies are needed to address modern marine antifouling applications.

In the following sections, the factors affecting marine biofouling and foul release are reviewed. New coating technologies, using both strategies for biofouling control, are the main focus of this literature review.

Factors on Marine Biofouling and Foul Release

The effect that surface properties (e.g., topography, chemistry, mechanics, and surface energy) have on the attachment, adhesion, and growth of living organisms was researched by the Brennan research group at the University of Florida [17-19, 21, 48]. Also surface charge has recently attracted more interest [49, 50].

Surface Chemistry/Energy

Surface chemistry and/or surface energy certainly play a role when a microorganism approaches and settle on a surface. Finlay *et al.* [51] found that *Ulva* spores tended to settle on hydrophobic rather than hydrophilic surfaces. The spores that settled on hydrophobic surfaces showed higher adhesion strength than those on hydrophilic surfaces, tested by water jet removal. Ista *et al.* [52] changed surface chemistry (and therefore surface energy) systematically via a self-assembled monolayers (SAMs) technique and tested the surfaces with marine bacteria and *Ulva* zoospores. They prepared two series of mixed SAMs on a gold surface: one was alkyl chains with mixed end groups of –COOH and $–CH_3$; the other was alkyl chains with mixed end groups of –OH and $–CH_3$. Although the adhesion of bacteria agreed with the prediction of the thermodynamic model, a spore test yielded more complicated bioresponses, indicating that a simple model cannot fully explain the interactions between the somewhat complex microorganisms and the surface. In a recent paper, Schilp *et al.* [25] studied *Ulva* spore and diatom attachment and removal on a hexa(ethylene glycol) (HEG) SAMs with various end groups (hydroxyl, methyl, ethyl, and propyl). The water sessile contact angles varied from ~30^o to ~90^o as the end groups varied. *Ulva* spores tended to settle on the hydrophilic surfaces (hydroxyl- and methyl- ended HEG), yet the adhesion strength was very weak: the surface-attached

“rafts” were easily removed by the operational procedures at the end of attachment assay and the subsequent flow test. As the diatom does not have any motile capability, its attachment depends on gravity (and Brownian motion when close to a surface). The adhesion between the diatom and the surfaces also increased with the hydrophobicity after rinsing. Therefore, the overall apparent attachment density increased with the hydrophobicity of the surface for both spores and diatoms. The recent work by Schilp *et al.* [53] showed that surfaces covered with poly(ethylene glycol) chains (MW ~2 and ~5 kg/mole respectively) were resistant to spore and diatom attachment.

Surface chemical patterns, resulting from the self-assembled monolayers (SAMs) technique, also showed an influence on the attachment of motile spores. As *Ulva* zoospores tend to settle on completely fluorinated surfaces rather than fully PEGylated surfaces, Finlay *et al.* [54] first showed that spores could not distinguish between patterned SAMs with alternating fluorinated stripes and PEGylated stripes when the width of the stripes was less than ~20 µm. In that case, the spores acted as if the alternating patterns were purely PEGylated surfaces. Gradient surface chemical patterns influenced the attachment characteristics of zoospores [55]. Unlike the sole hydrophilic or hydrophobic surfaces, the attachment of *Ulva* zoospores on this gradient pattern exhibited the opposite trend. Excluding the migration of the settled spores, the authors speculated that the gradient surface sent long-range signals to disturb the swimming directionality of the spores.

Surface Charge

Ederth *et al.* [56] found that *Ulva* spores were attracted to a cationic oligopeptide (aginine) self-assembled monolayer but were easily removed. In a recently published work, the zeta potential of the motile *Ulva* spores was determined to be -19.3±1.1 mV

[57]. This measurement could explain why spores tend to adhere to neutral or positively charged surfaces rather than negatively charged surfaces.

Mechanical Properties

Generalizing Kendall's model [58], Brady [59, 60] declared that the relative adhesion of marine organisms onto the surface of a polymer substrate is proportional to the square root of the product of the elastic modulus and the critical surface energy. Polydimethylsiloxane (PDMS), with low surface energy and elastic modulus, is therefore an ideal foul release coating material.

The mechanical properties of PDMS on spore attachment and removal was studied by Chaudhury *et al.* [26]. In their study, the elastic modulus of PDMS ranged from 0.2 to 9.4 MPa. These smooth samples showed no significant difference in spore attachment while spore and sporeling removal were highest on the lowest modulus sample [26]. When the mechanical property is fixed (modulus 0.8 MPa), the film thickness (16, 100, and 430 µm respectively) showed no significant effect on spore attachment, while spore and sporeling removal were more easily achieved on thicker films (430 µm film for spore, and > 100 µm films for sporeling) [26].

The effect of the substrate thickness on barnacle adhesion was studied by Sun *et al.* [61]. It has been known that barnacles can "feel" and "penetrate" through the upper layer to the underlying coats and thus settle firmly when the surface film thickness is below ~100 µm (dry film thickness) [41].

Surface Topography

The effect of surface roughness on the attachment of animals such as barnacle cyprids was extensively investigated [59-61]. Andersson *et al.* [62] prepared a microtextured PDMS surface by casting a PDMS prepolymer against metal mesh with

various sieve sizes. Their field test showed significant reduction of barnacle fouling [62]. Petronis *et al.* [63] replicated micron-sized pyramids and grooves onto PDMS from silicon wafers which were treated by photolithography and etching to define the sizes and shapes of the surface structures. They claimed that the groove structure could effectively reduce barnacle attachment while the pyramid structure was not able to do so (both compared with smooth surface) [63]. Berntsson *et al.* [64] carried out an investigation of surface microtexture on the exploration and attachment by barnacle cyprids. Their results showed a remarkable 92% reduction of cyprid attachment compared to smooth controls. It is important to note that they used poly(methyl methacrylate) (PMMA) and poly(vinylidene fluoride) (PVDF), which have higher surface energies and elastic moduli than PDMS.

Surface topography can also affect *Ulva* zoospore attachment. Callow *et al.* [65] found spores preferentially settled against the surface features when the spacings between the features were similar to or larger than the size of the spores. From these findings, a narrower spacing between the surface features could prevent spore attachment. This result was later demonstrated by Carman *et al.* [17].

New Coating Strategies

Polymeric materials

Many new polymeric coating materials are under investigation to replace the toxic organometal-based coatings which currently are in extensive use. Among all polymer materials, zwitterionic polymers showed promise in antifouling toward both protein adsorption and bacteria adhesion [11, 66, 67]. Ongoing research with this type of material also showed excellent resistance to marine microorganisms [68]. In order to combine the antifouling (AF) property of oligoethylene glycol and the foul release (FR)

property from perfrluoroalkanes, Krishnan *et al*. [69] synthesized an amphiphilic copolymer. Oligoethylene glycol and perfluoroalkyl moieties were present in the same side chains of their synthesized polymers. In an aqueous environment, the side chains bent with oligoethylene glycol segments sticking toward water and perfluoroalkyl segments “bowing” toward the coating surface. The obtained surface showed improvement against attachments of *Ulva* and *Navicula,* and a higher removal rate of sporelings compared with glass and PDMS surfaces. Linear-chain poly(ethylene glycol) (PEG) grafted surfaces have long been shown to be effective against protein adsorption and cell adhesion [10, 70, 71]. Statz *et al*. [72] coated a titanium surface with PEG chains via conjugation with L-3,4-dihydroxyphenylalanine and the resulting surface showed AF/FR against spore and diatom. Furthermore, an almost 100% removal rate was achieved when a 20-Pa shear stress was applied. Other polymeric materials, such as perfluoropolyethers (PFPE) and their PEG blends [73], and siloxane-polyurathane copolymers [74], also showed improved AF properties.

There are still potential issuesto be addressed with these polymeric materials. For zwitterionic polymers [67], hydrolysis may occur in the physiological environment with the help of enzymes, and the resulting products may contain quaternary ammonium salts, which are undesired leachants. For amphiphilic copolymer [69] and PFPE [73], the synthetic/processing procedures are time consuming and thus inefficient in terms of production. A disadvantage of PEGylated polymer coatings is that PEG can gradually degrade [9, 75], making it unfavorable for long term applications.

Surface catalysis

The Detty group [76] explored an innovative approach for marine antifouling applications. They used selenoxide or telluride as a catalyst and xerogel film as a carrier

to convert the low concentration of H_2O_2 (in the natural marine environment) into active oxygen atoms, in order to expel the un-welcome species. The initial lab test results showed an effective reduction of attachment from barnacle larva, tubeworm larva, and *Ulva* spores. A potential obstacle with this novel approach is the adsorption of organic matter onto the xerogel film. The contamination would gradually deactivate the catalyst. Another possible disadvantage of the xerogel film is its mechanical strength, which may not endure the shear forces arising from vessel at normal cruising speed.

Biomimetic measures

Marine bacteria communicate via signaling chemicals to form biofilms and this cue can strongly attract algal spore to deposit on the biofilms [77]. Therefore a strategy of "quenching" these signaling chemicals was proposed by biomimetic routes. Zosteric acid (*p*-(sulfo-oxy) cinnamic acid), a naturally occurring phenolic acid in eelgrass (*Zostera marina* L.) plants, was found to have antifouling activity toward a wide spectrum of species such as *Ulva* zoospore, marine bacteria and barnacle larvae [12]. This compound has also been used in antifouling against fresh water microorganisms [78-80] and fungal spores on plant leaves [81]. Recently, the search of effective antifoulants has been expanded to the extracts from some marine organisms, including plants [82-84] and animals [83, 85]. When these types of leachants are blended with coating materials for antifouling applications, there is still a concern that a higher leaching rate is needed so as to reach comparable antifouling efficacy as traditional organometallic agents [86].

Researchers have found that some marine animals are resistant to biofouling without secreting chemical signals. Instead, these animals grow complex outer surfaces with micro- or even nano-sized topographies [87, 88]. Another biomimetic route is thus

to explore the antifouling properties from these naturally evolved surface topographies. Direct replicas of rough surfaces from foul-resistant species such as tropical sea stars onto an epoxy resin did not lead to antifouling in a field test [89]. However, a further comparison of the surface properties of the two (sea stars and epoxy) in terms of chemistry and mechanics could have explained the difference in antifouling performance. Meanwhile, the direct deployment of the shells of bivalve molluscs [13], which can have regular or irregular surface microtopogaphies, showed resistance to the fouling species in a field test. Researchers at the University of Florida developed surface micro-patterns for antifouling applications. One biomimetic pattern, named Sharklet AF^{TM}, showed an up to 86% reduction of *Ulva* zoospore attachment [17], and 97% reduction of barnacle cyprids attachment [18]. By correlating spore attachment with various surface patterns, an engineering roughness index (ERI) model was proposed [19]. This model was further refined and showed predictive capability [27]. Engineered surface micro-topographies were mostly replicated onto PDMSe by the group, and other materials and surface chemistries are under investigation by the group.

In summary, there are many factors controlling the initial attachment of marine organisms onto a surface. From the point of view of long term application, coatings with various surface chemical compositions will not permanently resist the deposition of organic matter in natural marine environment. Therefore the surface will eventually attract microorganisms to grow on it, causing the subsequent accumulation of various larger plants and animals. On the other hand, a physical surface defense inspired from biomimetics may work effectively in the long run. Surface hierarchical structures (in both

chemical and physical patterns) may be needed to repel organisms with different sizes and attachment mechanisms.

Bacterial Biofilms in Medical Environment

Healthcare-associated infections (HAIs) have become familiar in the last decade. In the United States alone, more than 1.7 million people are affected by HAIs and approximately 100,000 people lose their lives due to the complications from HAIs annually [90]. HAIs also result in $4.5 billion of additional healthcare expenses [91]. As one important part of the healthcare industry, invasive medical devices from simple catheters to sophisticated artificial heart valves are improving human health and life quality while at the same time imposing substantial risk of infections. For example, it is estimated that up to 20,000 patients died annually of central line–associated bloodstream infections in U.S. intensive care units [5]. The annual cost of caring for patients with central venous catheter (CVC)-associated bloodstream infections could be as high as $2.3 billion.

In natural environments, bacteria tend to attach to surfaces and form colonies/biofilms for an increased rate of survival and proliferation [92]. According to Costerton *et al.* [93], a bacterial biofilm is defined as “matrix-enclosed bacterial populations adherent to each other and/or to surfaces or interfaces”. The process of bacterial adhesion to a surface occurs in five stages as shown in Figure 2-2 [94]. During the initial stage of attachment, there are specific interactions (e.g., cell-protein film or cell-sugar receptors interactions) and non-specific interactions (e.g., electrostatic or hydrophobic interactions) between the cell and the surface [95, 96]. Once irreversibly attached to the surface, the bacterial cells will activate specific genes which lead to the synthesis of extracellular polymeric substances (EPSs) or extracellular matrices (ECMs)

to encase the bacteria [97, 98]. A recent report on the adhesion of *Staphylococcus aureus* (*S. aureus*) to engineered PDMSe films clearly demonstrated the cycle of bacterial adhesion [21]. Due to the protection of the EPSs/ECMs secreted by the adhered bacteria, the colonies/biofilms are 500 times more resistant to common biocides, antimicrobial treatments and the antibodies of the host, when compared with the planktonic bacteria [93, 94]. The pathogens released from the bacterial biofilms can cause chronic infections in the host, and thus the formation of bacterial biofilms on the surface of biomedical devices is undesirable.

To avoid bacterial adhesion to biomedical devices, two primary strategies have been proposed and utilized for biomaterials: bioadhesion-free coatings and incorporated antimicrobial agents [99]. Due to the complex physiological environment, the surface of an inserted device will eventually be covered by biomatter. Therefore, the chemical cues will favor the recruitment of pathogens, if they are present. On the other hand, antimicrobial agents face the challenge of multi-drug resistant bacterial strains, which are increasingly common in current medical facilities world-wide [100]. From the standpoint of materials science and engineering, we may achieve antifouling by (1) carefully selecting the desired materials, (2) further adjusting the chemistry at the interfaces, and (3) biomimetically engineering the interfacial characteristics.

The initial adhesion of bacterial cells onto the surface is the critical step for biofilm formation. The types of interactions in bioadhesion were summarized by Glantz *et al.* [29]. Many factors, such as a protein conditioning film, surface charge, surface hydrophobicity, and surface micro-topography, can affect this step. A recent review [101] summarized the effects of these factors and suggested that the

attachment of bacterial cells to the solid surface is not only affected by the culture medium and surface properties, but also by the dynamic change of bacterial membrane structures. In the following section some other factors involving the characteristics of bacterial cells are reviewed, and recent advances in the prevention of biofilms are summarized.

Bacteria Mechanical Sensing

Mechanical senses originate from sensing such forces as osmotic force, thirst, touch, vibration and texture [102]. It was postulated that early cells developed two basic types of sensing mechanisms to ensure survival [102]. One is based on solute sensing with a key-lock type interaction at the cell wall. Another is based on solvent (i.e. water) sensing with ion-channel type gauges at the cell wall. After billions of years of evolution, cells living in an aqueous environment are usually equipped with mechanosensitive (MS) ion channels which are embedded in the cell membranes and which could respond to tension in proportion to the concentration of water [102]; it is believed that these channels are critical to osmotic pressure regulation in bacterial cells [103]. The bacterial MS ion channels were first found in *Escherichia coli (E. coli)* [104] and were well characterized. The MS ion channels are divided into three categories, i.e. MscL, MscS, and MscM, representing MS channel of large, small, and mini conductance, respectively [105]. MscL is non-selective, whereas MscS is selective to anions over cations and MscM slightly prefers cations over anions [105].

Tissue cells were reported to respond to the stiffness of the substrate [106, 107]. The cell membrane not only protects the inner environment, but also plays a critical role in exchanging materials and information (e.g., chemical and mechanical cues). The bioactivities occurring at the cell membrane certainly involve the energy: the biomotor

proteins (e.g., myosins) are powered by adenosine triphosphate (ATP). Recently, atomic force microscopy (AFM) has been used to reveal the characteristic vibrations of cell membranes. In an early report, Pelling *et al.* [108] determined the periodicity of the membrane motion of singe yeast cells ranging from 0.8 to 1.6 kHz depending on temperature, and they associated this vibration with membrane motor protein activity. A later investigation of body cells (rat cardiomyocytes (CM) and human foreskin fibroblasts (HFF)) [109] revealed that the vibrational frequency was 4.2 Hz for CM and 0.06~0.34 Hz for HFF.

There are few publications on the effect of the substrate mechanical properties on the adhesion of bacteria. Lichter *et al.* [110] investigated the adhesion of *Staphylococcus epidermidis* (*S. epidermidis*) and *E. coli* on a polymeric thin film with varying mechanical properties. They found a positive correlation between surface stiffness and adhesion for the two bacterial species.

Bacteria Quorum Sensing

Cell communication and activity coordination have long been considered a characteristic of “advanced” creatures. However, research in the past two decades has revealed that bacteria can also establish communication systems to synchronize biological activities such as biofilm formation [111]. As this communication is population (and signal concentration) dependent, the process of adjusting bacterial “social” activities is referred to as quorum sensing [112].

Quorum sensing may be divided into 4 steps [112]: (1) bacterial cells produce small signaling chemicals, (2) the chemicals are released into the local environment by active transport or passive diffusion, (3) the chemicals are “picked up” by the receptors on the cell wall of other bacterial cells, and (4) specific gene expressions are induced by

certain concentrations of signaling chemicals. This process is a positive feedback loop, which means that the concentration of signaling chemicals can increase exponentially above a threshold. (Thus quorum sensing signals are also referred to as autoinducers.)

Various bacteria species utilize different chemical signal molecules for quorum sensing. In general, Gram-negative bacteria use acylated homoserine lactones as autoinducers while Gram-positive bacteria use processed oligo-peptides to communicate [111]. Recent advances indicate that cell-to-cell communication via autoinducers occurs both within and between bacterial species [113]. Furthermore, evidence suggests that bacterial autoinducers can elicit specific responses from host organisms [114].

The effects of quorum sensing on biofilm formation vary with different species. *Pseudomonas aeruginosa (P. aeruginosa),* a Gram-negative bacterium, shows less tendency toward biofilm formation with one *lasI* mutant strain compared with a wild type [115]. This finding led to a new treatment method for biofilm associated infections using quorum sensing inhibitors [116]. Unlike *P. aeruginosa*, the quorum sensing in the Gram-positive *Staphylococcal* species does not facilitate biofilm formation. The quorum sensing system in *Staphylococcus aureus* (*S. aureus*), which is regulated by an accessory gene regulator (agr), suppresses adhesin production (hindering colony formation) and induces secreted exoprotein production. On the other hand, *agr* dysfunction or inhibition may increase the adhesive properties of *S. aureus*. Studies using fluorescent *S. aureus* confirmed that *agr* is not activated in all areas of the biofilm, except for the clusters that detached from the biofilm in a later stage [117].

Current Art in Inhibition of Biofilm Formation

The relationship between chronic infection and bacterial or fungal biofilms, and also the strategies to inhibit biofilm formation were summarized in several reviews [118, 119].

Surface grafted polymeric/oligomeric ethylene glycol brushes (PEG) have attracted much attention in the past two decades since the PEG layer is resistant to protein and cell adhesion. Though early investigation suggested longer chain PEG grafts (MW 18.5 kg/mole) on biopolymers were effective in protein and cell repelling [71], recent reports on PEG grafted surfaces for prevention of cell adhesion [10, 120-123] mainly focused on relatively shorter chains (MW 2 to 5 kg/mole) and were based on simulation and experimental data of protein adsorption.
Du *et al.* [120] deposited a PEG layer onto a lipid film by conjugation, which is relatively weak compared with covalent bonding. The brushes (with chain length of MW 5 kg/mole) provided sufficient protection to the underlying lipid layer from protein adsorption and cell adhesion after two hours of animal cell/protein-surface attachment. Cunliffe *et al.* [121] covalently bonded alkyl, perfluoroalkyl, alkylamide, or PEG (MW 5 kg/mole) chains onto a glass substrate and found that, after a 24 hr incubation, the PEG modified surface was the least fouled by the four bacteria types tested. In a later report [10], significant reduction of bacterial adhesion (on the order of 2-4 magnitudes) was achieved during five hour experiments on a PEG (MW 5 kg/mole) grafted poly(ethylene terephthalate) (PET).

Other surface modifying agents were also proposed and tested for anti-fouling purposes. Among them, the charged polymeric coatings/grafts seem to be very promising. Haldar *et al.* [124] tested branched and linear N,N-dodecyl methyl-

polyethylenimines (PEIs) and their derivatives against the influenza virus and bacteria. Four-log reduction was achieved for the virus test and complete bactericidal activity was obtained when *E. coli* and *S. aureus* were tested. The bacteicidal activity was not due to leaching from the coating, but rather due to the rupture of the bacterial cell membranes caused by sticking side chains [125]. Chen *et al.* [126] showed that a surface grafted poly(sulfobetaine methacrylate) layer (zwitterionic polymer) was resistant to biofilm formation for 48 hours against *S. epidermidis* (Gram-positive) and *P. aeruginosa* (Gram-negative).

Due to thermodynamic reasons, it may prove impossible to create a surface that is perfectly non-fouling. In fact, the surface of any inserted medical device *in vivo* is rapidly covered by plasma and connective tissue proteins. Thus the efficacy of the surface grafts may not last a required period of time for practical applications. Therefore, another concept for the prevention of implant-associated infections involves the impregnation of devices with various antimicrobial substances such as antibiotics, antiseptics, and/or metals. In fact, materials for clinical use (such as antimicrobial catheters) are commercially available, with considerable impact on subsequent infections [118].

Several quorum sensing (QS)-modulating therapies, such as macrolide antibiotics, QS vaccines, and competitive QS inhibitors, have been investigated. These therapies may prove to be helpful in diminishing the translation of QS-directed toxins or can prematurely activate the QS response so as to alert the immune system to bacteria hid in a low cell density. QS represents a recently discovered method of bacterial

communication and population control, which may prove to be a unique mechanism to prevent, suppress, and treat infectious diseases [127].

Biomimetic strategies have been adopted to develop antifouling coatings to prevent adhesion of marine microorganisms [17, 128]. Recent work by Chung *et al.* [21] showed the promising application of engineered PDMSe surface features in preventing biofilm formation. Since the first stage (reversible attachment of the cells on a surface) is the most critical in bacterial adhesion, surface engineering strategies should be developed to interrupt the cell's sensing of the surface and hinder the initial attachment. As surface-immobilized linear PEG chains and zwitterionic short chains show excellent performance in preventing protein adsorption and cell adhesion, a combination of an engineered surface covered with a tethered oligomeric layer may have a synergetic effect and therefore act as antifouling coatings for biomedical devices over an extended period of time *in vivo*.

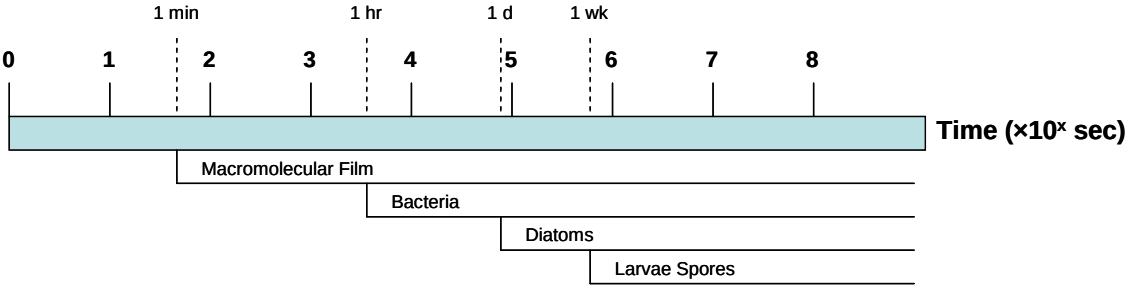

Figure 2-1. Time line of marine fouling event sequences [8].

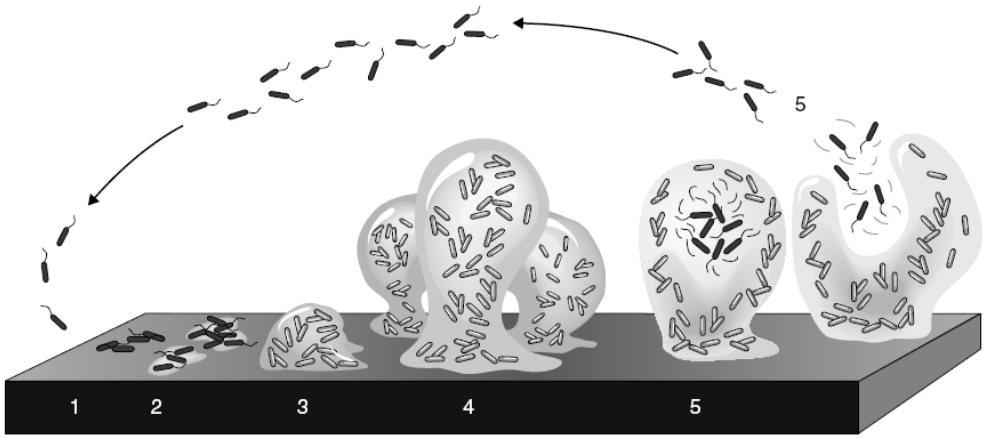

Figure 2-2. Illustration of the development of bacterial biofilm: (1) individual bacterial cells attach reversibly to the surface; (2) the cells anchor to the surface irreversibly by secreting exopolymeric substances, and the cells lose their flagella-driven motility; (3) early development of bacterial colonies indicates the first maturation phase is reached; (4) the fully grown and developed biofilm shows the second maturation phase is reached; (5) single motile cells (dark cells on the figure) disperse from the colonies to start another cycle [94].

CHAPTER 3
FABRRICATION AND CHARACTERIZATION OF MICROENGINEERED THERMOPLASTIC POLYMERIC FILMS

Introduction

One objective of this work was to establish an easy and efficient technique to produce various polymeric films with microengineered, surface topographic features. There are basically two ways of producing micropatterns on polymers: direct patterning (such as photolithography and reactive ion etching) and molding (such as hot embossing). Direct patterning can produce a desired surface pattern in a short period of time. However, there are several drawbacks associated with this method, such as high processing cost, limited size of the products, and restrictions on the substrates. Molding, on the other hand, is and attractive alternative due to its flexible processing choices, low operational costs, and high-quality and high-resolution products [129].

Molding technique involves mold fabrication and mold treatment. The mold fabrication was thoroughly reviewed by Campo and Arzt [129]. Demolding is the last step for surface patterning in micro-fabrication using the molding technique. This step determines the quality (fidelity and resolution) of the final products. Therefore an antisticking (or antiadhesive) surface treatment is usually performed for easy demolding. Previously, researchers deposited fluoropolymers onto the stamps with the help of a CF_4/H_2 or CHF_3 plasma treatment. This layer was not strongly bonded to the surface, and therefore repeated coatings were needed for multiple fabrications. Another antisticking coating was developed by applying self-assembled monolayers (SAMs). Perfluorosilanes have been used to treat silicon wafers for antisticking coatings [130, 131]. The SAMs coatings are strongly bonded to the substrate, but the perfluorosilanes are usually highly reactive with water. Thus the surface coverage and

stability of the SAMs are adversely affected by the water content in the processing environment and therefore the operation cost is increased for this technique.

When characterizing the thickness of thin films grafted onto surfaces, several methods, including x-ray reflectivity (XRR) [132-138], neutron reflectometry (NR) [134, 135, 139], x-ray photoelectron spectroscopy (XPS) [140], atomic force microscopy (AFM) [139-141], and ellipsometry [139, 142], were explored. XRR is an absolute technique for measuring film thickness [133, 137] and has been used to calibrate XPS and ellipsometry measurements [137, 139].

After preparation and characterization of the antisticking layer on a mold, polymer films with nano- or micro-sized topographical structures can be replicated with ease. Common replication techniques include solution casting and thermal embossing.

One important phenomenon associated with the surface roughness is that it influences the wetting and dewetting of the surface. An example from nature is the lotus leaf, which acquires superhydrophobicity through hierarchical nano- and micro-sized features, although the Young's contact angle is only ~74^{o} for the coating wax on the surface [143]. There are two generally accepted models to explain the effect of roughness: Wenzel's model [144] and the Cassie and Baxter [145] (C-B) model.

Wenzel's model assumes the liquid fully wets the total available surface of the substrate, giving the following expression for the apparent contact angle:

$$\cos\theta^* = r\cos\theta \tag{3-1}$$

where θ^* is the apparent contact angle on the rough surface, r is the Wenzel roughness factor (defined by the total surface area divided by the projected planar surface area),

and θ is the equilibrium contact angle on a smooth surface of the same material, and is determined by Young's equation:

$$\cos\theta = \frac{\gamma_{sv} - \gamma_{sl}}{\gamma_{lv}} \tag{3-2}$$

where γ refers to the interfacial tension and the subscripts *s*, *l*, and *v* refer to the solid, liquid, and vapor phases, respectively. Equation 3- shows that a rough surface will promote hydrophilicity (or hydrophobicity) if the material is hydrophilic (or hydrophobic).

The C-B model attributes the change of the contact angle on a rough surface to the composite solid-liquid-vapor interfaces. In other words, the rough surface is not fully wet as there are entrapped air pockets underneath the liquid. If f is the fraction of the solid in contact with the liquid, the C-B equation is

$$\cos\theta^* = -1 + f(1 + \cos\theta) \tag{3-3}$$

The C-B model predicts that a hydrophobic state can be reached even with intrinsically hydrophilic materials. Thermodynamic analysis supports this phenomenon: examples include re-entrant micro-structure [146] and hierarchical nano-micro sized surface features [147].

Here, the process of producing high-fidelity surface micro-patterns was developed. An anti-sticking layer, short-chain poly(dimethyl siloxane) (MW 5 kg/mole) was covalently grafted onto a mold surface with relatively simple treatment procedures. Solution casting was chosen for the fabrication of polymer films as it was simple and reproducible. Solvent was slowly removed so that the polymer film could fully replicate the surface nano- and micro-structures from the mold. Surface morphology, topography and wettability were characterized for better understanding the subsequent bioresponse studies.

Materials and Methods

Materials

Polystyrene (PS, M_w ~350 kg/mole) and poly methylmethacrylate (PMMA, M_w ~350 kg/mole) were purchased from Sigma-Aldrich (St Louis, MO). Kraton G1657M styrene-ethylene-butadiene-styrene triblock copolymer (SEBS, mass fraction of styrene block ~0.13) and G1650M (mass fraction of styrene block ~0.30) were purchased from Kraton (Houston, TX). 3-(aminopropyl triethoxysilane) (APTES), and monoglycidyl ether terminated PDMS (M_n 5 kg/mole, abbreviated as PDMS-5K) were purchased from Sigma-Aldrich (St. Louis, MO). Anhydrous ethanol, 1-propanol, and 2-propanol, hydrogen peroxide (30 wt%), and concentrated sulfuric acid (95%) were purchased from Fisher Scientific (Pittsburgh, PA). All chemicals were used without further purification. Nanopure water (>17.8 MΩcm) was prepared in the lab with a Barnstead Nanopure Diamond^{TM} lab water system from Millipore (Billerica, MA).

Surface Treatment of Silicon Wafers

The grafting of PDMS-5K onto Si wafer was carried out in three steps: (1) a silicon (Si) wafer was first soaked in xylenes overnight to remove possible organic matter, followed by immersion in a freshly mixed concentrated sulfuric acid (H_2SO_4) and hydrogen peroxide (H_2O_2) water solution (30 wt%) (1:1 volume ratio) [148] for 30 min to generate surface hydroxyl groups; (2) after thorough rinsing with nanopure water, the Si wafer was dried with a nitrogen flow and neat APTES was dropped to cover the entire surface for 10 min; (3) after rinsing with anhydrous ethanol, the APTES treated Si wafer was covered by neat PDMS-5K and heated in oven at 80 ^{o}C for 4 hr. The wafer was then rinsed with 2-propanol and 1-propanol (alternately) in an ultrasonic bath. The

PDMS-5K treated Si wafer was blown dry with an Ar flow [149]. A schematic flow chart for the treatment is given in Figure 3-1.

Fabrication of Microengineered Thermoplastic Polymeric Films

Both smooth and topographical surfaces were transferred to the three polymers by solution-casting of a polymer/toluene solution (0.15 g polymer per 1 ml solvent) onto the patterned silicon wafers. The resultant topographies contain feature elements with a width of 2 µm, a distance (between the neighboring elements) of 2 µm, and a varying height of approximately 2 or 3 µm. The short name of this pattern was Sharklet +2SK2x2 (for 2 µm height) and +3SK2x2 (for 3 µm height). Pattern fidelity was evaluated with light and scanning electron microscopy (SEM). As the PMMA and PS films were curling after the removal of the solvent, thermal-pressing was used to ease the unbalanced residual stress. To do this, a PMMA or PS film was sandwiched between two poly(ethylene terephthalate) (PET) sheets, and two glass plates were preheated in an oven. The desired processing temperature was 88 ^{o}C for PMMA, and 97 ^{o}C for PS. The polymer film (in between the PET sheets) was placed on the preheated glass plate, and covered by another preheated glass plate in the oven. The polymer film was thermal-pressed for approximately 30~60 sec under ~2,000 Pa pressure. After cooling, the curling was removed.

Surface Characterization of Polymer Films

X-ray photoelectron spectroscopy (XPS) spectra were obtained on a Perkin Elmer PHI5100 ESCA system (Waltham, MA) operated with an Al Kα X-ray source (hv = 1486.6 eV) at 12 kV and 9 mA in FRR (fixed retardance ratio) mode with analyzer chamber pressure at ~10^{-9} torr.

Atomic force microscopy (AFM) was used to determine the nano-scale surface roughness of the Si wafer and the morphology of the smooth polymer films obtained from solution casting. A Dimension 3100 AFM with a Nanoscope V controller (Digital Instruments, CA, USA) was used for all measurements. The probes were silicon nitride cantilevers (Veeco Metrology, CA, USA), with a spring constant of 0.06 N/m. All samples were imaged in air without using liquids. Contact mode imaging was used to obtain high resolution topographic images of all of the smooth Si wafers and polymer films. The scanned surfaces were 2x2 μm^2 or 5x5 μm^2 at a scan rate of 1 Hz.

The water contact angles were measured using both dynamic and sessile drop methods with a Ramé-Hart goniometer (Netcong, NJ) coupled with DROPimage Advanced software (for image capturing). The dynamic drop technique was adopted for advancing and receding contact angle measurements. The liquid used was nanopure water (>17.8 MΩ·cm resistivity) and droplets were placed on the surfaces via Ramé-Hart Auto Pipetting system. Advancing contact angles were initially measured with 2~3 µl drops, followed by a gradual total increase of ~0.3 µl in increments of 0.05 µl, and five images were taken at one location. Receding contact angles were measured with ~40 µl drops, followed by a gradual intake of the liquid from the drops at 1~2 µl per time at the same spot, with five images taken at the same location. For each sample, two locations were randomly chosen for measurements with both advancing and receding modes, and thus ten images were recorded for each sample. Contact angles were measured with ImageJ software (public software developed by NIH).

The sessile drop contact angles were measured with ~5 µl drops, and Six drops were placed at the randomly chosen locations on the test surface. immediately after

placing the liquid, images were taken in two directions: the spreading direction parallel to the surface feature, and the spreading direction perpendicular to the surface feature. Six images were taken for one test surface. The sessile drop contact angles were also measured with ImageJ software. Surfaces were blown by nitrogen flow at room temperature prior to testing.

Results and Discussion

PDMS-5K Grafted Si Wafers

PDMS-5K was grafted onto Si wafers according to the treatment scheme in Figure 3-1. After an oxidative piranha wash and thorough rinsing with water, the Si wafer (with a patterned or flat region) was evenly covered by a water layer, which indicated abundant surface hydroxyl groups. When grafting of PDMS-5K was completed, water droplets could not spread on the patterned or flat regions on the Si wafer, providing a rough indication of the PDMS-5K layer on the wafer surface.

The surface silanization with APTES was the most critical step in the Si wafer treatment because this process determined the surface density of the $–NH_2$ end group, which reacts with glycidyl group of the short-chain PDMS (PDMS-5K). Processes using dilute solutions of APTES in water [149] or in toluene [150] were employed. The PDMS-5K layers grafted on the Si wafer following the two silanization treatments, however, were not acceptable for demolding. PMMA and PS films had to be peeled off from the mold with the help of dry ice to cool down the Si wafer. Furthermore, the micro-topographical features on the obtained PS films were deformed and damaged during demolding, as shown in Figure 3-2. For the PS +2SK2x2 film, the smallest feature (2 µm width, 4 µm length) was broken (Figure 3-2 A and C), and most features were bent toward one direction (Figure 3-2 D). Although longer immersion time (18 hr) in 2~12%

APTES/toluene solution may give higher surface coverage [151], the solution treatment was abandoned due to time constraints.

A neat APTES treatment was thus adopted from Sui's report [152] and only took 10 minutes to silanize the Si wafer. The resulting PDMS-5K layer on Si wafers was robust: the whole series of polymer samples in this work were cast more than 50 times, and the polymer films from the patterned wafers were peeled off with ease without the aid of dry ice. The patterned polymer films showed a high fidelity (see next section) and thus the antisticking treatment protocol was successfully established.

Dynamic water contact angle measurements of both smooth and patterned regions on Si wafers (before and after PDMS-5K grafting) are shown in Table 3-1. The advancing (θ_a) and receding (θ_r) water contact angles of PDMSe with +2SK2x2 pattern are also listed as references.

For the flat regions on the Si wafers, the PDMS-5K grafted surface showed no difference in both θ_a and θ_r compared with a hexamethyldisilazane (HMDS) treated surface. For the mold regions, which had the recessed Sharklet pattern (2 µm depth, denoted as -2SK2x2), the advancing contact angles were the same for the two treating methods, while the receding contact angles were not, with the higher θ_r for the PDMS-5K treated surface than the HMDS treated one.

The low surface energy methyl groups ($–CH_3$) on PDMS-5K chains would be in contact with the atmosphere, as are methyl groups in the case of HMDS treated surface. The advancing contact angle is less sensitive to surface roughness and heterogeneity than the receding angle [153], which explains why the advancing contact angles are the same for both patterned and flat regions with the two treatment methods.

Contact angle hysteresis, *H*, is defined as the difference of the advancing angle θ_a and receding angle θ_r:

$$H = \theta_a - \theta_r \quad (3\text{-}4)$$

The contact angle hysteresis can be influenced by many factors, such as the solid surface roughness, the chemical heterogeneity, swelling, penetration of liquid into the solid surface, and reorientation of functional groups [154, 155]. The contact angle hysteresis was the largest for the PDMS-5K treated Sharklet mold on a Si wafer (52^o, see Table 3-1), while it was the least for the smooth PDMSe surface (24^o). Therefore, surface roughness together with chemical heterogeneity may explain the difference.

The XPS survey scans clearly showed that C content (C 1s, ~284 eV) increased and Si content (Si 1s and Si 2p, ~100 eV) decreased after silanization with APTES and surface grafting of PDMS-5K on the Si wafers (Figure 3-3). Graf *et al.* [150] recently developed a protocol for cleaning the Si surface and surface silanization with APTES. Their XPS survey spectra for the bare and APTES-coated Si surfaces showed the same trend as in this study. Si $2p^3$ peaks were scanned for the Si wafers after each treatment. After the oxidative wash, the chemical states of the Si wafer were mainly Si-$(O)_4$ (~103 eV) and Si(0) (~99 eV) [156-159], indicating the presence of surface oxidized layer with elemental Si below, as shown in Figure 3-4 (A). After the grafting of the short-chain PDMS (Figure 3-4(C)), the surface chemical states shifted to a (C_2SiO_2) peak (~102 eV) [156] ; the Si(0) peak still appeared in the spectra, thoughwith a significant intensity drop (see Figure 3-4(A)). The spectra in Figure 3-4 clearly shows that the Si wafer was covered with short-chain PDMS after the process.

Micro-engineered Polymer Films

After solvent evaporation and the removal of residual solvent under reduced pressure, the polymer films with micro-topographical features were either easily peeled off (for PDMSe, G1657M, G1650M, and PS/G1650M) or self-peeled (for PMMA and PS) from the PDMS-5K treated silicon wafers. As an example, the whole patterned film (Sharklet AF^{TM}, +2SK2x2) replicated onto PMMA is shown in Figure 3-5 (A). The fidelity of the microstructure was examined under a light microscope (see Figure 3-5 (B)). Typically twelve (12) microscopic images were taken of random locations from the entire 2.5x2.5 cm^2 patterned surface. The number of deformed features was counted and the fidelity was calculated by dividing the number of deformed features by the total number of features in the same area. In this work, all micro-patterned samples showed greater than 99% fidelity.

SEM images showed the detailed features of the Sharklet pattern replicated to various polymeric substrata. Figure 3-6 shows the SEM images of the +2SK2x2 pattern on G1657M, PMMA and PS. Images with higher magnifications shows that the etching marks, resulting from photolithographic process of Si wafers, were also replicated to the micro-sized features on the PMMA and the PS Sharklet textured surfaces (Figure 3-7 and 3-8). However, high-magnification images of PDMSe +2SK2x2 micro-features (Figure 3-9) do not show the nano-sized fine features. The reason may be that PDMSe is a soft material and allows surface shrinkage to minimize surface area after curing. Figure 3-10 shows the successful replication of the +3SK2x2 pattern onto the G1650M and PS/G1650M blend. The actual feature size was measured from SEM images. For the +2SK2x2 pattern, the measured feature height was 2.1 µm of height, 2.0 µm of width, and 2.0 µm of spacing.

Wettability of the polymer films

The type of wetting regime (Wenzel, Cassie-Baxter, or a wicking regime) can be determined by using a lower (θ_{LC}) and upper (θ_{UC}) critical contact angle, according to the following equations [160, 161]:

$$\theta_{LC} = \cos^{-1}\left(\frac{1-f}{r-f}\right) \quad (3\text{-}5)$$

$$\theta_{UC} = \cos^{-1}\left(\frac{f-1}{r-f}\right) \quad (3\text{-}6)$$

Here, r is the Wenzel roughness factor (i.e., the total surface area divided by the projected planar surface area) and f is the fractional area of the projected surface area that is filled by topographical feature tops. When the contact angle on the smooth surface is higher than the upper critical value, the wetting regime is Cassie-Baxter wetting regime; if the contact angle is between the lower and upper critical value, it is in the Wenzel wetting regime; if the contact angle is less than the lower critical value, then it is a wicking regime. The calculated surface parameters are listed in Table 3-3. According to the measured water contact angles on the smooth materials (Table 3-5), the wetting regime for the various Sharklet textured surfaces on the selected materials are predicted and listed in Table 3-4. The calculation predicts that the Sharklet PDMSe, the G1657M, and the PS/G1650M blend are in the Cassie-Baxter wetting regime (air entrapment) while the Sharklet G1650M, the PMMA, and the PS are in the Wenzel regime.

The sessile drop water contact angle was measured for all of the smooth and Sharklet textured polymer films that were solution cast (Table 3-3). The contact angle of the smooth PDMSe, PS and PMMA was 113 ± 4^{o}, 89 ± 1^{o} and 76 ± 2^{o}, respectively. The

results were in agreement with the literature report of 113 ± 1^{o} for PDMSe [160], 90.0 ± 0.5^{o} for PS [162] and 76 ± 4^{o} [163] for PMMA. The contact angle measured for the smooth G1657M, G1650M, and PS/G1650M blend materials showed that these surfaces were all hydrophobic. Due to the anisotropy of the Sharklet pattern, the shape of the water droplet on the patterned surfaces tends to be skewed, and the contact angle measured from different directions should be different. Water droplets sitting on the Sharklet patterned PDMSe, G1657M, G1650M, and PS/G1650M blend are not obviously deformed. However, on PMMA and PS films, elliptical shapes with higher apparent contact angles (in two directions) than on the corresponding smooth films were observed (Figure 3-12, Table 3-5).

From Table 3-5 we can see that the Sharklet textured surfaces on PDMSe, G1657M, G1650M, and PS/G1650M blend can be fitted into the Cassie-Baxter wetting regime. Of interest are the PMMA and PS Sharklet topographies, which show large differences in the two directions (parallel or normal to the surface feature). None of the models can predict contact angles in different directions on an anisotropic surface. The Cassie-Baxter regime may fit in the perpendicular direction, but not in the parallel direction for the PMMA and the PS Sharklet patterns.

If the walls and tops of the micro-sized features of the Sharklet textured topographies were perfectly smooth, the measured contact angles should agree with the predicted wetting regimes. However, the solution-cast polymer films replicate well the etching marks on the side-walls of all the protruding features. As evidenced in a recent work by Nosonovsky [147], the nano-sized curvatures on the side walls can help pin the liquid-solid contact lines and therefore stabilize the metastable interfaces. In this

work, the side walls of the topographical features on all of the materials show convex lines. This may explain why the measure water contact angles are usually larger than the predicted values.

Surface characteristics of the polymer films

The smooth polymer films were scanned by an AFM to compare the nanometer-sized features of the various surfaces obtained by solution casting against the PDMS-5K grafted Si wafer (Figure 3-11). All 3-D images of the film surfaces were obtained from 2x2 μm^2 regions. The average surface root-mean-square roughness (R_q) values were obtained from analysis of 5 different 2x2 μm^2 areas on each sample. The R_q values were calculated from [153]

$$R_q = \sqrt{\frac{\sum_{i=1}^{n}(z_i - \bar{z})^2}{n-1}} \tag{3-7}$$

where z_i is the height of a randomly chosen location on the scanned surface, $\bar{z}$ is the mean height of all measured heights, and n is the sample size (i.e., number of height measurements).

From Table 3-2 and Figure 3-11, the surfaces of PDMSe and G1657M are smooth (R_q < 0.3 nm), the PMMA and PS surfaces are relatively rough (R_q ~1 nm), and the G1650M and PS/G1650M blend surfaces show high roughness (R_q > 1.8 nm) due to the phase separation between the PS block and the ethylene/butadiene block.

Conclusion

A simple and effective method was developed to covalently graft short chain Polydimethylsiloxane (PDMS, Mw ~5 kg/mole) onto the surface of a silicon wafer. This process did not require an inert atmosphere and moisture sensitive chemicals.

Moreover, the resulting antisticking layer had a long life-cycle. This antisticking layer, together with the solution casting process, served to replicate high-fidelity (>99%), microengineered topographic patterns onto polymeric substrata with varied mechanical properties and surface energetics.

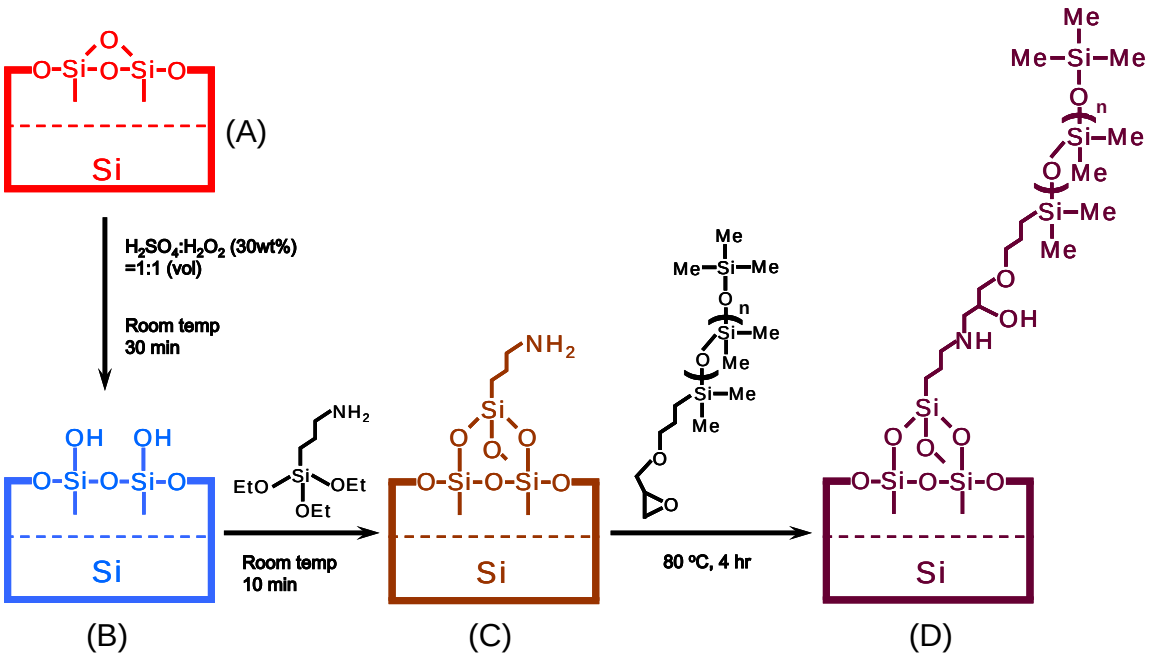

Figure 3-1. Schematic description of surface treatment of a Si wafer: (A) Untreated Si wafer, (B) Si wafer with surface hydroxyl groups, (C) anchored amine groups on Si surface, (D) short-chain PDMS covered Si wafer.

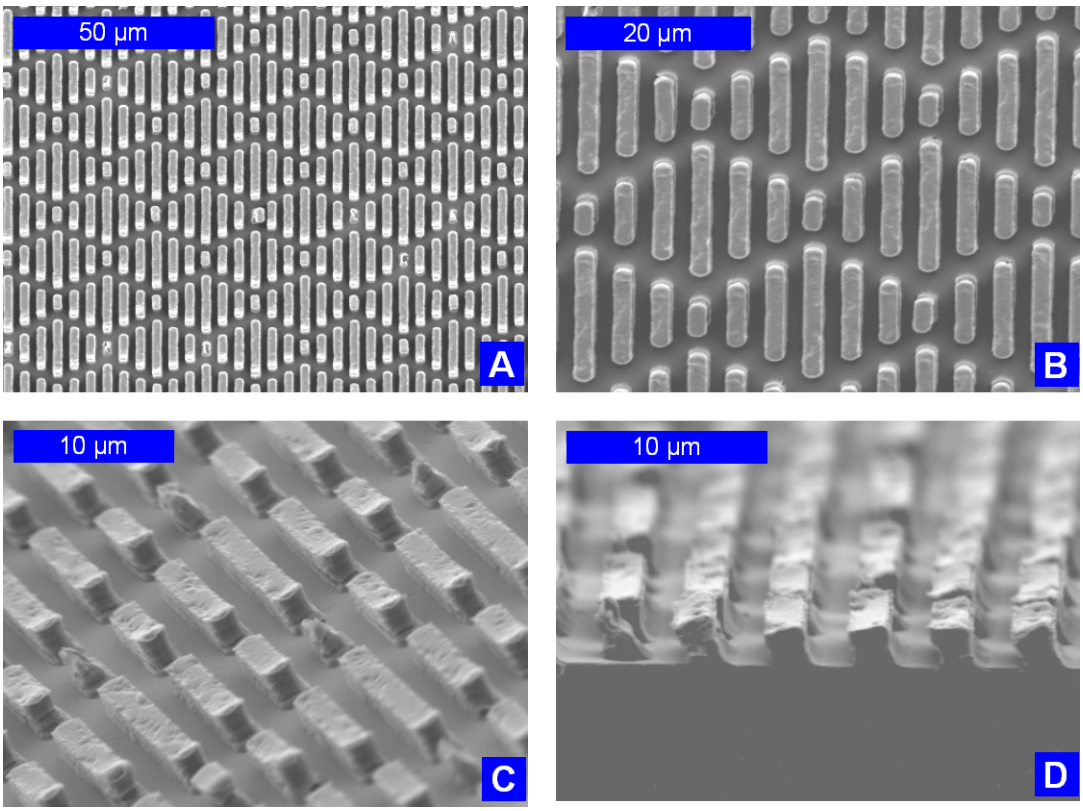

Figure 3-2. SEM images of PS film with +2SK2x2 pattern: (A) Top-down view at 1000x magnification, (B) Top-down view at 2000x magnification, (C) taken at 45^{o} tilt to show the protruding features, (D) cross-sectional view.

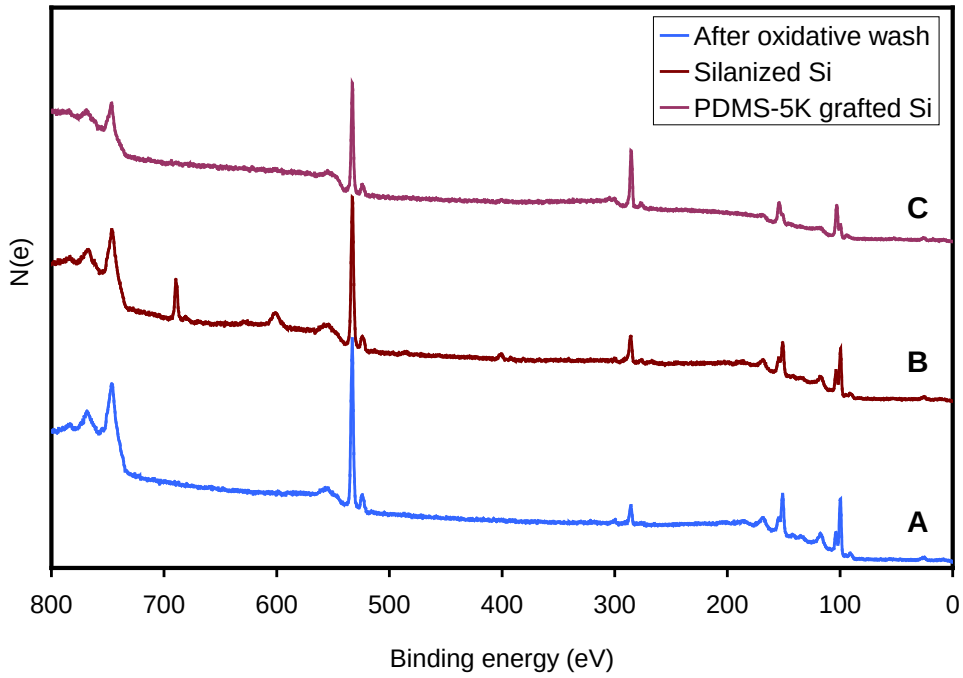

Figure 3-3. XPS survey spectra for Si wafer under various treatments: (A) after H_2SO_4-H_2O_2 (oxidative) wash, (B) after oxidative wash and APTES treatment, (C) after oxidative wash, APTES treatment, and PDMS-5K grafting.

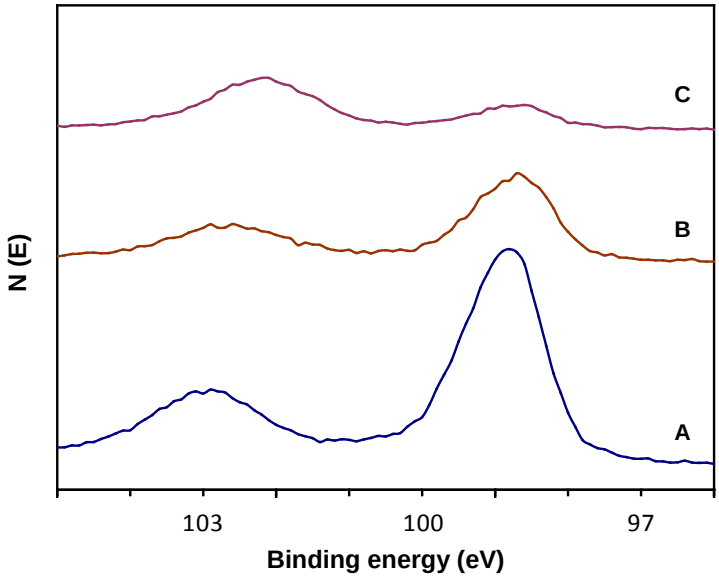

Figure 3-4. XPS spectra of Si $2p^3$ peaks for Si under various treatment: (A) after H_2SO_4-H_2O_2 (oxidative) wash, (B) after oxidative wash and APTES treatment, (C) after oxidative wash, APTES treatment, and PDMS-5K grafting.

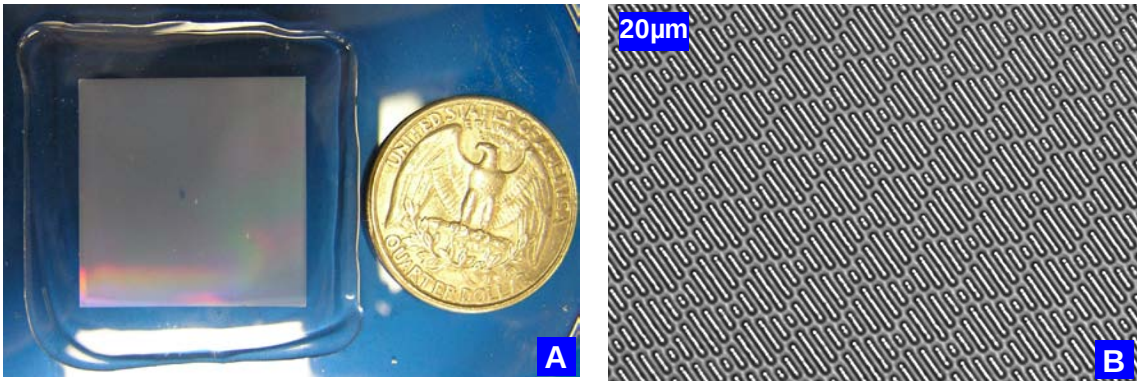

Figure 3-5. (A) Photo of the replicated PMMA film with Sharklet AF™ (+2SK2x2) pattern; (B) Light micrograph of the PMMA Sharklet AF™ (+2SK2x2) pattern (top-down view).

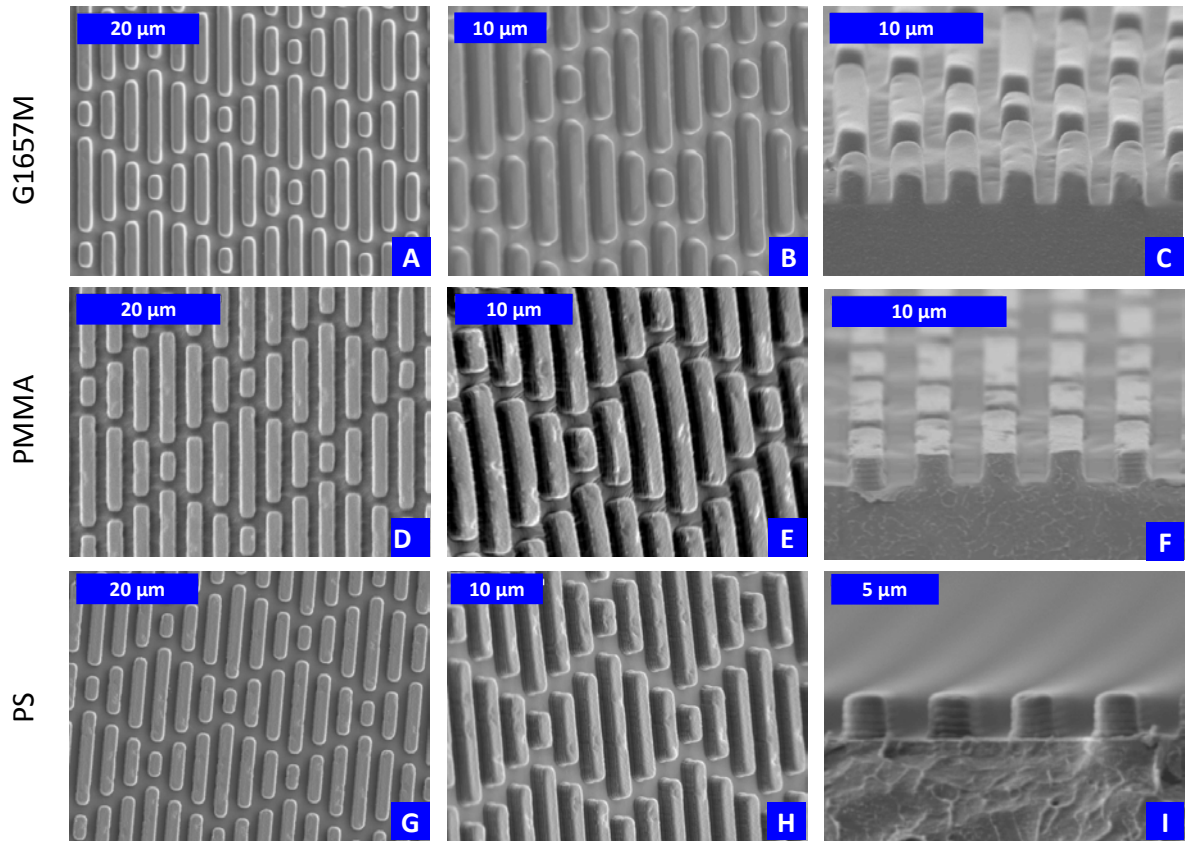

Figure 3-6. SEM images of polymers with Sharklet AF™ (+2SK2x2) pattern: (A-C) G1657M, (D-F) PMMA, (G-I) PS.

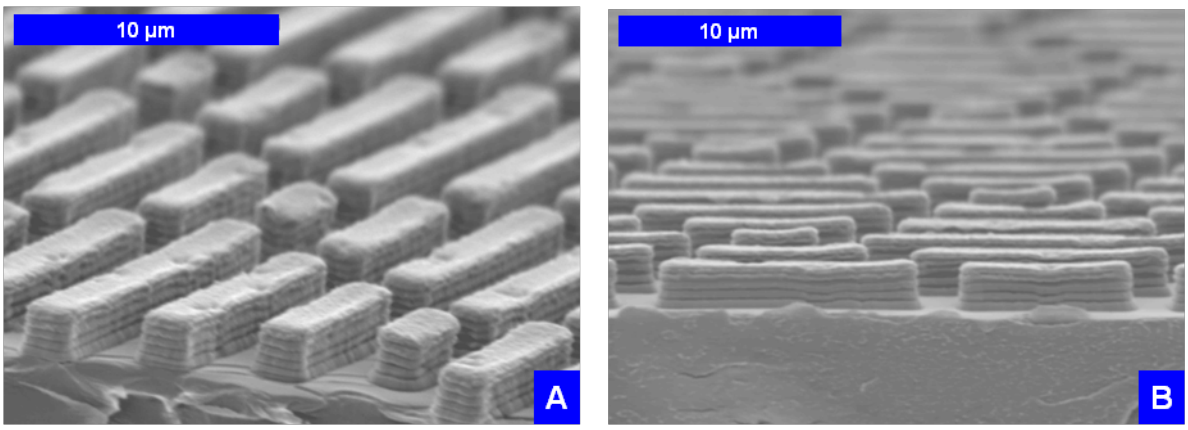

Figure 3-7. SEM images of PMMA +2SK2x2 film, showing the fine structure on the side walls of the features: (A) tilted view, (B) cross-sectional view.

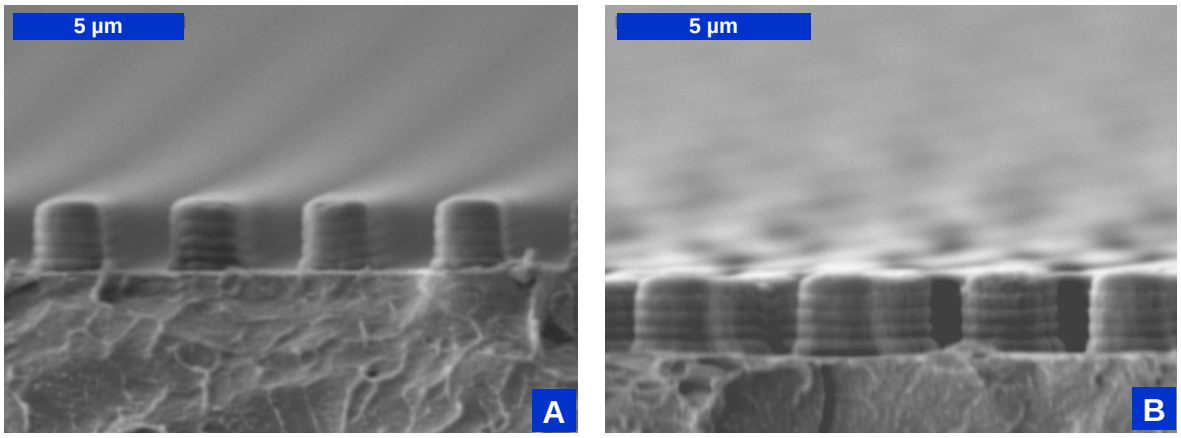

Figure 3-8. SEM images of PS +2SK2x2 film, showing the fine structure of the surface features: (A) Cross-section at 7000x (B) cross-section at 8000x.

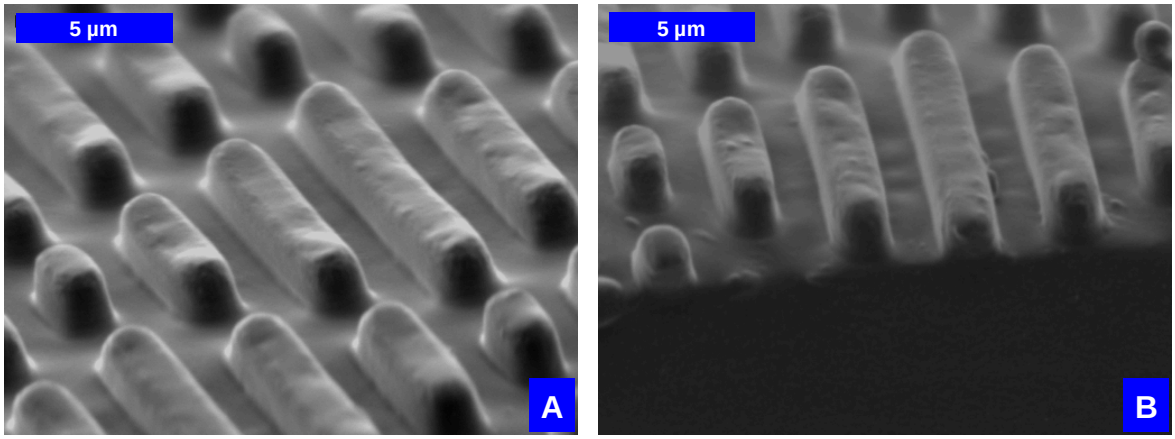

Figure 3-9. SEM images of PDMSe +2SK2x2 film, not showing the nano-structure of the surface features: (A) tilted view at 35^{o} (B) cross-section view.

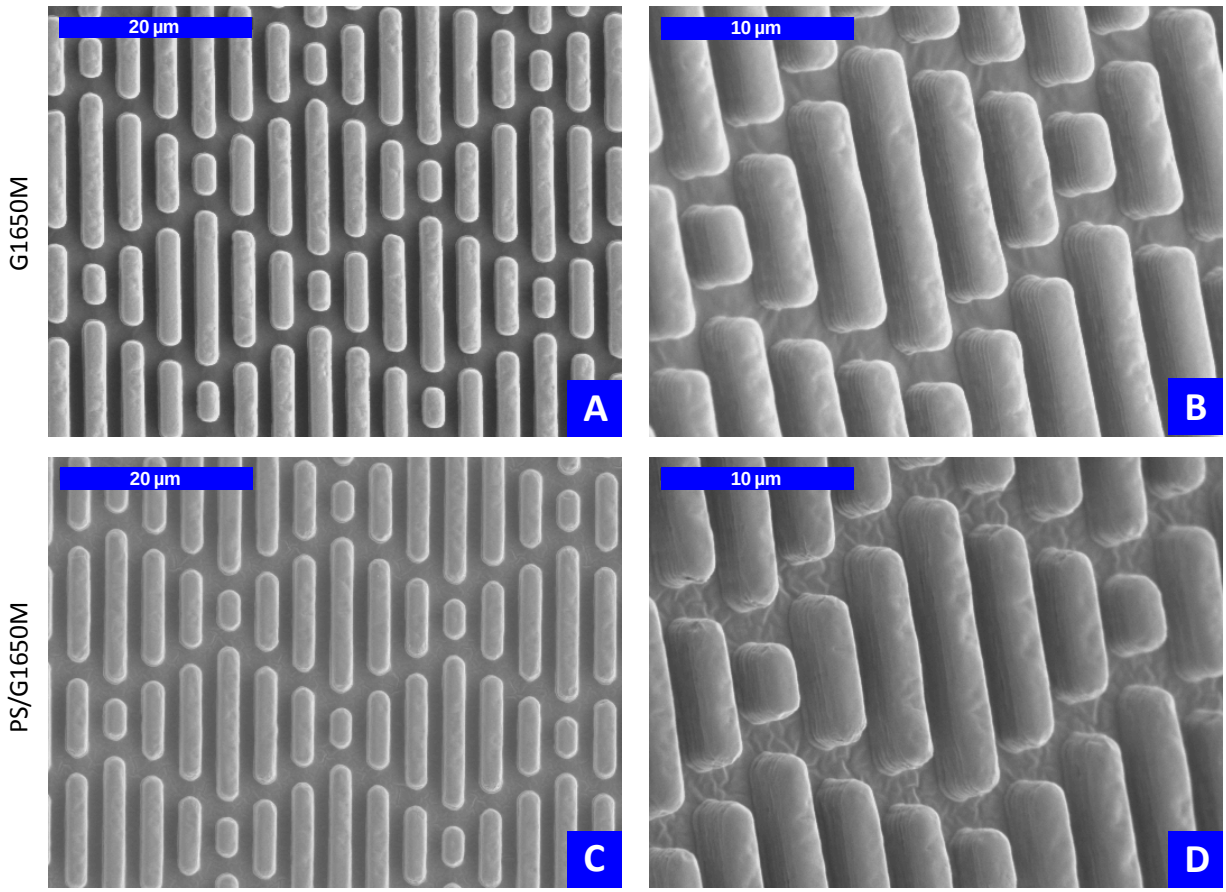

Figure 3-10. SEM images of +3SK2x2 polymer film: (A, B) G1650M; (C, D) PS/G1650M.

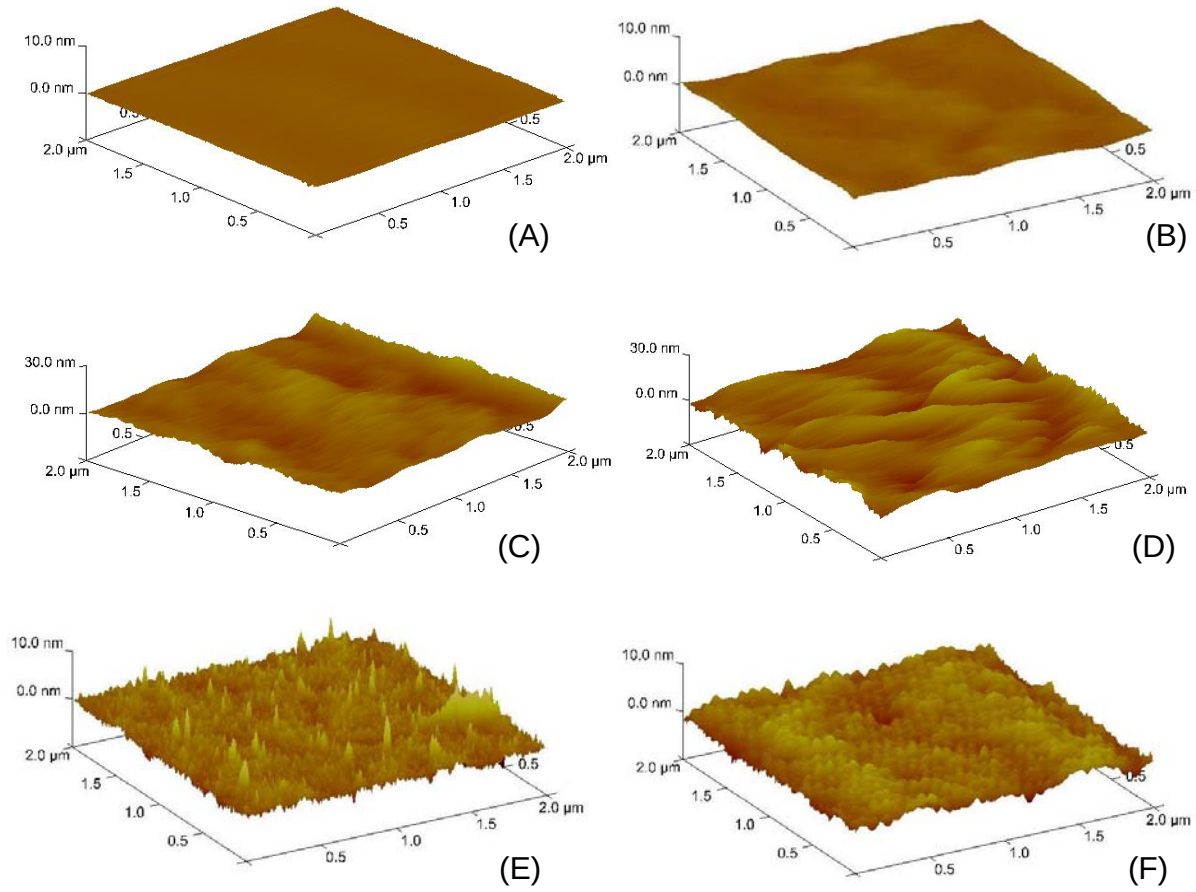

Figure 3-11. AFM images of various smooth polymer surfaces obtained from solution casting against PDMS-5K treated silicon wafer: (A) PDMSe, (B) Kraton G1657M, (C) Kraton G1650M, (D) PS/G1650M blend, (E) PMMA, (F) PS.

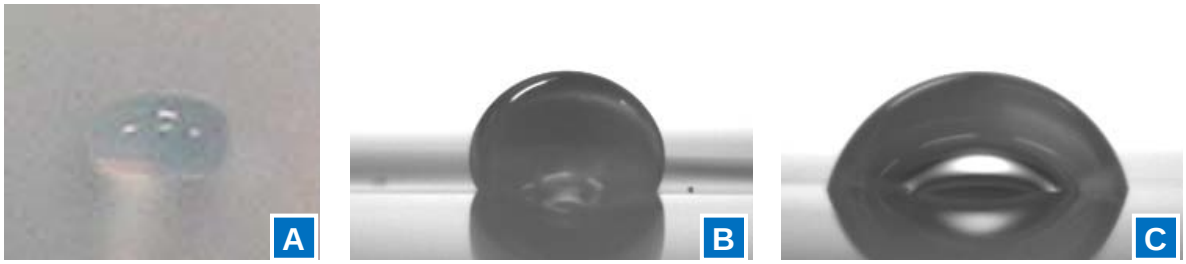

Figure 3-12. Photo images of an elliptical water droplet sitting on +2SK2x2 PMMA film. (A) top-down view of a water droplet sitting on the pattern; (B) side view (direction of water spreading is perpendicular to the surface features); (C) side view (direction of water spreading is parallel to the surface features).

Table 3-1. Dynamic water contact angle on the Si wafers.

Surface feature		Contact angle (^{o})		H (^{o})
		θ_a	θ_r	
+2SK2x2 PDMSe		160 ± 2	112 ± 3	48
Smooth PDMSe		113 ± 6	89 ± 5	24
HMDS treated Si wafer	Sharklet Mold	141 ± 4	98 ± 6	43
	flat region	117 ± 2	87 ± 4	30
PDMS-5K grafted Si wafer	Sharklet Mold	141 ± 3	89 ± 5	52
	flat region	118 ± 2	85 ± 2	33

* HMDS: hexamethyldisilazane

Table 3-2. Root mean square roughness of the flat polymer films via solution casting on PDMS-5K treated silicon wafer

Material	R_q, nm
PDMSe	0.11
G1657M	0.30
G1650M	1.87
PS/G1650M	2.14
PMMA	1.01
PS	1.01

Table 3-3. Calculated surface parameters for microengineered topographies

+2SK2x2				+3SK2x2			
r	f	θ_{LC} (^{o})	θ_{UC} (^{o})	r	f	θ_{LC} (^{o})	θ_{UC} (^{o})
2.0	0.42	69	111	2.5	0.44	74	106

Table 3-4. Predicted wetting regime for the polymer films with varied feature height

Material	+2SK2x2	+3SK2x2
PDMSe	Cassie-Baxter	Cassie-Baxter
G1657M	Cassie-Baxter	Cassie-Baxter
G1650M	Wenzel	Wenzel/Cassie-Baxter
PS/G1650M	Cassie-Baxter	Cassie-Baxter
PMMA	Wenzel	Wenzel
PS	Wenzel	Wenzel

Table 3-5. Sessile drop contact angles on polymer films, with water as testing medium.

Material	Feature	Contact Angle (^{o})		
		Measured	Wenzel	C-B
PDMSe	Smooth	113 ± 4		
	+2SK2x2 (parallel)	137 ± 5	143	138
	+2SK2x2 (perpendicular)	141 ± 2		
	+3SK2x2 (parallel)	139 ± 4	169	137
	+3SK2x2 (perpendicular)	143 ± 1		
G1657M	Smooth	111 ± 5		
	+2SK2x2 (parallel)	144 ± 1	137	137
	+2SK2x2 (perpendicular)	146 ± 2		
	+3SK2x2 (parallel)	145 ± 2	154	136
	+3SK2x2 (perpendicular)	149 ± 3		
G1650M	Smooth	103 ± 6		
	+2SK2x2 (parallel)	135 ± 4	117	133
	+2SK2x2 (perpendicular)	142 ± 3		
	+3SK2x2 (parallel)	139 ± 2	124	131
	+3SK2x2 (perpendicular)	147 ± 1		
PS/G1650M	Smooth	112 ± 2		
	+2SK2x2 (parallel)	140 ± 5	140	138
	+2SK2x2 (perpendicular)	147 ± 2		
	+3SK2x2 (parallel)	144 ± 5	160	137
	+3SK2x2 (perpendicular)	152 ± 3		
PMMA	Smooth	76 ± 2		
	+2SK2x2 (parallel)	86 ± 1	60	119*
	+2SK2x2 (perpendicular)	120 ± 6		
	+3SK2x2 (parallel)	86 ± 1	52	117*
	+3SK2x2 (perpendicular)	133 ± 2		
PS	Smooth	89 ± 1		
	+2SK2x2 (parallel)	95 ± 3	88	125*
	+2SK2x2 (perpendicular)	139 ± 2		

* C-B estimation for PMMA and PS with Sharklet patterns was based on the air-entrapment mode.

CHAPTER 4
ULVA ZOOSPORE ATTACHMENT ON THE MICROENGINEERED POLYMERIC FILMS

Introduction

Biofouling, accumulation of biomass at the interfaces, has been attracting much interest from researchers worldwide. Some of the adverse influences of biofouling include the increased fuel cost for ships [3], accelerated corrosion of marine structures [164], and spread of invasive species [4]. With stringent regulations on coating materials applied to marine vessels, the need for cost-efficient and environmental-friendly coatings is urgent. Many strategies, in terms of materials chemistry, surface energetics, micro-topographical features, and mechanical properties, have been proposed by various research groups to construct antifouling/foul-release (AF/FR) coatings.

The study of polymer based materials are among the most active fields for AF/FR coatings. Among all the efforts on polymer materials, zwitterionic polymers showed promising applications in both antifouling of both protein adsorption and bacteria adhesion[11, 66, 67]. Ongoing research with this type of materials also showed excellent resistance to marine organisms [68]. In order to combine the AF property of oligoethylene glycol and the FR property from perfrluoroalkanes, Krishnan *et al.* [69] synthesized an amphiphilic copolymer. There were oligoethylene glycol and perfluoroalkyl moieties in the same side chains of their synthesized polymers. In an aqueous environment, the side chains bent with oligoethylene glycol segments sticking toward water and perfluoroalkyl segments “bowing” toward the coating surface. The obtained surface showed improvement against settlements of *Ulva* and *Navicula* and higher removal rate of sporelings compared with glass and polydimethylsiloxane

(PDMS) surfaces. Linear-chain poly ethylene glycol (PEG) grafted surfaces have long been shown to be effective against protein adsorption and cell adhesion [10, 70, 71]. Statz *et al.* [72] coated Ti surface with PEG chains via conjugation with L-3,4-dihydroxyphenylalanine and the resulting surface showed AF/FR against spore and diatom. Other polymeric materials, such as perfluoropolyethers (PFPE) and their PEG blends [73], and siloxane-polyurathane copolymers [74], also showed improved AF properties.

Surface chemistry certainly plays a role when a cell determines if it will settle on the surface. Ista *et al.* [52] changed surface chemistry (and therefore surface energy) systematically via self-assembled monolayers (SAMs) technique and tested the surfaces with marine bacteria and *Ulva* zoospores. In their work, they prepared two series of mixed SAMs on gold surface: one was alkyl chains with mixed end groups of –COOH and $–CH_3$. The other was alkyl chains with mixed end groups of –OH and $–CH_3$. Although the adhesion of bacteria complied with the prediction of a thermodynamic model, spore test gave more complicated bioresponses, indicating simple model cannot fully explain the interactions between the somewhat complex microorganisms and the surface. Diatoms were used as test subject on various chemically modified surfaces [165].

The concern with all the non-toxic material and surface chemistry work lies in the fact that the surface will eventually be conditioned with organic matter [8], which will recruit microorganism subsequently. One disadvantage of PEGylated polymer coatings is that PEG can be degraded gradually [9, 75], making it unfavorable for long term applications.

Although the adhesion strength between the fouling organisms and the surface energy and mechanical properties of a substratum was investigated [59, 166], there are few reports on the effect of surface mechanical properties on the settlement/attachment behavior of the marine microorganisms. Recently, Chaudhury *et al*. [26] varied the elastic modulus of polydimethylsiloxane (PDMS) from 0.2 to 9.4 MPa and found no significant difference on the settlement of *Ulva* spore. A recent work [110] suggested that surface mechanical stiffness may influence the adhesion and colonization of bacteria (*Staphylococcus epidermidis* and *Escherichia coli*), on polyelectrolyte multilayer thin films.

Surface topographical features as a strategy of physical defense have also attracted much attention. One approach, which is based on the biomimetic analogy to the shark scale, has shown effectiveness in antifouling towards many species such as bacteria, spore, and barnacle cyprids [18, 19, 21, 48]. Schumacher's work [20] on a nanoforce gradient design didn't show a correlation between the spore settlement and the force gradient. However, the data fitted well with a predicting model in a later work [27], shown below:

$$\log\left(\frac{A}{A_{SM}}\right) = a \cdot ERI_{II} \tag{4-1}$$

where A is the spore settlement density on the topographical surface, A_{SM} is the spore settlement density on the smooth surface of the same material, and a is fitting constant, engineered roughness index (ERI) ERI_{II} is defined as

$$ERI_{II} = \frac{r \cdot n}{1-f} \tag{4-2}$$

where *r* is the Wenzel roughness index, *n* is the number of discrete features on the surface, and f is the fraction of solid in contact with liquid in the Cassie-Baxter model. This prediction model suggests that surface thermodynamic properties are the main controlling factors for microorganisms' attachment/settlement onto a surface in the case of PDMSe material.

One key issue about this prediction model is the influence of the surface chemistry/energy and substrate mechanical properties. Therefore, the objective of this study was to test the hypothesis that the Sharklet AF^{TM} pattern is the effective antifouling design in itself no matter on which substrate it is replicated. Thus, thermoplastic polymers with systematically varied mechanical and energetic properties were selected to help test the hypothesis. Styene-ethylene/butyldiene-styrene triblock copolymer (SEBS) as a thermoplastic elastomer was chosen as a hydrophobic, low modulus (Young's modulus 6~30 MPa) material. Poly methyl methacrylate (PMMA) was chosen due to its higher modulus (~ 3,300 MPa) and relatively high surface energy. Another objective of this study was to explore simple technique of fabricating micropatterned polymer films. The Sharklet pattern was replicated onto five polymeric substrate. The polymers were: poly(dimethyl siloxane) elastomer (PDMSe) (the standard material on which most topographical studies have been conducted), two types of Kraton SEBS polymers (varied ratio of styrene blocks), a polystyrene/SEBS blend, and poly(methyl methacrylate) (PMMA). *Ulva* zoospore settlement assays were performed on the samples.

Materials and Methods

Materials

Poly(methyl methacrylate) (PMMA, 350 kg/mole) was purchased from Sigma-Aldrich (St Louis, MO). Styrene-ethylene/butyldiene-styrene (SEBS) triblock copolymers, Kraton G1657M (styrene block mass percentage 13%) and Kraton G1650M (styrene block mass percentage 30%), were purchased from Kraton (Houston, TX). Polystyrene (PS, molecular mass 30 kg/mole) was purchased from Polysciences (Warrington, PA). 3-(aminopropyl triethoxysilane) (APTES), and monoglycidyl ether terminated polydimethylsiloxane (PDMS, MW 5 kg/mole, abbreviated as PDMS-5K) were purchased from Sigma-Aldrich (St. Louis, MO). Anhydrous ethanol, 1-propanol, 2-propanol, hydrogen peroxide (30 wt%), and concentrated sulfuric acid (95%) were purchased from Fisher Scientific (Pittsburgh, PA). All of the chemicals were used without further purification. Nanopure water (>17.8 MΩ·cm) was prepared in the lab with a Barnstead Nanopure Diamond^{TM} lab water system from Millipore (Billerica, MA).

Topographical Replication

The thermoplastic polymeric films were prepared by a solution-casting method. The polymer toluene solution (0.15 g polymer dissolved in 1 ml toluene) was cast onto a smooth or a pre-patterned silicon wafer. The pattern was transferred to a silicon wafer (2.5x2.5 cm^2 in area) by a photolithographic technique [19, 21]. To lift the polymer films from the wafer, an antisticking layer (short-chain polydimethylsiloxane, or PDMS-5K) was grafted onto a silicon (Si) wafer in a three-step manner: (1) a Si wafer was immersed into a freshly mixed concentrated sulfuric acid (H_2SO_4) and hydrogen peroxide (H_2O_2) water solution (30 wt%) (1:1 volume ratio) [148] for 30 min to generate surface hydroxyl groups; (2) after thorough rinsing with nanopure water, the Si wafer

was dried with a nitrogen flow. Neat APTES was added dropwise to cover the entire surface for 10 min. (3) After rinsing with anhydrous ethanol, the APTES treated Si wafer was covered by neat PDMS-5K and heated in an oven at 80 ^{o}C for 4 hr. The wafer was then rinsed with 2-propanol. The PDMS-5K treated Si wafer was dried with an Ar flow [149]. Enough of the polymer solution was placed on the wafer dropwise to cover the smooth or patterned area of the wafer. After slow removal of solvent, the desired polymer films were obtained with the size of about 8 cm in length, 3 cm in width and 150 µm in thickness. The Sharklet patterned area was located in the middle of the film with a 2.5x2.5 cm^2 coverage. Polydimethylsiloxane elastomer (PDMSe) was used as a reference material as described previously by Chung *et al*. [21] Silastic T2^{TM} (from Dow Corning Corp, Midland, MI) base material and curing agent were mixed at a 10 to 1 mass ratio and cast against the silicon wafer described above. After one day curing at room temperature, the resulting PDMSe films were easily lifted from the silicon wafers.

The resultant topographies contain feature elements with a width of 2 µm, a distance (between the neighboring elements) of 2 µm, and a varied height of approximately 2.1 or 3 µm,. The short name of this pattern was Sharklet +2SK2x2 (for 2 µm height) and +3SK2x2 (for 3 µm height). Pattern fidelity was evaluated with light and scanning electron microscopy (SEM).

The surface free energy of each sample was determined by a two-liquid method, known as Owens-Wendt-Kaelble (OWK) approach (geometric mean method) [167, 168]. The surface energy of the solid (γ_S) was the sum of the polar component (γ_s^p) and dispersive component (γ_s^d). In this method, at least a pair of liquids, one polar and one non-polar was needed to determine the surface energy by Equation 4-3:

$$\gamma_L = \frac{2\left(\sqrt{\gamma_s^d \gamma_L^d} + \sqrt{\gamma_s^P \gamma_L^P}\right)}{1+\cos\theta} \quad (4\text{-}3)$$

The parameters γ_L, γ_L^d, and γ_L^P, which are known, refer to the total surface free energy, dispersion and polar components of the probe liquid, respectively. Two probe liquid tests produce two equations from which the γ_S^P and γ_S^d can be calculated. In order to get a more precise surface energies, three probe liquids, water (WT), ethylene glycol (EG) and diiodomethane (DM), which have γ_L= 72.8, 48.0 and 50.8 mJ/m^2, γ_L^d= 21.8, 29.3 and 49.5 mJ/m^2, and γ_L^P= 51.0, 18.9 and 1.3 mJ/m^2 respectively, were chosen and we took the mean value resulted from the two pair tests, WT-DM and EG-DM, as shown in Table 4-1 and 4-2.

Sample Preparation

The polymeric films were cut into 1.3×1.0 inch^2 pieces and were then glued to the glass slides by a fast-cure epoxy glue, Araldite 2012, purchased from Huntsman (The Woodlands, Texas, USA). Minimal amount of glue (~0.05 g) was spread onto glass slides followed by attaching of the polymer samples. The covered area of epoxy glue was larger than the area of the polymer sample. Usually there were two narrow epoxy glue regions exposed to air after attaching the polymer films. The fidelity of each topographical sample was checked under a microscope before shipping.

Samples were shipped dry to University of Birmingham, UK, and were immersed in seawater for 24 hours prior to the experiment. The samples were not exposed to sonication. Any air visibly trapped in the features was dispersed using a jet of seawater from a pipette.

Spore Attachment Assay

Spore attachment assay was performed by Dr John Finlay and Dr Maureen Callow at the University of Birmingham, UK. Fertile plants of *Ulva linza* were collected from Wembury beach, the United Kingdom (50°18”N; 4°02”W). *Ulva* zoospores were released and prepared for attachment experiments as previously described [169].

Samples were transferred to artificial seawater (Tropic Marin) for 1 hour prior to experimentation without exposure to air. Samples were then rapidly transferred to assay dishes to minimize any dewetting of the topographical areas. Ten milliliter of spore suspension (adjusted to 1.5×10^6 ml^{-1}) were added to each dish and placed in darkness for 45 minutes. The slides were then rinsed and fixed with 2% glutaraldehyde in artificial seawater as described in Callow *et al.* [170].Spore counts were quantified using a Zeiss epifluorescence microscope attached to a Zeiss Kontron 3000 image analysis system [171]. Thirty images and counts were obtained from each of three replicates at 1 mm intervals along both the vertical (15) and horizontal (15) axes of the slide.

The spore concentration was 1.5×10^6 spores ml^{-1}; the settlement time was 45 min, 3 replicates of each sample were tested.

Statistical Methods

Spore density was reported as the mean number of settled spores per mm^2 from 30 counts on each of three replicate slides +/- standard error . Statistical differences between surfaces were evaluated using a nested analysis of variance (ANOVA) followed by the Tukey test for multiple comparisons. Replicate slides (3) of each surface (5) were treated as a nested variable within each surface.

Principal component analysis was performed with Minitab V15.0 software (Minitab Inc, State College, PA). Many factors, including surface chemistry, surface energy,

mechanical properties, surface topography, tortuosity, and feature dimensions, can affect the attachment of spores onto a surface. Five parameters that can be quantified for the topographical surfaces were selected as independent variables: the bulk elastic modulus (Young's modulus, *E*), the surface free energy (γ), the spacing between the two adjacent surface features (a), the discrete number of surface features (n), the Wenzel roughness factor (r), and the area fraction of the surface top relative to the projected planar area (f). The data source came from this study as well as previous work of the Brennan research group, shown in Table 4-2.

Results and Discussion

Spore Attachment Affected by the Epoxy Glue

The attachment density of *Ulva* spore on all of the tested surfaces was reported in Figure 4-1. It was found that the spore settlement density was abnormally high on +3SK2x2 PDMSe surface. As PDMSe was used as the baseline for the spore attachment test, the data for other materials were therefore questionable. It was necessary to investigate the reasons so that the spore attachment data could be further analyzed.

After finishing the spore attachment assay, all the tested samples were shipped back to the lab at UF. All the 51 glass slides with polymer samples were scanned under light microscope thoroughly. The typical images of each region were shown in Figure 4-2, using +2SK2x2 PS as an example. It was noticed that the spores settled on the epoxy region with extremely high coverage. This high attachment density on epoxy region can be observed on each glass slide. Spores were also attracted to the cavities between the polymer film and the epoxy layer, as shown in Figure 4-3. These observations demonstrated that the epoxy glue had high attractiveness to the spores.

To test if there was any chemical leaching from the glue, Araldite2012 epoxy glue was spread on two clean glass slides. After one day curing, each slide was immersed in 45 ml D.I. water in a centrifuge tube. A clean glass slide was also soaked in the same amount of D.I. water to serve as reference. After 38 days of soaking, UV-Vis spectra were taken and shown in Figure 4-4. According to the MSDS provided by Bostik Findley, Araldite 2012 epoxy glue consists two parts: one is epoxy resin containing bisphenol A diglycidyl ether polymer (CAS # 25068-38-6), butanediol diglycidyl ether (CAS # 2425-79-8) and acrylonitrile butadiene styrene polymer (CAS # 9003-56-9), the other part is a polyamine hardener. The UV spectra showed that the leachant may be amine/amide with aromatic groups, having similar structures to N-(3,4-dimethoxybenzyl)phthalamic acid, compared with a report from the Occupational Safety and Health Administration (OSHA) [172].

The topographical regions of each sample were carefully examined under a microscope. Except for +3SK2x2 PDMSe surface, all other topographical samples kept their fidelity after spore settlement assay (Figure 4-5). Flopped top is prevailing on +3SK2x2 PDMSe surfaces, see Figure 4-6. The retained +3SK2x2 PDMSe sample was examined under microscope before and after soaking in D.I. water for 24 hr. No flopped top was observed in both cases. The damage of surface features may have occurred during shipping and handling of the samples. Based on the observations, the spore attachment density on +3SK2x2 PDMSe was not considered in the following analysis.

Spore Attachment on Various Surfaces

It was shown that the chemical attractant from the exposed epoxy regions is strongly influential. The instinct assumption was that the influence of the epoxy glue

would be the same among all the samples. The following observation and statistical analysis were based on this assumption.

The attachment density of spores on the smooth surfaces greatly varied on the different substrate (Figure 4-1). Spore densities ranged from ~300 mm^{-2} on the PDMSe to ~1900 mm^{-2} on the PS/G1650 blend. Plotting the spore attachment densities against the square root of the product of elastic modulus and surface energy indicated that spore density increased as elastic modulus increased up to 240 MPa (PS/G1650M blend)(Figure 4-7), but above this the density of settled spores decreased. The correlation was weak, as R^2 was only about 0.363. In an earlier report, Chaudhury *et al.* [26] found no significant difference in spore attachment on PDMSe over a small range of moduli (0.2 ~ 9.8 MPa).

Compared to attachment densities on the smooth surfaces spore attachment was reduced on the +2SK2x2 patterns on the PDMSe, G1650, PS/G1560 and PMMA. On the G1657 attachment density was slightly higher on the pattern, and on the polystyrene it was much higher (over double). Although the density of settled spores was low on the smooth PDMSe, the reduction of 41% on the patterned area (+2SK2x2) is low compared with previous studies (commonly higher than 70% reduction). Plotted as a function of force gradient, spore density increased to a force gradient value of 2100 nN (PS/G1650M blend) and then fell in a pattern similar to that seen for the elastic modulus of the smooth surfaces (Figure 4-7).

The +3SK2x2 Sharklet reduced spore attachment on the G1657M, G1650M and the PS/G1650M blend (Figure 4-1). In the case of PMMA the attachment density was considerably greater than on the +2SK2x2 Sharklet pattern. It is interesting that the

small change in height can cause such a difference in attachment density and shows just how sensitive the sensory apparatus of the spores must be. Although, it should be remembered that a difference of 1μm in height is a difference of approximately 15% of the body length of a spore.

A plot of spore attachment density (on the +2SK2x2 and +3SK2x2 patterns) against nanoforce gradient indicated that there was a possible increase in spore density with force gradient at (Figure 4-8). However, the trend was weak ($R^2 = 0.38$) and might again reflect other parameters rather than force gradient per se.

An alternative view of the influence of the leachant from the epoxy glue could be based on the concentration differences of the aromatic amide(s) in the different substrata. The chemical could diffuse into the polymer films. As it contains aromatic rings, it has higher affinity to the substrate containing higher concentration of benzene rings. In this study, G1657M, G1650M, PS/G1650M blend, and PS have higher benzene ring content along the list. Therefore, the concentration of aromatic amide(s) dissolved in the polymer film may be in the following rank: G1657M < G1650M < PS/G1650M blend < PS. The data in Figure 4-1 exhibited the higher spore attachment density following the trend. The film thickness will determine the concentration gradient of the dissolved amin/amide. The abnormally high attachment densities on the patterned sample of+2SK2x2 PS, may be caused by the variations in the thickness of the polymer films, compared with the smooth PS film. The solubility of the aromatic amides may be smaller in PDMSe and PMMA compared with PS-containing polymers, but they could still disturb the attachment behavior of the spores.

If, in the worst case of scenario, the leachant from the epoxy glue is overwhelmingly strong to disturb the sensory functions of the spores, the spores would show random attachment behavior on all the samples, i.e., there would be no statistical difference among all of the smooth and the Sharklet textured surfaces for all of the materials. However, the attachment density data did show difference among different material groups. Therefore, it could be concluded that material properties may have influence on the spore attachment process.

Site Selection by Spores

Images of the spores on the patterns are shown in Figure 4-9 and 4-10. On both types of pattern, on all substrates the spores selected the wider channels which separated the diamond patterns to settle in. They were especially prevalent at either end of the diamond where the smallest features were placed (probably the widest part of the channel). The channels between the individual bars of the pattern were narrower and proved less favorable for attachment.

Correlation between the Surface Parameters and *Ulva* Spore Attachment

The three surface parameters (*n, r, f*) were used to construct the concept "engineered roughness index" (ERI_{II}) in previous works and excellent predictive correlation was obtained for the *Ulva* spore attachment on PDMSe material [27]. The principal component analysis (PCA) method was first applied to the three parameters to determine if any of the three parameters contribute more to the total variance. The data set was shown in Table 4-3. PCA analysis on the three parameters shows that the first component has an Eigenvalue of 2.4, explains 80.4% of the total variance in the group. The eigenvalues of the other two components are all less than 1 (0.359 and 0.230 respectively) and should not be considered. For the first component, the loading of each

variable is 0.560 (n), 0.590 (r), and 0.581 (f), respectively. The results show that the three surface parameters contribute equally to the total variance and should all be considered in the correlation with the response. However, the plot of the $Ln(A/A_{SM})$ against ERI_{II} values gave weak correlation ($R^2 = 0.24$, Figure 4-11).

When three more surface parameters (E, γ and a) were introduced, principal component analysis (PCA) method was used to reduce the surface parameters (listed in Table 4-3) into two groups of components. As seen in Table 4-4, the two components can explain a total of 72.9% of the variance of the quantified surface parameters, which describe the surface energy, mechanical property, surface topography (roughness) and tortuosity. In the first component, the three parameters n, r, and f, showed the highest loadings (higher than or close to 0.5). In the second component, E and γ are the main contributors with loadings (absolute values) higher than 0.6.

The grouping of the surface parameters inspired new correlation of spore attachment vs. surface properties. Brady [59] showed that the relative adhesion of fouling organisms is proportional to the square root of the product of elastic modulus and surface energy. Callow et al. [170] demonstrated that when a spore is in touch with a surface, it secrets a small amount of adhesive to “test” if this is a suitable spot for it to settle. It suggests that the mechanical strength of the initial “test” adhesion is among the factors that determine the likelihood of the spore to settle on the surface. Considering the second component in PCA analysis, it is reasonable to introduce new parameters into the spore attachment model. When all the data from this study and previous works by Wilson [173], Schumacher [19, 20] and Long [27] were included, the reduction of spore attachment density on a surface is expressed as follows (shown in Figure 4-12),

$$Ln\left(\frac{A}{A_{SM}}\right) = -10.7\frac{ERI_{II}}{\sqrt{E\gamma}} \quad (R^2 = 0.49) \tag{4-3}$$

As observed in the data set from Wilson's work [173], the spacings between the neighboring features were all no less than 5 µm, which is about the diameter of the spores. Spacing of 5 µm channeled PDMSe surface greatly increased spore attachment [17]. Later surface designs all considered spacings less than this critical size. Therefore, when the data from Wilson's work were not included, the predictive correlation is (also in Figure 4-13)

$$Ln\left(\frac{A}{A_{SM}}\right) = -11.6\frac{ERI_{II}}{\sqrt{E\gamma}} \quad (R^2 = 0.68) \tag{4-4}$$

In Figure 4-13, there are still data points higher than point zero when ERI_{II} values are small. It is possible that other factors such as surface chemistry play significant role in some cases. In a bacteria-surface interaction study [174], the surface energy term was considered as a sum of Lifsthitz-van der Waals (LW) and acid-base (AB) interactions; and AB term was further subdivided into electron-donor and electron-acceptor contributions. These divisions may be more accurately describing the contributions from the variation of surface chemistry to the surface energy term for the different materials.

It should be noted that PCA analysis was to find the correlations among the independent variables and to simplify the multi-dimensional correlation to 2- or 3-dimensional correlation. The PCA method used in this section could help group the surface parameters for correlation with the spore attachment data. As the spore attachment was greatly influenced by the epoxy glue in this study, the data obtained and the correlation results should be interpreted with caution. Nevertheless, the

statistical analysis gave a potential direction for the predictive model in the future. A new spore attachment study on the samples without using epoxy glue will be performed and should clarify the above concerns.

Conclusions

Sample analysis showed that the epoxy glue used for adhering the polymeric films onto the glass slides could leach out strong attractant (aromatic amide) to the *Ulva* spores. Therefore, the spore attachment data in this study should be interpreted with caution. New batch of polymeric films was prepared and the spore attachment test will be performed with future studies to eliminate the concerns about the leachant.

Observations showed that regardless of which material the patterns were made from, the majority of spores settled in the channels between the “diamonds” which were larger than the channels between the individual elements. The data would suggest that either G1650 or PS/G1650 would probably be the best of the more rigid materials from which to make a Sharklet patterned coating.

The principal component analysis (PCA method) showed that the two groups of surface parameters, one composed of n, r and f, and the other composed of E and γ, were important in interpreting the relationships among the surface parameters. Since the analyses were performed for the surface parameters, the grouping of the surface parameters provided potential direction for the correlation of the spore attachment and the surface properties in the future.

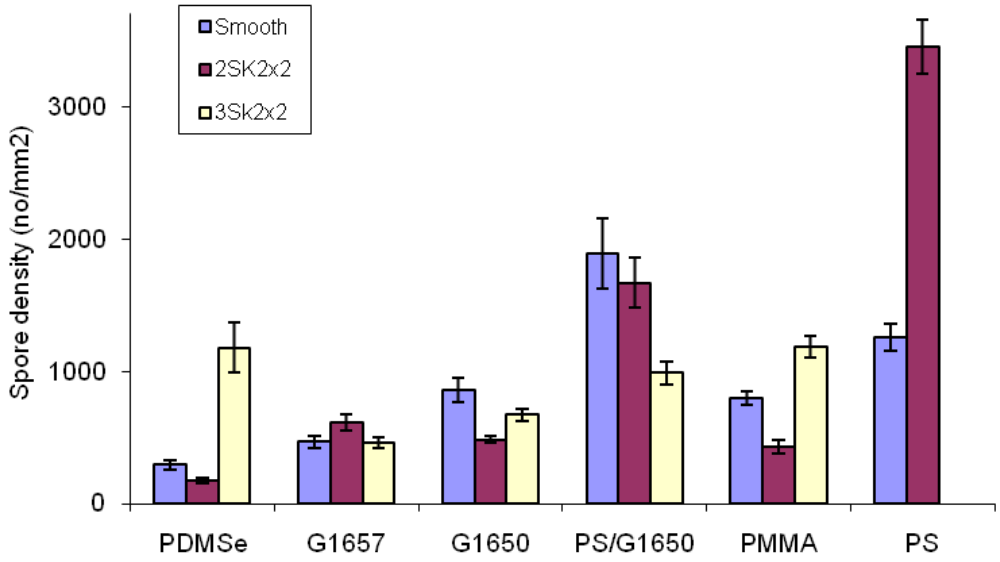

Figure 4-1. The attachment densities of *Ulva* spores on sharklet patterns. Each point is the mean from 90 counts on 3 replicate slides. Bars show 95% confidence limits.

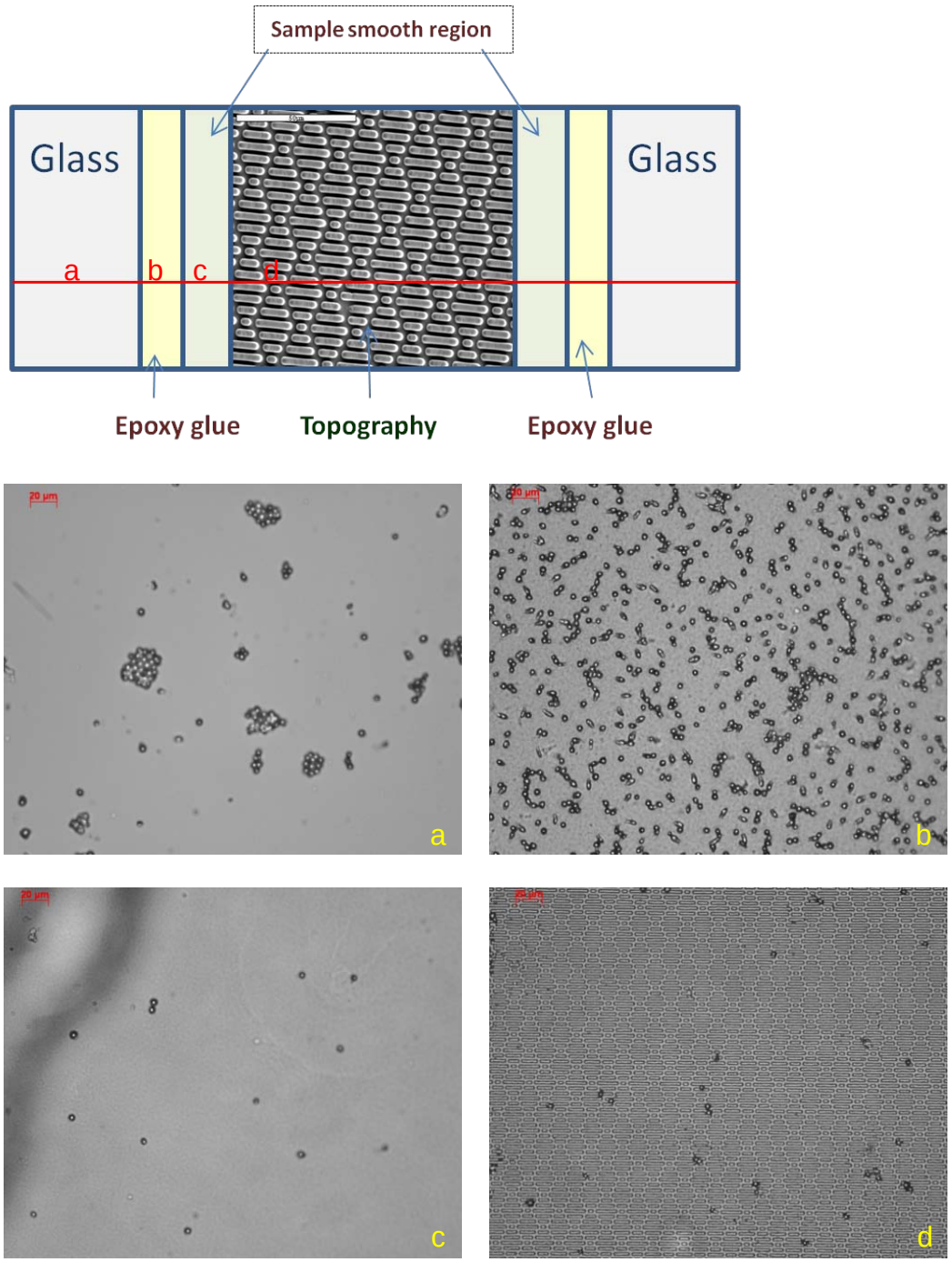

Figure 4-2. The schematic drawing of +2SK2x2 PS film attached to a glass slide. Microscopic images were taken from each region of the sample-attached glass slide: (a) glass region, (b) Araldite2012 epoxy region, (c) smooth polymer region, (d) topographical region. Scale bars were all equal to 20 µm.

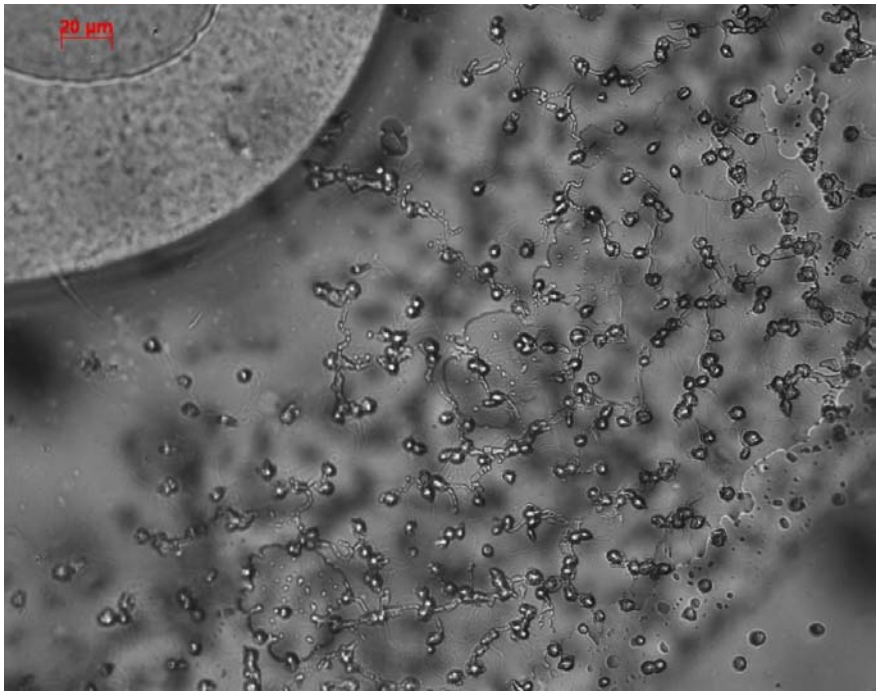

Figure 4-3. Spores can be observed in the cavity between the PS film and the underneath epoxy glue.

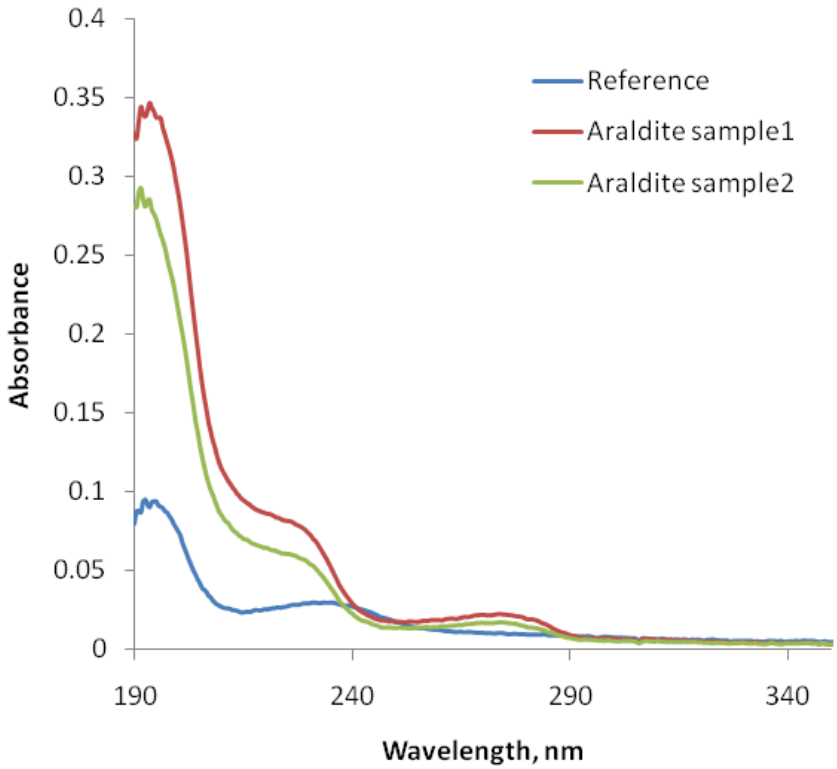

Figure 4-4. UV-Vis spectra of water extracts from Araldite layer and glass slide stored in D.I water in centrifuge tubes.

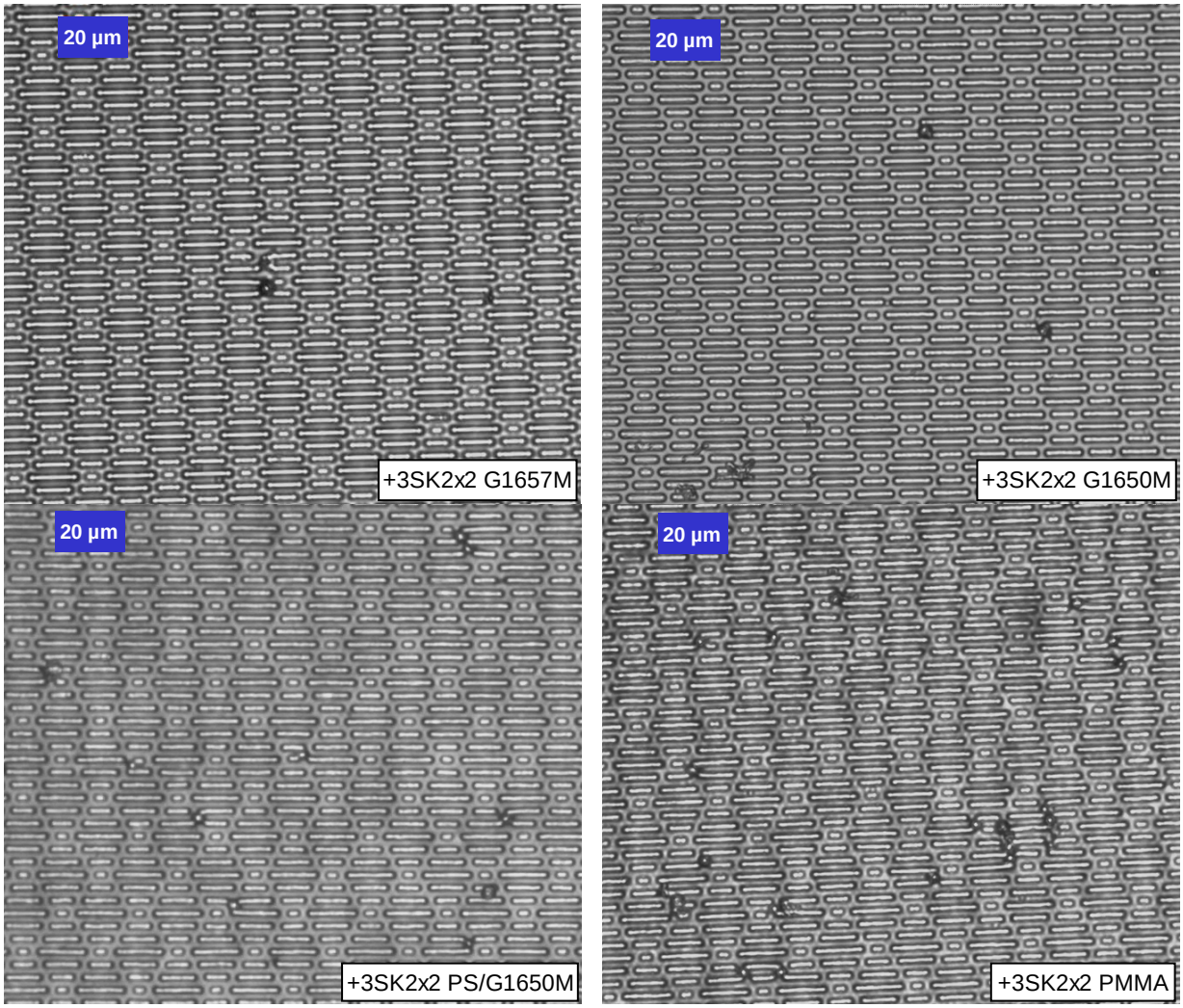

Figure 4-5. Some representative micro images of topographical features on various substrates.

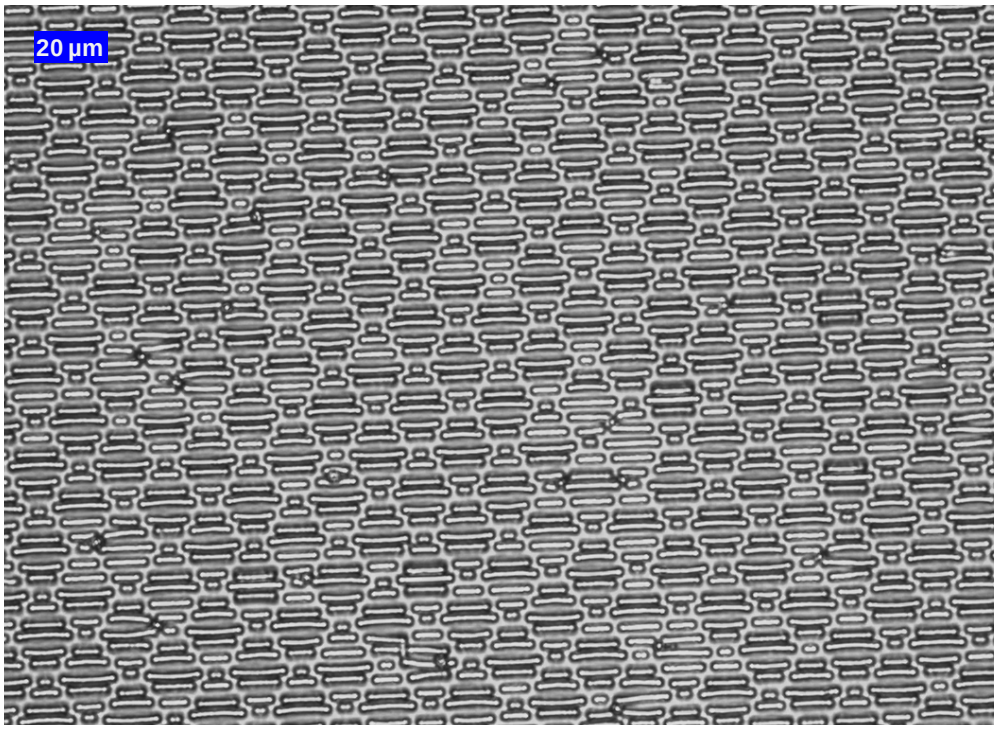

Figure 4-6. Micrograph of +3SK2x2 PDMSe surface after spore attachment assay. Flopped tops of the features were prevailing on the whole sample.

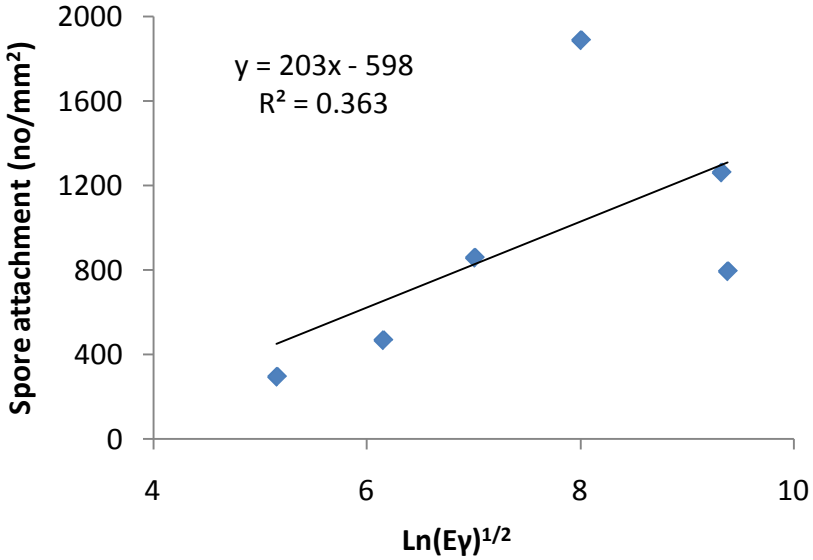

Figure 4-7. The attachment densities of *Ulva* spores on smooth surfaces vs. natural logarithm value of the square root of the product of elastic modulus and surface energy of the corresponding material. Each point is the mean from 90 counts on 3 replicate slides.

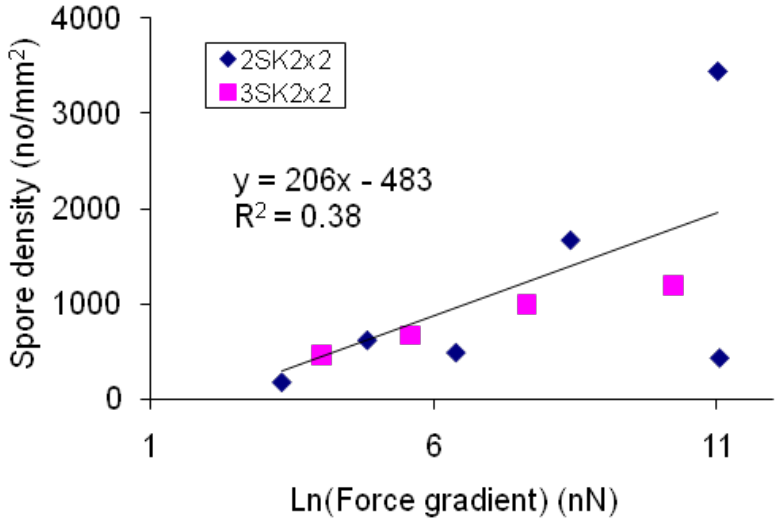

Figure 4-8. The attachment densities of *Ulva* spores on the Sharklet patterns plotted as a function of nanoforce gradient. Each point is the mean from 90 counts on 3 replicate slides.

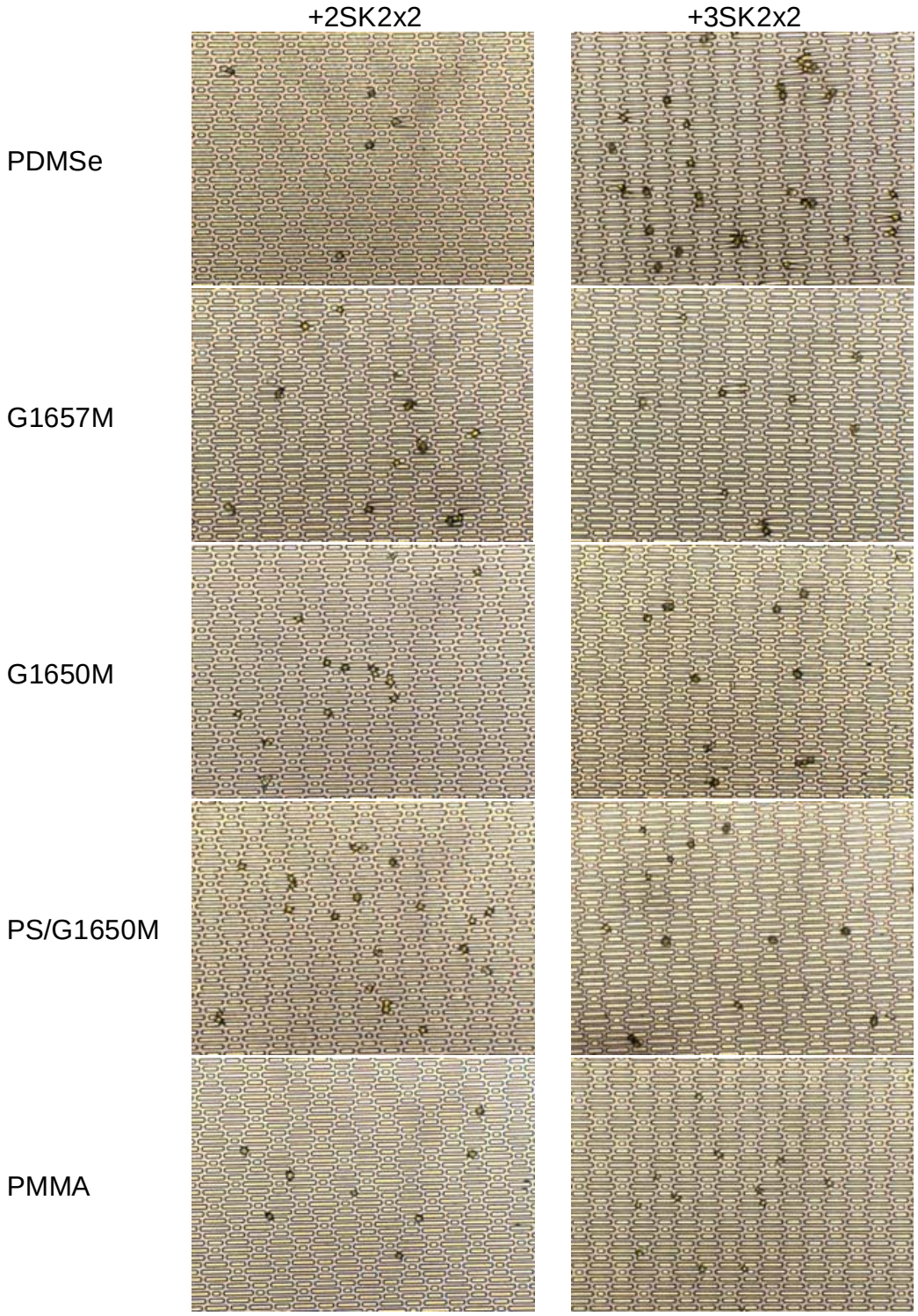

Figures 4-9. Images of spore settled on the Sharklet patterns (fixed sample). Image width approx.180 µm. Many of the spores choose to settle in the wider spaces that exist between the “diamonds units” of the pattern.

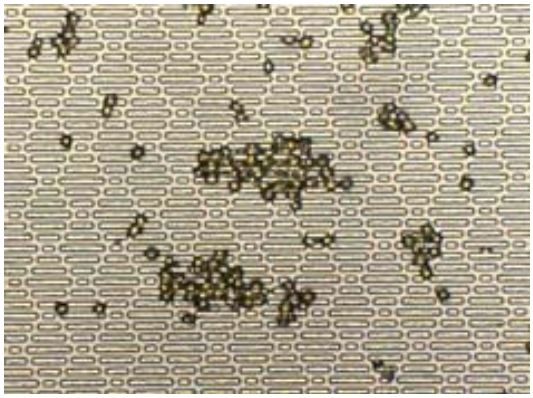

Figures 4-10. Image of spores settled on the +2SK2x2 PS patterns (fixed sample).

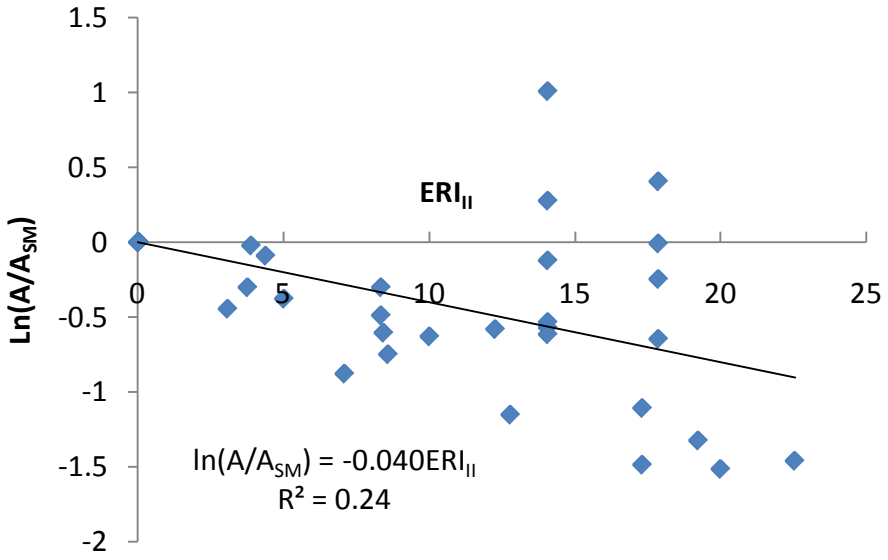

Figure 4-11. Correlation of the spore attachment density on the topographical relative to the smooth surface vs. ERI_{II}. The data sets used were from this study, Schumacher [19, 20], and Long [27].

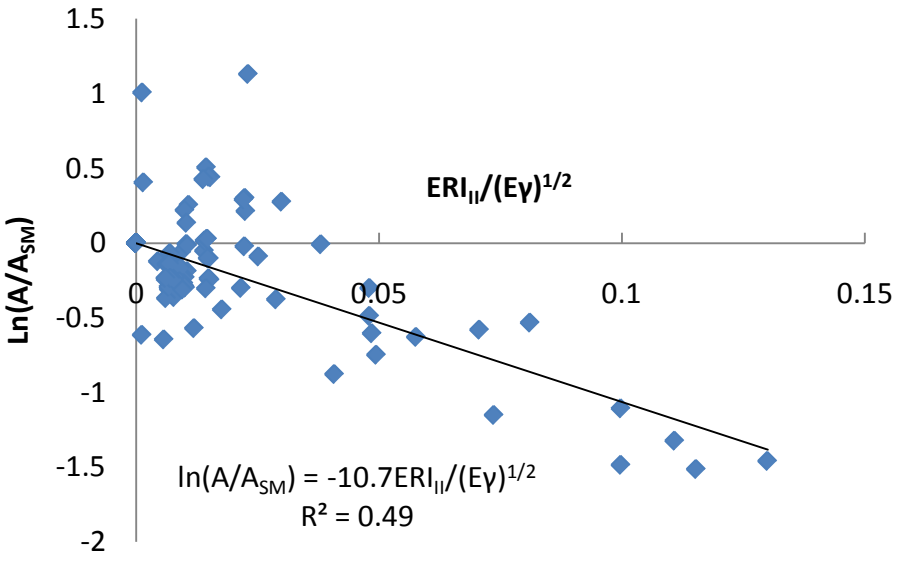

Figure 4-12. Correlation of the spore attachment density on the topographical relative to the smooth surface vs. ERI_{II} divided by the square root of ($E\gamma$). The spore attachment data were from this study and previous works of Wilson [173], Schumacher [19, 20], and Long [27]. Notice that in Wilson's work the spacings between the neighboring features were no less than 5 µm while all others the spacings were about 2 µm.

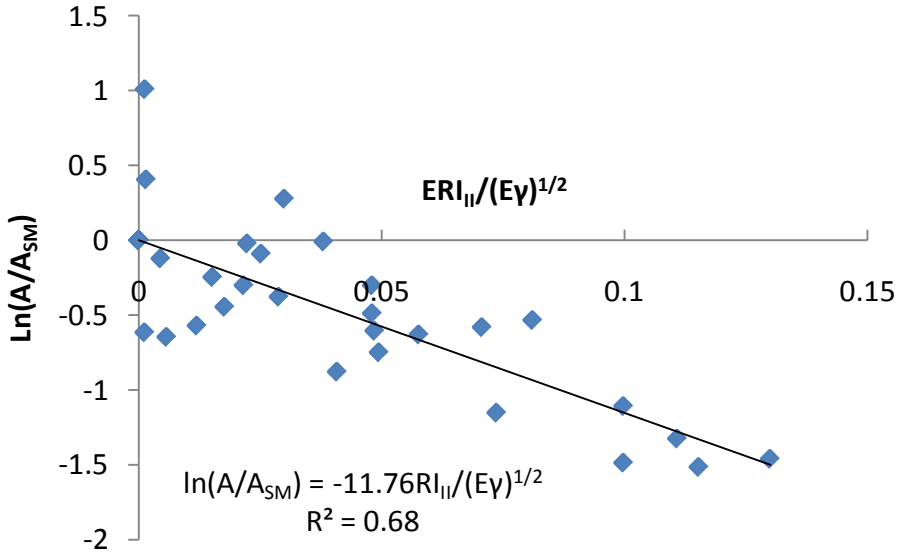

Figure 4-13. Correlation of the spore attachment density on the topographical relative to the smooth surface vs. ERI_{II} divided by the square root of ($E\gamma$). The spore attachment data were from this study and previous works of Schumacher [19, 20] and Long [27]. The spacings between the neighboring features were all about 2 µm, which was less than the diameter of the spore (~5 µm).

Table 4-1. Static contact angle measurement on various smooth surfaces with different probe liquid.

Material	Water (WT)	Diiodomethane (DM)	Ethylene glycol (EG)
PMMA	75.9 ± 1.2^o	36.0 ± 1.1^o	51.6 ± 0.8^o
G1657M	111.8 ± 0.8^o	54.2 ± 1.5^o	82.3 ± 1.2^o
G1650M	103.0 ± 3.1^o	42.1 ± 1.9^o	72.0 ± 1.8^o
PS/G1650M	108.6 ± 1.4^o	44.4 ± 1.2^o	68.6 ± 1.3^o

Table 4-2. The mechanical property and surface free energy of the selected materials.

Material	E, MPa	γ, mJ/m^2	
		Literature report	Measured
PDMSe	1.4 [175]	22 [176]	21.5 [48]
Kraton G1657M	6.3	-	35.0
Kraton G1650M	34	-	40.8
PS/G1650M blend	2.4×10^2	-	40.7
PMMA	3.3×10^3 [177]	41.2 [178]	42.4
PS	3.1×10^3	40.2 [178]	-

Table 4-3. Surface parameters in the current and previous spore attachment studies.

Material	Surface	*E, MPa*	γ, mJ/m^2	*a,* µm	*n*	*r*	*f*
PDMSe	SM	1.4	21.5	0	0	1	0
	+2SK2x2	1.4	21.5	2.0	4	2.05	0.417
G1657M	SM	6.3	35	0	0	1	0
	+2SK2x2	6.3	35	2.0	4	2.05	0.417
	+3SK2x2	6.3	35	1.9	4	2.51	0.438
G1650M	SM	34	40.8	0	0	1	0
	+2SK2x2	34	40.8	2.0	4	2.05	0.417
	+3SK2x2	34	40.8	1.9	4	2.51	0.438
PS/G1650M	SM	240	40.7	0	0	1	0
	+2SK2x2	240	40.7	2.0	4	2.05	0.417
	+3SK2x2	240	40.7	1.9	4	2.51	0.438
PMMA	SM	3300	42.4	0	0	1	0
	+2SK2x2	3300	42.4	2.0	4	2.05	0.417
	+3SK2x2	3300	42.4	1.9	4	2.51	0.438
PS	SM	3100	40.2	0	0	1	0
	+2SK2x2	3100	40.2	2.0	4	2.05	0.417
PDMSe	SM	1.4	21.5	0	0	1	0
(Schumacher)	triangle-pillar	1.4	21.5	2.0	2	2.23	0.37
	ridge	1.4	21.5	2.0	1	2.5	0.5
	pillar	1.4	21.5	2.0	1	2.36	0.23
	SK	1.4	21.5	2.0	4	2.51	0.42
	SM	1.4	21.5	0	0	1	0
	GR0	1.4	21.5	2.0	1	2.5	0.333
	GR1	1.4	21.5	2.0	2	2.78	0.444
	GR2	1.4	21.5	2.0	2	2.5	0.4
	GR3	1.4	21.5	2.0	2	2.5	0.417
	GR4	1.4	21.5	2.0	2	2.5	0.4
	GR5	1.4	21.5	2.0	1	2.5	0.428
	SK	1.4	21.5	2.0	4	2.51	0.42
PDMSe	SM	1.4	21.5	0	0	1	0
(Long)	SK(+1.8)	1.4	21.5	2.0	4	1.9	0.38
	SK(-2.0)	1.4	21.5	2.0	4	2	0.6
	SM	1.4	21.5	0	0	1	0
	SK(2.7)	1.4	21.5	2.0	1	2.4	0.38
	SK(2.7)	1.4	21.5	2.0	2	2.4	0.43
	SK(2.6)	1.4	21.5	2,0	3	2.3	0.46
	SK(2.9)	1.4	21.5	2.0	4	2.5	0.48
	SK(2.6)	1.4	21.5	2.0	5	2.3	0.49

Table 4-3. Continued

Material	Surface	*E, MPa*	γ, mJ/m^2	a, µm	n	r	f
PDMSe	sm	1.4	21.5	0	0	1	0
(untreated)	channel(5x5)	1.4	21.5	5	1	2	0.5
(Wilson)	channel(5x10)	1.4	21.5	10	1	1.67	0.333
	channel(5x20)	1.4	21.5	20	1	1.5	0.2
	pillar (5x5)	1.4	21.5	5	1	2	0.25
	pillar (5x10)	1.4	21.5	10	1	1.44	0.111
	pillar (5x20)	1.4	21.5	20	1	1.16	0.04
	channel (1.5x5)	1.4	21.5	5	1	1.3	0.5
	channel (1.5x10)	1.4	21.5	10	1	1.2	0.333
	channel (1.5x20)	1.4	21.5	20	1	1.12	0.2
	pillar (1.5x5)	1.4	21.5	5	1	1.3	0.25
	pillar (1.5x10)	1.4	21.5	10	1	1.13	0.111
	pillar (1.5x20)	1.4	21.5	20	1	1.05	0.04
(Si-oil 50 cst,	sm	1.4	22.8	0	0	1	0
5%)	channel(5x5)	1.4	22.8	5	1	2	0.5
	channel(5x10)	1.4	22.8	10	1	1.67	0.333
	channel(5x20)	1.4	22.8	20	1	1.5	0.2
	pillar (5x5)	1.4	22.8	5	1	2	0.25
	pillar (5x10)	1.4	22.8	10	1	1.44	0.111
	pillar (5x20)	1.4	22.8	20	1	1.16	0.04
	channel (1.5x5)	1.4	22.8	5	1	1.3	0.5
	channel (1.5x10)	1.4	22.8	10	1	1.2	0.333
	channel (1.5x20)	1.4	22.8	20	1	1.12	0.2
	pillar (1.5x5)	1.4	22.8	5	1	1.3	0.25
	pillar (1.5x10)	1.4	22.8	10	1	1.13	0.111
	pillar (1.5x20)	1.4	22.8	20	1	1.05	0.04
(Si-oil 50 cst,	sm	1.4	22.5	0	0	1	0
20%)	channel(5x5)	1.4	22.5	5	1	2	0.5
	channel(5x10)	1.4	22.5	10	1	1.67	0.333
	channel(5x20)	1.4	22.5	20	1	1.5	0.2
	pillar (5x5)	1.4	22.5	5	1	2	0.25
	pillar (5x10)	1.4	22.5	10	1	1.44	0.111
	pillar (5x20)	1.4	22.5	20	1	1.16	0.04
	channel (1.5x5)	1.4	22.5	5	1	1.3	0.5
	channel (1.5x10)	1.4	22.5	10	1	1.2	0.333
	channel (1.5x20)	1.4	22.5	20	1	1.12	0.2
	pillar (1.5x5)	1.4	22.5	5	1	1.3	0.25
	pillar (1.5x10)	1.4	22.5	10	1	1.13	0.111
	pillar (1.5x20)	1.4	22.5	20	1	1.05	0.04

Table 4-3. Continued

Material	Surface	*E, MPa*	γ, mJ/m^2	a, µm	n	r	f
(Si-oil 5000	Sm	1.4	23.3	0	0	1	0
cst, 5%)	channel(5x5)	1.4	23.3	5	1	2	0.50
	channel(5x10)	1.4	23.3	10	1	1.67	0.33
	channel(5x20)	1.4	23.3	20	1	1.5	0.20
	pillar (5x5)	1.4	23.3	5	1	2	0.25
	pillar (5x10)	1.4	23.3	10	1	1.44	0.11
	pillar (5x20)	1.4	23.3	20	1	1.16	0.040
	channel (1.5x5)	1.4	23.3	5	1	1.3	0.50
	channel (1.5x10)	1.4	23.3	10	1	1.2	0.33
	channel (1.5x20)	1.4	23.3	20	1	1.12	0.20
	pillar (1.5x5)	1.4	23.3	5	1	1.3	0.25
	pillar (1.5x10)	1.4	23.3	10	1	1.13	0.11
	pillar (1.5x20)	1.4	23.3	20	1	1.05	0.040

Table 4-4. Loadings for the two components generated from principal component analysis using the variables from the five variables data set (Table 4-3).

Surface parameter	Component 1	Component 2
Elastic modulus (E)	0.212	**-0.633**
Surface free energy (γ)	0.269	**-0.619**
Spacing between the adjacent features (a)	-0.340	0.145
Number of discrete features (n)	**0.511**	0.090
Wenzel roughness factor (r)	**0.520**	0.272
Area fraction of solid in contact with liquid (f)	**0.485**	0.336
Percent of total variance explained	45.4%	27.5%

CHAPTER 5
BIOFILM INHIBITION ON SURFACE MICROENGINEERED POLYMERIC FILMS

Introduction

Invasive medical devices from catheters to artificial heart valves are being increasingly employed to improve health and life quality. However, inserted or implanted medical devices have a substantial risk of infections. Deaths due to hospital-acquired infections was estimated to be about 100,000 cases in the US alone in the year 2002 [179]. *Staphylococcus aureus* (*S. aureus*), a common bacterium that exists on the skin and in the nose, is among the major sources of healthcare associated infections [180]. Although treated with various antibiotic agents, *S .aureus* is evolving to be resistant to many of them. Now more than 63% of the isolated strains from hospitalized patients are methicillin-resistant *S. aureus* (MRSA) [181].

Bacterial biofilms are often responsible for the chronic infections among patients [182]. To avoid bacterial adhesion to biomedical devices, two basic strategies have been proposed and used for biomaterials: bioadhesion-free coatings, and incorporated antimicrobial agents [99]. As the effectiveness of the antibiotic treatment is increasingly challenged by MRSA, alternative methods are needed which take advantage of the surface characteristics on the inhibition of biofilm formation.

A biomimetic surface microtopographical design, Sharklet AF^{TM} (Figure 5-1), has been shown to be effective against the settlement of various marine species [17-19]. Recent work showed qualitatively that this pattern could delay the formation of a *S. aureus* biofilm [21]. The quantitative characterization of biofilm is difficult and still under intensive investigation. Recently, new dyes were found to distinguish the matrix and the

bacterial cells buried in it [183]. Still, quantifying the cell counts in an aged biofilm is difficult.

One objective of this work was to test the hypothesis that the surface micro-engineered topographical features alone can inhibit the formation of the bacterial biofilms. To test this we fabricated micro-engineered polymer films (all in Sharklet pattern) with systematically varied mechanical and energetic properties, and the micro-engineered surfaces were challenged with *S. aureus* inocula for 7 days. Another objective of this study was to explore possible mechanism for the inhibition of the biofilm formation on the micro-engineered surfaces. Therefore new clinical treatment strategies for medical device associated infections could be inferred from this work. The 7-day cultured polymer samples were challenged with a high dose of antibiotic culture medium for extended period of times, and the bioactivity of the bacterial microcolonies was examined with a relatively simple and accurate means called BioTimer assay. The microbial colonies/biofilms formed on the surfaces of these polymeric samples were evaluated by the BioTimer method reported by Pantanella *et al.* [184]. This method takes advantage of the metabolic process of *Staphylococcus*: the bacteria can fully digest glucose in the culture medium, converting it to CO_2 and water in the presence of air. The dissolved CO_2 will gradually lower the pH of the culture medium in an enclosed culture well and thus a pH-sensitive reagent serves as an indicator for the level of metabolic activity of the bacteria. The time required for the pH sensitive color switch of the culture medium can be correlated to the initial bacterial concentration. The bioactivity in terms of metabolic behavior was statistically analyzed between microcolonies formed on the control (smooth surface) and the Sharklet textured surface.

Materials and Methods

Materials

Poly(methyl methacrylate) (PMMA, MW 350 kg/mole) was purchased from Sigma-Aldrich (St Louis, MO). Styrene-ethylene-butyldiene-styrene (SEBS) triblock copolymers, Kraton G1657M (styrene block mass percentage 10%) and Kraton G1650M (styrene block mass percentage 30%), were purchased from Kraton (Houston, TX). Polystyrene (PS, MW 30 kg/mole) was purchased from Polysciences (Warrington, PA). 3-(aminopropyl triethoxysilane) (APTES), and monoglycidyl ether terminated polydimethylsiloxane (PDMS, M_n 5000 g/mole, abbreviated as PDMS-5K) were purchased from Sigma-Aldrich (St. Louis, MO). Anhydrous ethanol, 1-propanol, 2-propanol, hydrogen peroxide (30 wt%), and concentrated sulfuric acid (95%) were purchased from Fisher Scientific (Pittsburgh, PA). All chemicals were used without further purification. Nanopure water (>17.8 MΩ·cm) was prepared in the lab with Barnstead Nanopure Diamond ^{TM} lab water system from Millipore (Billerica, MA).

Tryptic soy broth (TSB) and Mueller Hinton broth (MH) were purchased from BD Biosciences (Franklin Lakes, NJ), and D-(+)-glucose and phenol red were obtained from Sigma-Aldrich (St Louis, MO). Cetylpyridinium chloride (CPC) was purchased from Acros (Thermal Fisher Scientific, Rockford, IL). These materials for the bioassays were used as received.

Fabrication of Microengineered Polymeric Films

The thermoplastic polymeric films were prepared by a solution-casting method. The polymer toluene solution (0.15 g polymer dissolved in 1 ml toluene) was cast onto a smooth or a pre-patterned silicon wafer. The pattern was transferred to a silicon wafer via a photolithographic technique [19, 21]. To lift the polymer films from the wafer, an

antisticking layer (short-chain polydimethylsiloxane, or PDMS-5K) was grafted onto the Si wafer in a three-step manner: (1) a silicon (Si) wafer was immersed in a freshly mixed concentrated sulfuric acid (H_2SO_4) and hydrogen peroxide (H_2O_2) water solution (30 wt%) (1:1 volume ratio) [148] for 30 min to generate surface hydroxyl groups; (2) after thorough rinsing with nanopure water, the Si wafer was dried with nitrogen flow and neat APTES was dropwise added to cover the whole surface for 10 min; (3) after rinsing with anhydrous ethanol, the APTES treated Si wafer was covered by neat PDMS-5K and heated in an oven at 80 ^{o}C for 4 hr. The wafer was then rinsed with 2-propanol. The PDMS-5K treated Si wafer was dried with an Ar flow [149]. Enough polymer solution was placed on the wafer dropwise to cover the smooth or patterned area of the wafer. After slow removal of the solvent, polymer films with the desired thickness of about 150 µm were obtained. Polydimethylsiloxane elastomer (PDMSe) was used as a reference material as described previously by Chung *et al.* [21]. Silastic T2^{TM} (from Dow Corning Corp., Midland, MI) base material and curing agent were mixed at a 10:1 mass ratio and cast against the silicon wafer described above. After curing at room temperature for one day, the resulting PDMSe films were easily lifted from the silicon wafers.

The resultant topographies contain feature elements with a width of 2.1 µm, a distance (between the neighboring elements) of 1.9 µm, and a height of approximately 3.0 µm. The short name of this pattern was +3SK2x2 (for 3 µm height). Pattern fidelity was evaluated with light and scanning electron microscopy (SEM). The pattern is shown in Figure 5-1.

The surface free energy of each Kraton samples was determined by a two-liquid method [167]. Nanopure water (with resistivity higher than 18.0 MΩ·cm) and methylene iodide were used as test liquid.

Sample Preparation

All of the smooth and patterned polymeric films were cut into approximately 3x3 cm^2 squares and placed in 8-cm Petri dishes as shown in Figure 5-2.

For the biofilm formation assays involving only the PDMSe samples, the samples were adhered to the Petri dishes with the help of a 70% ethanol/water solution. After removing the ethanol/water solution in a biological hood, the PDMSe samples were attached to the Petri dishes. Standard ethylene oxide gas sterilization was employed.

For the biofilm formation assays performed on various materials (PDMSe, SEBS, PS/SEBS blend, and PMMA), the polymeric films were secured to the Petri dishes with a petroleum-based grease Lubriseal® (Thomas Scientific, Swedesboro, NJ). The samples were then sterilized in a dessicator with a mixture of commercial bleach and dry acetic acid (1:2 volume ratio) at room temperature for 30 min. A Petri dish with a layer of the grease was also sterilized and served as a positive control. This sealant was found not to be non-toxic to *S. aureus*.

Biofilm Formation Assay

S. aureus (ATCC 35556) was subcultured in a tryptic soy broth (TSB) growth medium and grown at 37 °C overnight with shaking. Optical absorbance measurements were correlated with the colony forming units (CFUs) to obtain the bacteria growth curve. The bacterial concentration was determined by spectrophotometry by interpolating CFUs per milliliter from the linear optical density-CFUs regression. The samples were statically immersed in a 10^7 CFUs/ml bacterial suspension and kept in a

5% CO_2 incubator for 7 days. The dishes were daily put on a rocker for 1 min at 40 rpm and the medium was then replaced to allow for continued bacterial growth. When the 7-day culture is completed, the dishes were rinsed three times by a 20 ml Tween 80 (5 ppm)-PBS (phosphate buffered saline) solution, followed by three rinses with 20-ml sterilized, distilled water each time.

After thorough rinsing of the samples, an antibiotic agent oxacillin was used to treat the samples which had been cultured with *S. aureus* for 7 days. Oxacillin was dissolved in a sterilized TSB medium at a concentration of 1 g/l. This concentration is considerably higher than the minimum inhibitory concentration (MIC) for *S. aureus*, to kill any bacterial cells that are not well protected by their extracellular polymeric substance (EPS). The three Petri dishes were handled in the following manner: (1) a randomly picked Petri dish was not treated with the antibiotic medium, and the samples were punched for the BioTimer assay described in the next section; (2) 20 ml of the antibiotic medium was placed into the remaining two Petri dishes; the two dishes were put into the CO_2 (5%) incubator, cultured for 12 hr and 24 hr, respectively; then the samples were rinsed with sterilized water three times after culturing and were then ready for the BioTimer assay.

Except for the BioTimer assay, the samples were fixed with 10 mM CPC water solution and two disks punched out from each samples were thoroughly scanned under SEM. Typical images were recorded for each punch-outs.

BioTimer Assay

The BioTimer medium (BTM) was prepared according to the following recipe [185]: Mueller Hinton broth (21 g), glucose (10 g), and phenol red (25 mg) were dissolved in

1000 ml distilled water. The medium was sterilized at 121 °C for 15 min. The pH value was the determined to be 7.1, and the final medium was red and transparent.

A calibration curve can be obtained by correlating the initial concentration of the bacteria with the time required for the pH sensitive color switch of the BTM. A volume of 0.1 ml of *S. aureus*/TSB overnight cultures was injected into 0.9 ml BTA in a 48-well plate. Then serial ten-fold dilutions in a 0.9 ml BTM were performed. A volume of 220 µl of the mixed culture medium was drawn from each of the wells and the plate counting (for CFUs) was performed immediately. The 48-well plate, which had 680 µl of *S. aureus*-BTM remaining in each well, was put into an incubator at 37 ^{o}C. The color of the inoculated BioTimer assay was checked at regular time intervals. For each dilution, the time required for the color switch of the BTM was recorded and plotted versus the $\log_{10}$ of CFUs.

Statistical Methods

The mean number of cell counts on each of four punched coupuns +/- standard deviation was reported. Statistical differences between surfaces were evaluated using a nested analysis of variance (ANOVA) followed by the Tukey test for multiple comparisons [186]. Minitab (version 15, Minitab Inc, State College, PA) was used for this purpose.

Results

Characterization of Bacterial Colonies on the PDMSe Samples

The calibration curve for the planktonic CFUs counts and time used for color switch shows (Figure 5-3) a good correlation (R^2 ~0.97). The time required for the medium to switch color was correlated to the initial bacterial concentration (in CFUs/ml). A smaller color switch time corresponds to a higher initial concentration of planktonic

bacterial cells (in CFUs). The calibration curve was used to estimate the planktonic-equivalent CFUs counts for the bacteria attached to or colonized on the surfaces of the polymer samples after a 7-day culture. As all culture media were prepared specifically for a series of experiments, the BioTimer calibration was also performed each time to account for the slight variation in the amount of the phenol red used in the BioTimer medium.

The BioTimer assay results for the antibiotic treatment are shown in Figure 5-4. The results showed that without the antibiotic treatment, the time for a color switch (red to yellow) was longer on smooth samples than on the Sharklet pattern on the PDMSe material. The difference was statistically significant ($P<0.05$). This observation means that there were more metabolically active *S. aureus* cells on the Sharklet textured surface than on the smooth surface. A further examination by SEM imaging showed that multi-layered colonies were observed all over the smooth PDMSe surfaces (Figure 5-5 (A) and (B)). However, on the surfaces of the Sharklet pattern, only single-layer to three-layer small colonies dwelling in between the protruding features were prominent (Figure 5-6 (A) and (B)). In some regions of the Sharklet surfaces, there were small multi-layered colonies observed (Figure 5-6 (C)), which were usually smaller in size than those on the smooth surfaces and covered less than 5% of the whole punched disk (8-mm diameter) by a rough estimation.

After the 12 hr antibiotic treatment, the concentration of the active bacteria on the Sharklet surface dropped more than that on the smooth surface. Compared with the untreated samples, the planktonic-equivalent CFUs counts on the Sharklet surface showed about a two-log reduction, while less than a one-log reduction occurred on the

smooth surface. Furthermore, after the antibiotic treatment, the planktonic-equivalent CFUs counts on the Sharklet surface were significantly less than those on smooth surface (72% reduction, $p<0.01$) as determined by the BioTimer assay.

After a 24 hr antibiotic treatment, the BioTimer assay gave the same planktonic-equivalent CFUs count estimates for smooth and Sharklet surfaces (~2,000 CFUs/ml). The SEM imaging (Figure 5- 6) shows that although there were not many continuous bacterial colonies formed on the Sharklet pattern, some material covered the spacing between adjacent features. This material may come from the deposition of the culture medium or the secreted/metabolic products from the bacterial cells dwelling in the space between features. Therefore, the PDMSe feature, together with the thick organic capsule material, may have protected some of the bacterial cells on the surface of Sharklet pattern.

Bacterial Biofilm Formation on Various Substrates

As shown in Table 5-1, a series of polymeric substrates with systematically varied mechanical properties and surface energies were selected to determine the characteristics of biofilm formation on the smooth and Sharklet-patterned surfaces. The BioTimer assay results for the smooth and Sharklet surfaces (Figure 5-7) showed that it took less time for the BTM to change color on the Sharklet samples than on the smooth samples for the same material ($P<0.05$), except for Kraton G1650M surfaces where they were statistically not distinguishable. Thus the numbers of metabolically active bacteria on the surface of the Sharklet textured surface are more than those on the corresponding smooth surfaces. Tukey test was performed for the group of the smooth samples and the Sharklet textured samples. For the color switch time, there was no difference among the smooth surfaces and among the Sharklet textured surfaces.

Typical images obtained from SEM imaging (Figure 5-8) showed the opposite trend compared with the BioTimer assay results. Biofilms were observed on the smooth surfaces (except G1657M), while there were no biofilms observed on the Sharklet patterns. As the secreted materials from the biofilm covered the bacterial cells and the bioactivity of the biofilms cells is less than the planktonic cells, finding the opposite result from the BioTimer assay is understandable.

Discussion

Development of Bacterial Microcolonies on the Surfaces

The metabolic activities are different for the bacterial cells buried in the microcolonies. The work on *Escherichia coli* (*E. coli*) and *Pseudomonas putida* (*P. putida*) by Sternberg *et al*. [187] demonstrated that the metabolic activity of bacterial cells in the centers of the largest biofilm microcolonies is less than that of the cells at the outer layers. While investigating the metabolic activity in the biofilms of *Staphylococcus epidermidis* (*S. epidermidis*) and *S. aureus*, the Stewart group [188] found a depth-dependence within the biofilm microcolonies; they categorized the physiological states of the bacterial cells into at least four groups: aerobically growing, fermentatively growing, dormant and dead. Since they found about 10% of the total population was dead cells in the report [188] and the dead cells are considered a constituent of the biofilm, we decided to analyze two types of cells in the microcolonies on a surface: bioactive and dormant cells after a 7-day culture. After antibiotic challenge, we considered dead cells also.

Based on the SEM imaging and BioTimer assay results on the smooth and Sharklet patterned PDMSe surfaces, one possible scheme was proposed to illustrate the time-dependent development of bacterial microcolonies on the two surfaces, see

Figure 5-9. On both the smooth and Sharklet patterned surfaces, planktonic cells attach on the surface and begin to secret EPS to enclose themselves (Figure 5-9. both images (A) and (B), steps (a) and (b)), followed by the increase of the microcolonies and the beginning of differentiation of cell phenotype (Figure 5-9 both images (A) and (B), step (c)). With time, the microcolonies on the smooth surface increase in size without any limitation (Figure 5-9 (A), step (d)), therefore the quorum sensing (QS) system is triggered and the cells/cell clusters are then dispersed into the culture medium (Figure 5-9 (A), step (e)). This is in agreement with the work by Yarwood *et al*. [189]. However, on the Sharklet surface, the microcolonies are separated by the micro-sized features (Figure 5-9 (B), step (c)). Physically, the microcolonies are disrupted. To develop larger microcolonies, bacterial cells need to either grow from the microcolonies or deposit from the culture medium to fill the spacings between the protruding features. This becomes a rate limiting step. By the time mature biofilms are dominant on the smooth substrate, there are only a few continuous microcolonies distributed in a few regions on the Sharklet patterned surface (Figure 5-9 (B), step (d)). Since the culture medium is changed every day, the entire process occurs all the time. Therefore, we can observe all forms of cell aggregates: from individual cells to microcolonies on the Sharklet surface, and from individual cells to mature biofilms on the smooth surface (as shown in Figure 5-10 (A) after 7-day TSB culture).

From one report [188], in a thick *S. aureus* biofilm, which was cultured in a capillary tube under continuous flow of culture medium with access to air, the bioactive cell layer marked by an active expression of green fluorescent proteins showed an average ~40 µm thickness out of the total ~170 µm thick biofilm. Oxygen concentration

was determined to reach as deep as ~50 μm in the 2-day old biofilm in the report [188]. In another work [190], cells become more densely packed in a *S. aureus* biofilm as it aged in a 2-day culture. In our study, the inoculated samples were kept in a 5% CO_2 atmosphere in an incubator. The large and densely packed biofilms could be observed everywhere on the smooth PDMSe surface. However, on the Sharklet textured surface, the prominent colony patterns are the discontinuous, several-layered (commonly less than 3 layers as compared by the 3-μm feature height) microcolonies. With aging, the biofilm cells seemed to be less bioactive and in a dormant or dead state [189]. Therefore we speculate (supported from the BioTimer assay results) that most of the cells dwelling on the Sharklet textured surface are exposed to the culture medium and in a bioactive state. This indicates (as was observed) the time required for the color switch for the BioTimer assay would be less for the Sharklet textured surface than that for the smooth samples.

Many antibiotic agents showed penetration and killing to some degree on the cells in the form of biofilms for *S. epidermidis* [191, 192] and *S. aureus* [190, 193]. Fux *et al.* [194] examined the oxacillin resistance of the detached aggregates from *S. aureus* biofilms formed in a flow mode. They found that large clumps were far more resistant to oxacillin challenge compared with the mechanically dispersed clusters detached from the same biofilms [194]. Therefore, oxacillin treatment is expected to kill more cells in small microcolonies on a surface than large ones. After 12-hr of oxacillin treatment, it is postulated that most cells in small clusters separated by the protruding features on the Sharklet surface are killed (although some dormant cells residing in the center of the microcolonies were protected). Similarly, the EPS protected the cells in the inner portion

of the microcolonies and mature biofilms on the smooth surface. Upon removal of the antibiotic medium and submerging into the BTM, the cells in the center regions become nuclei of regrowth (Figure 5-10 (B)). As there may be more large microcolonies on the smooth surface than on the Sharklet as shown from SEM imaging, the BioTimer assay results show a longer time required for the color switch for the Sharklet samples than the smooth ones.

When treated by 1000 µg/ml oxacillin for 24 hr, most cells on the surfaces are killed, with less than 1% of the total population on both the smooth and the Sharklet textured surfaces surviving. In a recent review, Lewis [195] summarized works on persister bacterial cells, which are described not as antibiotic-resistant mutants, but tolerant to antibiotics by maintaining a dormant and non-dividing state. Upon removal of the antibiotic treatment, the persister cells can revive in a non-toxic culture medium and will still be killed by antibiotics. Singh *et al.* [196] provided direct evidence that persister cells exist among *S. aureus* cells in both planktonic and biofilm forms. It is postulated that the persister cells that are protected by the thick EPS in the microcolonies on the smooth and Sharklet textured surfaces survive the harsh treatment. This hypothesis could explain why it takes a long time for the dormant cells to regrow in the fresh BTM after 24-hr antibiotic treatment, and why the CFUs counts are not statistically different for the two types of surfaces.

Surface Properties on the Development of Bacterial Microcolonies

The influence of surface properties on the adhesion of bacterial species has been investigated extensively. In a recent paper, Lichter *et al.* [110] reported the positive correlation of surface stiffness on the adhesion of various bacterial species. Surface

chemical composition and surface charge [124, 126, 197] also play important roles in the inhibition of adhesion and development of bacterial cells on surfaces.

In our study, five materials with systematically varied mechanical and energetic properties were tested. For the smooth surfaces, the SEM images show differences in the morphologies of the bacterial microcolonies/biofilms (Figure 5-7), which might suggest that there is an effect on the development of microcolonies from the mechanical and/or nano-sized topographical properties of the substrata. The BioTimer assay results, however, do not show a statistical difference in the CFUs counts for the smooth samples. This can be interpreted to mean that the numbers of the active cells on the surfaces are statistically the same. For the Sharklet patterned surfaces, the SEM images show that most microcolonies are found between the features. Thus the physical obstacles appear to play the major role in separating the clusters of the bacterial cells in the case of Sharklet patterned surfaces. This observation provides the basis for proposing that the application of the microengineered surface features disrupt the formation of bacterial biofilms. In contact with culture medium, all the surfaces can be conditioned with organic matter, therefore disguising the chemical/energetic cues of the substrate[8].

Based on the results and the above discussion, it appears that *S. aureus* cells tend to form thin-layered, discontinuous microcolonies on the Sharklet textured surface in a 7-day *in vitro* culture. About 98% of the bioactive cells dwelling on the Sharklet textured surface can be killed by the antibiotic agent oxacillin in a 12-hr treatment. This t gives a new possible treatment method for biofilm associated infections, i.e., the physical disruption of the microcolonies combined with antimicrobial treatment.

Conclusion

The experimental protocol for a biofilm formation assay with *S. aureus* as test bacterium was established. Based on the BioTimer assay results, there was no difference in the colony forming units attached to the smooth polymer films with varied mechanical and energetic properties, and the same results held for the Sharklet AF™ patterns. However, the BioTimer assay results showed that there were more metabolic activity from the bacteria formed on the Sharklet patterns than on the smooth surfaces. SEM imaging showed that biofilms were formed on the smooth surfaces while no or little biofilm formed on the Sharklet AF™ patterns. After a high-dose antibiotic treatment for 12 hr, the measured metabolic rate from the Sharklet surfaces was less than that from the smooth surfaces. In terms of planktonic equivalent CFUs, there was about a 2-log reduction of the population of bioactive cells on the Sharklet textured surface while less than a 1-log reduction of bacterial population was achieved on the smooth surface, as determined by the BioTimer assay. Therefore the physical obstruction of the micro-sized features on the surface may inhibit the development of microcolonies. The bacterial cells attached to the Sharklet textured surface may mostly keep their bioactive state and may be easy to kill with antibiotics due to less protection from thick cell layers and EPS, compared with the large biofilms formed on the smooth surface. New treatment strategies for the medical devices can be inferred from this work, i.e. the combination of micro-textured surfaces with antibiotic treatment, taking advantage of the inhibition of biofilm formation and easily killed bioactive cells on the microengineered surfaces.

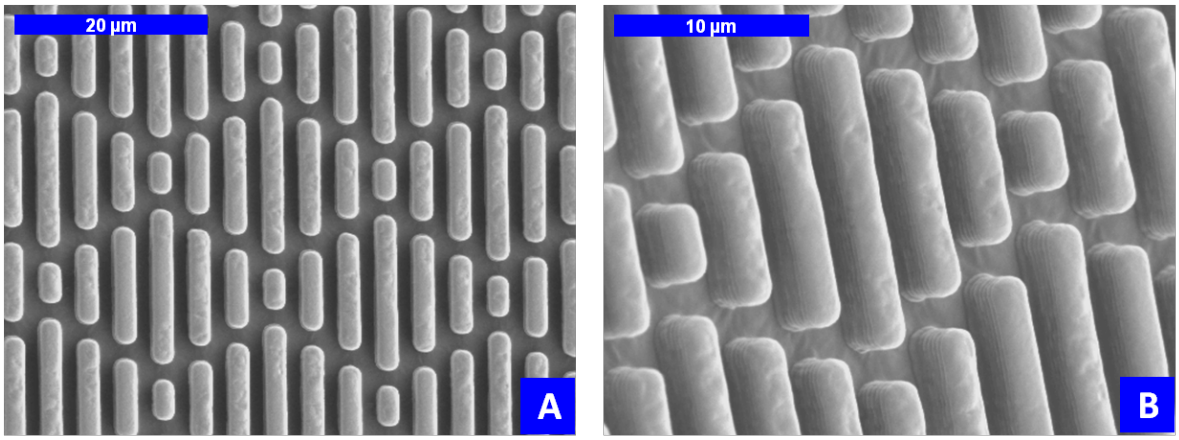

Figure 5-1. SEM images of Kraton G1650M with +3SK2x2 pattern: (A) top-down view, (B) 40^{o} tilted view to show the protruding features.

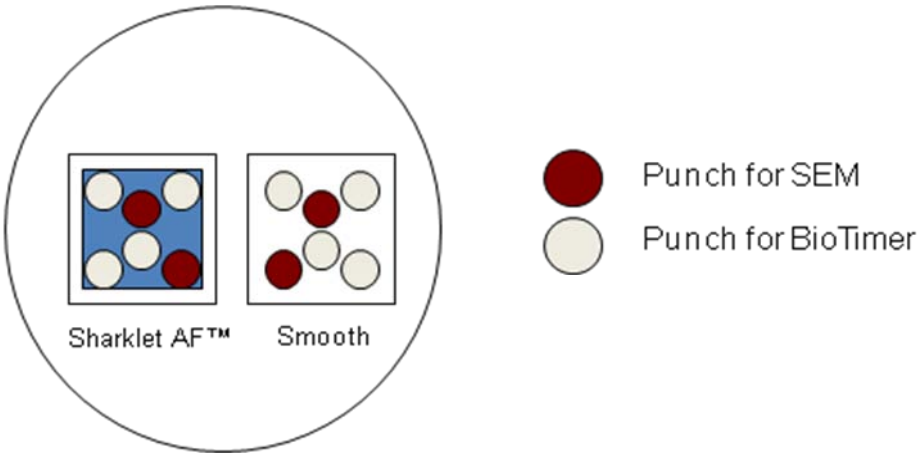

Figure 5-2. Layout of sampling plan for biofilm formation assay. The two polymeric films (3x3 cm^2) were adhered to the bottom of one polystyrene Petri dish. After 7-day culture with S. aureus/TSB, the surfaces were rinsed and then four 8-mm punches were obtained for the BioTimer assay to estimate the colony forming units (CFUs) on the surfaces. Two punches were used for SEM imaging.

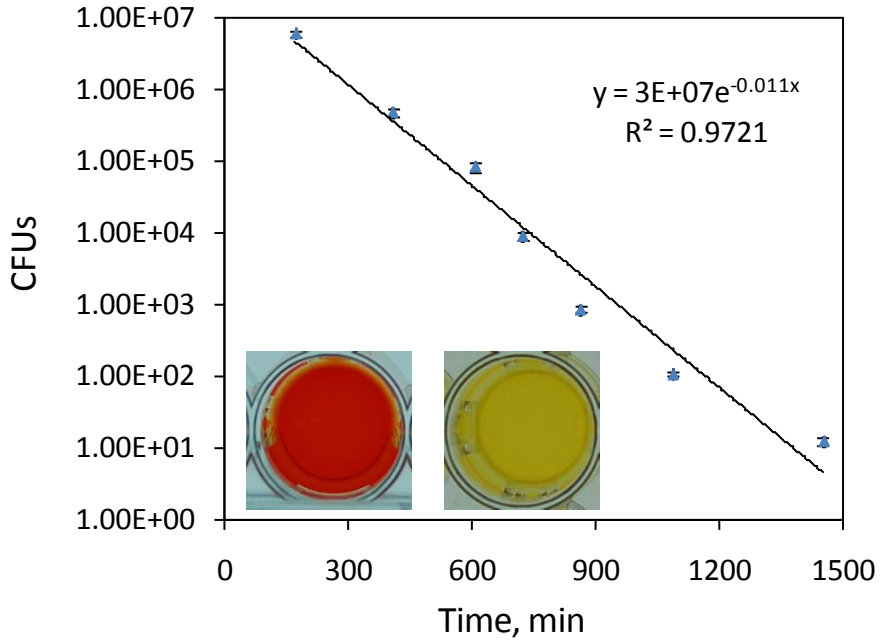

Figure 5-3. The correlation of the CFU counts in the BioTimer assays and the time required for color switch (from red to yellow). The inset pictures show the color of the BioTimer medium before (red) and after (yellow) planktonic *S. aureus* culture.

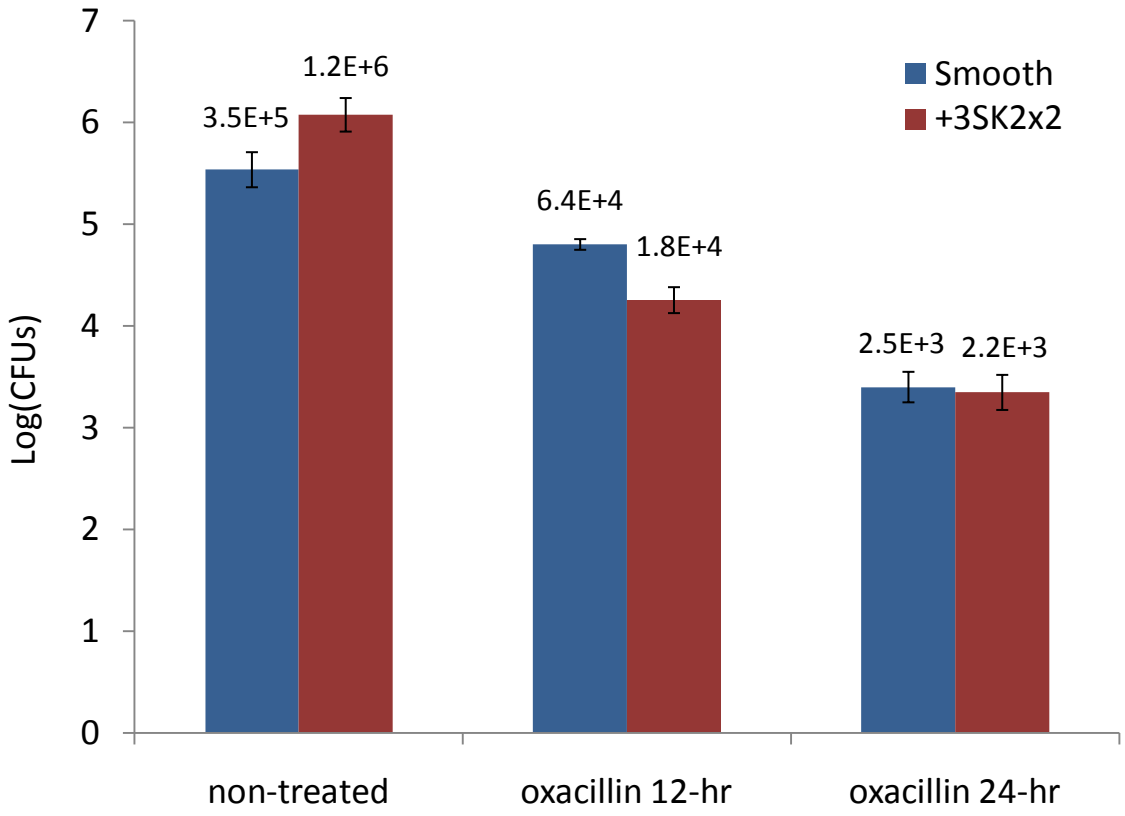

Figure 5-4. Planktonic-quivalent CFUs counts on PDMSe samples after 7-day culture followed by an antibiotic treatment. The numbers on top of the columns are the mean planktonic-equivalent CFUs counts from 4 BioTimer assays in a triplicate set of experiments for each surface.

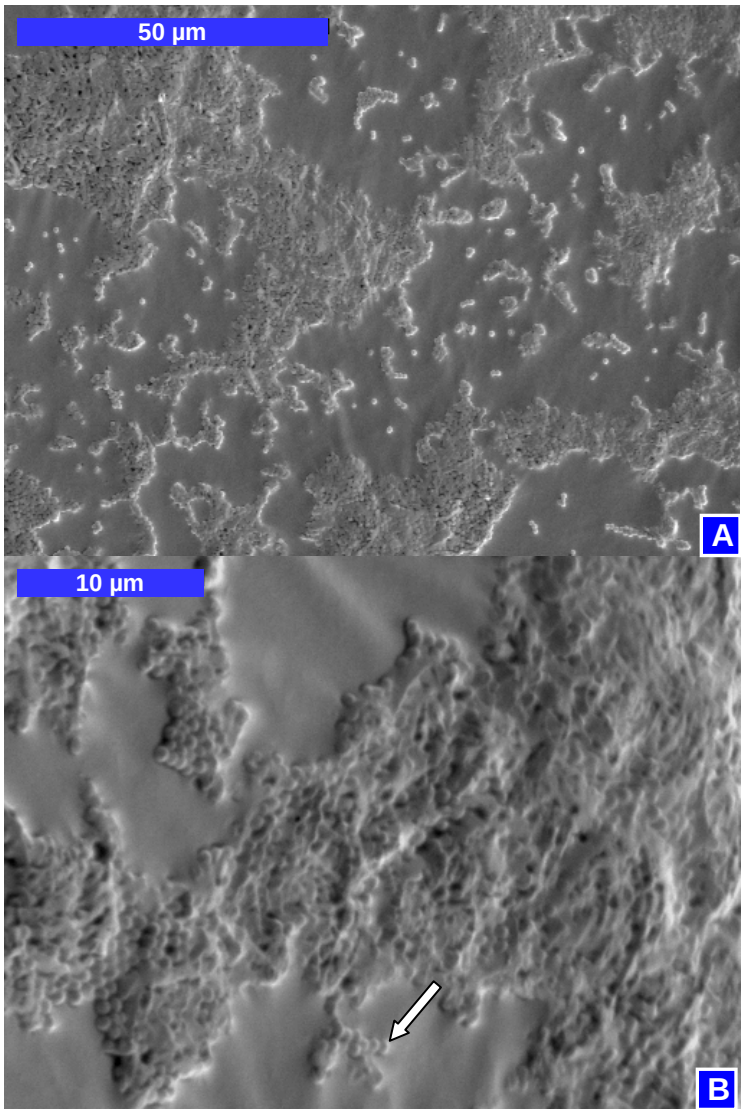

Figure 5-5. SEM images of the smooth surface after 7-day *S. aureus* culture: (A) Top-down view, (B) 40^{o} tilted view.

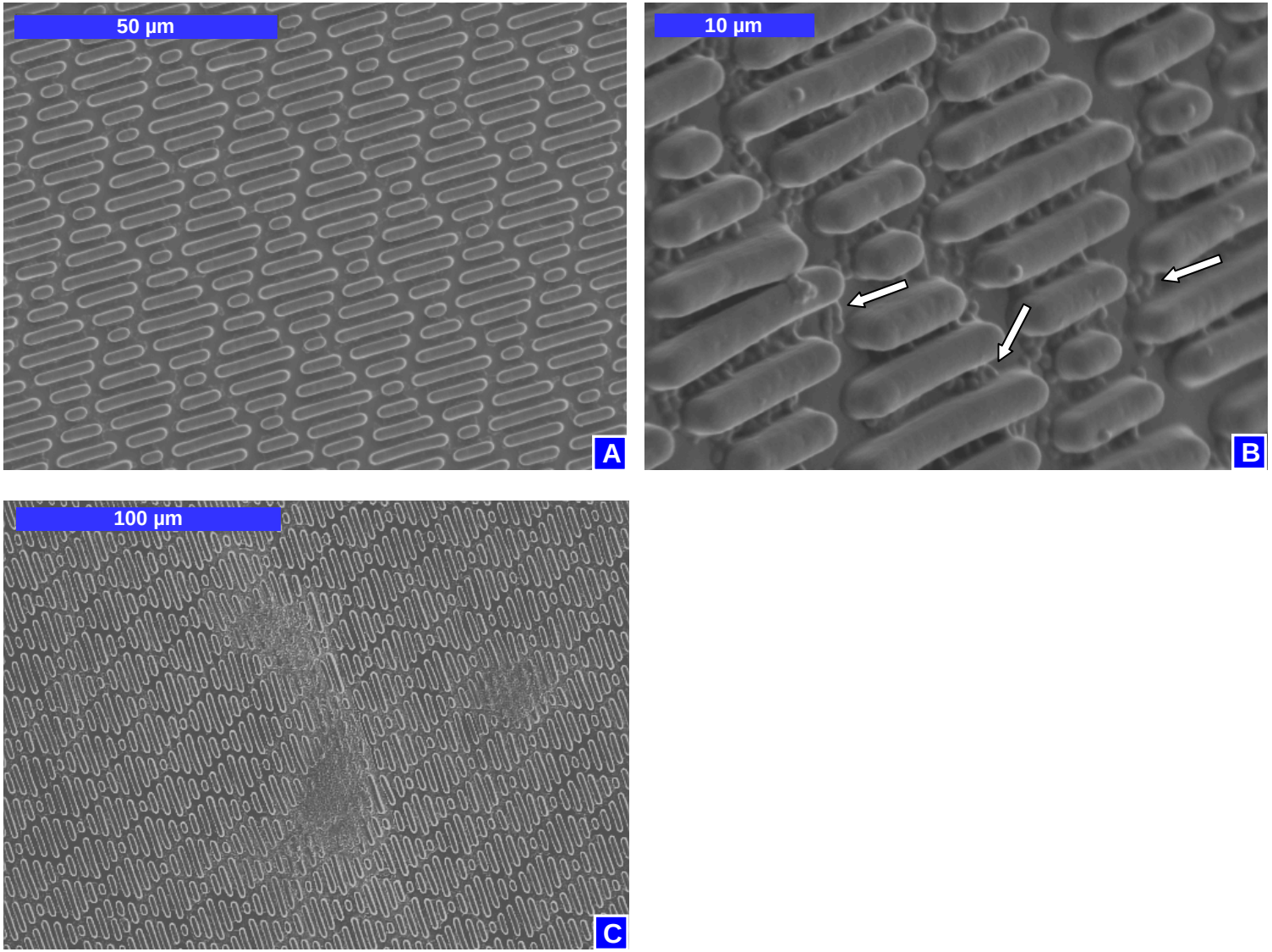

Figure 5-6. SEM images of the Sharklet patterned surface after 7-day *S. aureus* culture: (A) Top-down view, (B) 40^{o} tilted view, arrows clearly showing EPS covered cell clusters, (C) bacterial colonies that were sporadically observed on Sharklet surface.

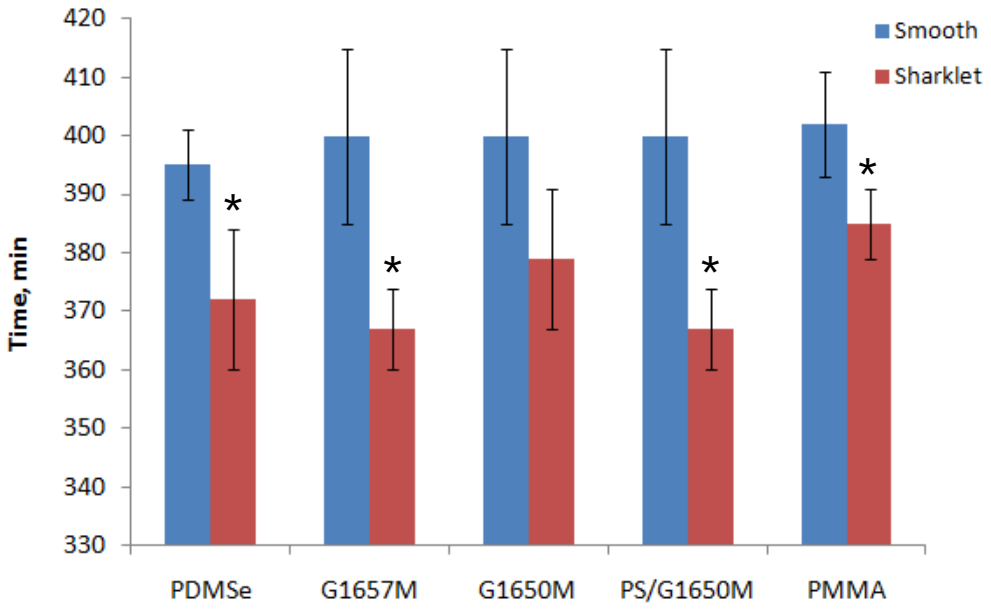

Figure 5-7. The time required for color switch on smooth and Sharklet surfaces after 7-day culture. Star (*) denotes statistically different data pair ($P<0.05$).

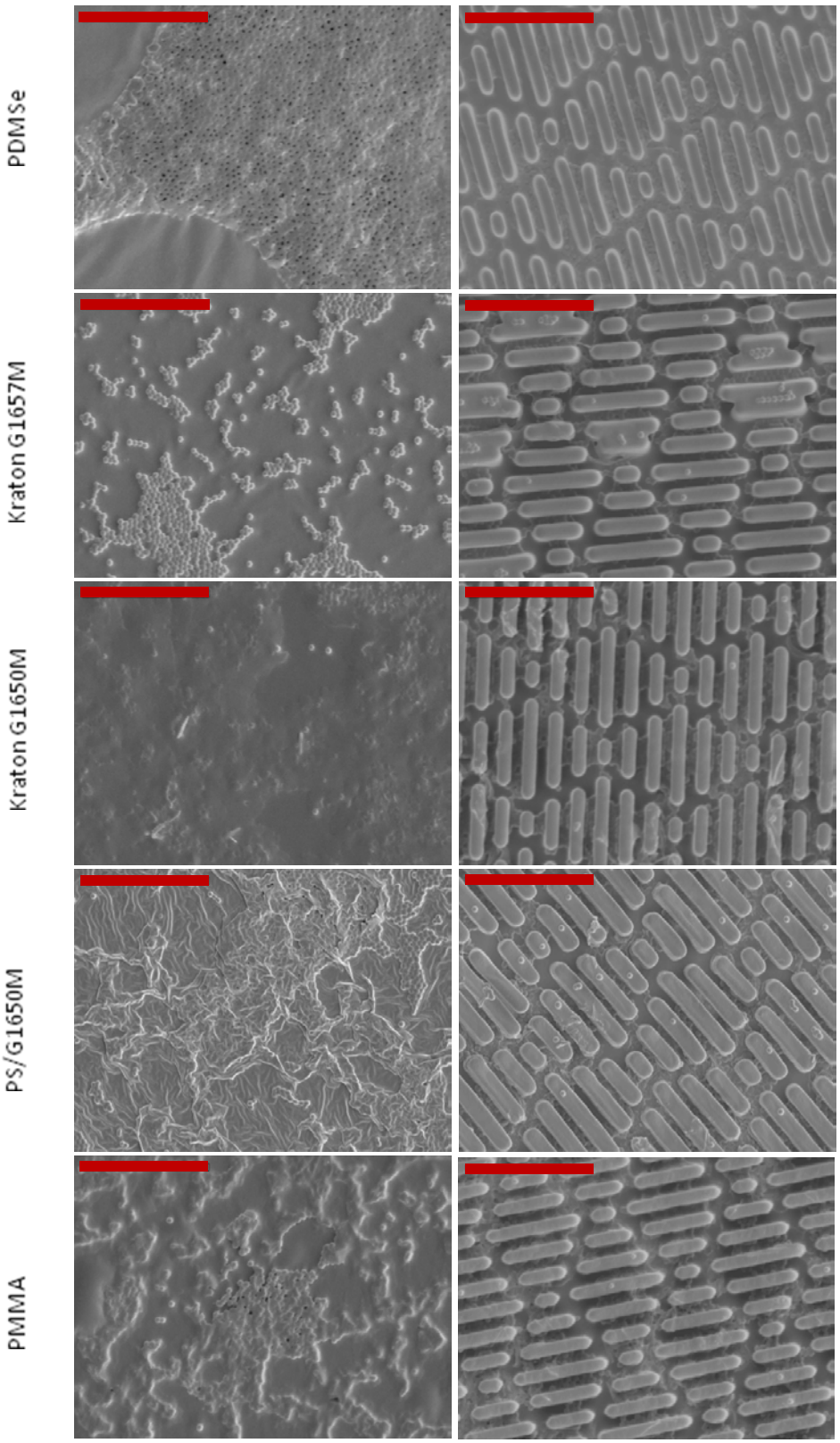

Figure 5-8. SEM images of the surfaces of smooth and Sharklet polymer films after 7-day *S. aureus*/TSB culture. Scale bars all equal to 20 µm.

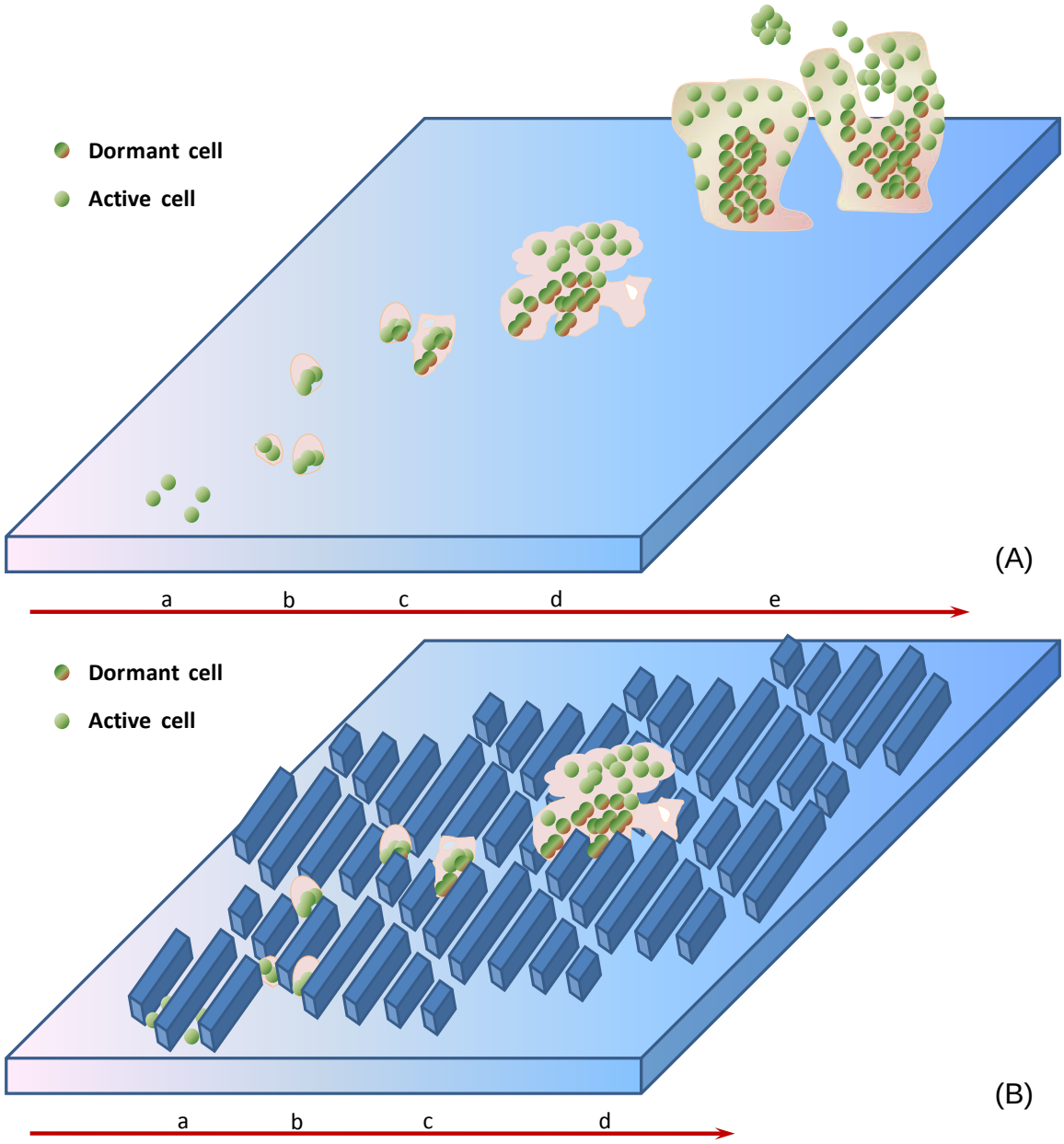

Figure 5-9. Schematic illustration of bacterial microcolonies which developed on the smooth (A) and microengineered (B) surface with time: (a) individual bacterial cells attach reversibly to the surface; (b) the cells anchor to the surface irreversibly by secreting extracellular polymeric substances (EPS), and the cells lose their motility; (c) early development of discrete bacterial colonies with start of differentiation of enclosed cells; (d) cells in the microcolonies differentiate into two main types: one is more active and dwells in the outer layer in contact with the culture medium and another is hibernating in the center and bottom layer ; (e) single cells or cell clusters disperse from the mature biofilm to start a new cycle.

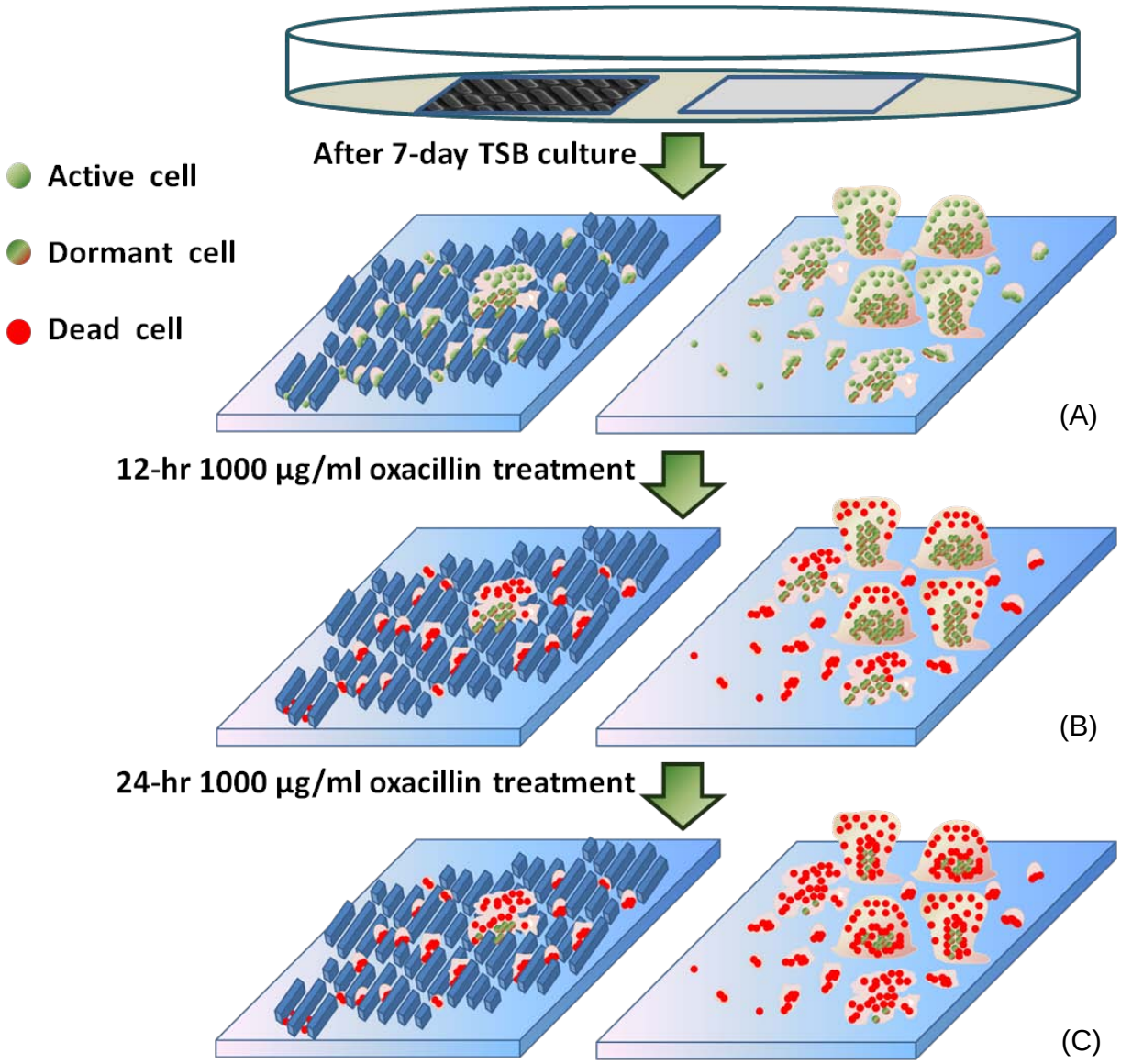

Figure 5-10. Schematic illustration of the microcolonies formed on the topographical and smooth surfaces and the states of the cells after antibiotic treatment. (A) Microcolonies are well established on the surfaces after 7-day culture. (B) When treated by oxacillin for 12 hr, most cells in small microcolonies and in the outer layers of biofilms were killed. (C) After a longer period of antibiotic treatment, most cells attached to the surface of the smooth and the microengineered pattern are killed, while some dormant (persister) cells in the center and bottom of the microcolonies are protected by the EPS and/or the surface features.

Table 5-1. Physical properties of the selected materials.

Materials	Young's modulus, MPa	Surface free energy, mJ/m^2
PDMSe	1.4 [a]	21.5 [c]
Kraton G1657M	6.3	35.0
Kraton G1650M	34	40.8
PS/G1650M blend	2.4×10^2	40.7
PMMA	3.3×10^3 [3, b]	42.4

[a] From previous work [175]
[b] From reference [198]
[c] From reference [48]

CHAPTER 6
NEW UNDERCUT SURFACE FEATURE AND BIORESPONSE

Introduction

Biofouling, the undesired attachment and accumulation of biological matter on surfaces, imposes huge economic losses on society. For example, it is estimated that the US Navy spends an extra amount of over one billion dollars per year on fuel costs due to the increased drag resulting from biofouling [3].

Due to biotoxicity and accumulation along the food chain, previously employed organo-tin based coatings were banned and phased out by the year 2008. Other biocides containing metal oxides (such as copper) also showed hazardous effects on marine organisms. Thus environmental friendly coatings are needed for antifouling applications.

For some time, it has been known that surface topography play a significant role in how surfaces are wet by liquids. Wenzel [144] examined the effects of added surface area arising from surface features upon wetting. Micro-surface features can also inhibit wetting by forming vapor-liquid interfaces .This phenomenon was examined by Cassie and Baxter [145].

On smooth surfaces, wettability has a profound influence upon *Ulva* zoospore attachment and removal [51]. Surface topographical features can significantly change the apparent water contact angle for a material. However, there are no reports on fouling studies for a compound surface which has stable liquid-vapor-solid interfaces. It may be attributed to the instability of the air pockets in the underwater environment for most of the surface microstructures.

With under-cut surface micro-features, obtaining stable liquid-vapor-solid interfaces is possible. Therefore, the surface wetting regime may be changed on a surface with undercut micro-patterns [199, 200]. Furthermore, stable air pockets will hide some of the surface in contact with the liquid, causing microorganisms to have a reduced chance of touching the surface. These facts inspired the design of under-cut surface features on thermoplastic materials.

Theory

The concept of the engineering roughness index (ERI), based upon surface wetting, was first proposed by Schumacher *et al*. [19] in a model for the bioresponse of marine spores toward micro-engineered surfaces.

To account for the effect of various distinct surface features on the designed micro-engineered surfaces, the calculation of ERI was modified into the following form by Long *et al.* [27]

$$ERI_{II} = \frac{r \cdot n}{1 - f} \quad (6\text{-}1)$$

where, *r* is the Wenzel roughness factor defined by the total surface area divided by the projected planar surface area [144], *n* is the number of the distinct surface features, and f is the fractional area of the solid surface in contact with the liquid in the Cassie-Baxter (C-B) model [145].

The basis for the predictive model was built upon the bioresponse assays performed on polydimethylsiloxane elastomer (PDMSe) material. To apply this model to various other materials with different surface chemistry (and thus surface energy and wettability) and nano-sized topographies, we proposed to use the water contact angle to estimate *r* or f depending on whether the wetting regime is in the Wenzel, C-B, or

wicking regime. It can be determined by a lower (θ_{LC}) and upper (θ_{UC}) critical contact angle, according to the following equations [160, 161]:

$$\theta_{LC} = \cos^{-1}\left(\frac{1-f}{r-f}\right) \tag{6-2}$$

$$\theta_{UC} = \cos^{-1}\left(\frac{f-1}{r-f}\right) \tag{6-3}$$

When the contact angle on the smooth surface is larger than the upper critical angle, the wetting regime is Cassie-Baxter; if the contact angle is between the lower and upper critical angles, the surface is in the Wenzel wetting regime; if the contact angle is less than the lower critical angle, the surface is in the wicking regime. After determining the wetting regime for a topographical surface, the terms in Equation (6-1) can be estimated by the following equations:

$$r = \frac{\cos\theta^*}{\cos\theta} \tag{6-4}$$

$$\begin{cases} f = \dfrac{\cos\theta^* + 1}{\cos\theta + 1} & \text{Air entrapment} \\ f = \dfrac{\cos\theta^* - 1}{\cos\theta - 1} & \text{Liquid wicking} \end{cases} \tag{6-5}$$

where, θ^* is the apparent contact angle and θ is the intrinsic contact angle (liquid in contact with a flat surface). Therefore, if the wetting regime is in the Wenzel state, then Equation 6-4 is used to calculate the roughness index value, and f is calculated by the feature dimensions; if the wetting regime is in the C-B state, then the upper line in Equation 6-5 is used to estimate the value of f, and the Wenzel roughness ratio is calculated from the topographical dimensions. The aim of this approach is to estimate

the actual area fraction (relative to the planar surface area) in contact with the liquid. It should be noted that there are constraints for r ($r \geq 1$) and f ($0 \leq f < 1$). The engineered roughness index value calculated from the water contact angle data is denoted as ERI_{II}^{*} in this work.

Chapter 3 showed that the Sharklet textured PDMSe surfaces were all in the C-B regime. ERI_{II}^{*} vavlue can be calculated using equations 6-1 and 6-5 (the air pocket situation). Good correlation can be obtained for spore attachment density change relative to smooth surface vs. ERI_{II}^{*} (see Figure 6-1):

$$Ln\left(\frac{A}{A_{SM}}\right) = -0.058 \cdot ERI_{II}^{*} \quad (R^2 = 0.82) \tag{6-6}$$

In Equation 6-6, A denotes the spore attachment density on the topographical surfaces and A_{SM} is the spore attachment density on the smooth surface.

The correlation between Ln(A/A_{SM}) and ERI_{II}, which was based on the measured dimensions of the topographical features in Long's work [27], is cited below for comparison:

$$Ln\left(\frac{A}{A_{SM}}\right) = -0.071 \cdot ERI_{II} \quad (R^2 = 0.88) \tag{6-7}$$

Materials and Methods

Materials

The polymer films used in this work were all +3SK2x2 films made from Kraton G1650M, PS/G1650M blend, and PMMA. The preparation method was described in detail in Chapter 3.

Process of Making Undercut Micro-features on Polymer Films

To produce undercut micro-features, pressure and heat were applied to deform the tops of the micro-features, as illustrated in Figure 6-2. The softening and melting ranges of some common polymers are listed in Table 6-1.

Specifically, the pre-patterned polymer film was placed on a flat substrate. A hot plate was then driven in contact with the polymer film to exert sufficient pressure for a specified amount of time. The top of the micro features was deformed; Figure 6-3 shows some examples of the flattened surface structures.

The experimental setup is shown in Figure 6-4. Two stacks of glass slides (two pieces in each stack) were put on a flat glass plate as spacers. The polymer film was placed on one glass slide and placed in between the two stacks. A PDMS-5K grafted silicon wafer was then put on top of the polymer film and the spacer. The preheated glass beaker with silicone oil (total weight 205 g) was placed on the silicon wafer for 30 sec to deform the top of the micro-features without damaging the entire surface structure. The applied pressure was about 2200 Pa on the polymer film. The silicone oil in the container was preheated to (1) 160 ^{o}C for G1650M, (2) 170 ^{o}C for PS/G1650M, and (3) 200 ^{o}C for PMMA.

Surface Characterization of Polymer Films

The water contact angle was measured using the sessile drop method with a Ramé-Hart goniometer (Netcong, NJ) coupled with DROPimage Advanced software (for image capturing). Nanopure water (>17.8 MΩ·cm resistivity) droplets were placed on the surfaces via a Ramé-Hart Auto Pipetting system. On each sample, six 5-μl droplets were randomly placed; the images of each droplet were taken in two directions: parallel and perpendicular to the surface features. In this manner, twelve images were recorded

for each sample and contact angles were measured with ImageJ software (public software developed by NIH). For each sample, the contact angles were reported in two directions.

Sample surfaces were imaged using scanning electron microscopy (SEM). The samples were sputter coated with Au/Pd under Ar (~45 mTorr) at 38 mA for 1 min. A Jeol 6400 SEM was used to take the images. The operational conditions were: (1) working distance 15 mm, (2) accelerating voltage 5 kV, (3) beam current $3\sim6x10^{-10}$ mA.

Statistical Methods

Statistical differences between surfaces were evaluated using a nested analysis of variance (ANOVA) followed by the Tukey test for multiple comparisons.

Results and Discussion

Polymer Films with Undercut Micro-Topographical Features

The three polymer materials (G1650M, PS/G1650M, and PMMA) with surface feature +3SK2x2 (Sharklet AF^{TM} pattern, feature height ~3 μm, feature width ~2 μm, and spacing between two neighboring features ~2 μm) were thermal-pressed. Each treated sample was observed with a light microscope to ensure there were no obvious defects after the treatment. The SEM images were taken for all three materials with Sharklet AF^{TM} pattern after thermal pressing (Figures 6-5, 6-6, and 6-7). The images showed a wider feature width at the top than the other part of the same feature from the cross-sectional SEM images. The feature width and spacing on each polymeric material were measured and are listed in Table 6-2. The dimensions of the features were measured using more than 5 features in one SEM picture. Usually more than 4 pictures were used for a dimension measurement. The standard deviation was small (<0.05 nm), and therefore was not included in Table 6-2. The measured dimensions showed that the

tops were flattened. The features on G1650M and PS/G1650M after thermal pressing showed an upside-down wedge shape. Features on PMMA after thermal pressing (Figure 6-7) more closely resembled the cross-sectional view shown in Figure 6-4.

Estimation of Fouling Reduction on the Undercut Surfaces

The undercut Sharklet pattern was formed on the three test materials (G1650m, PS/G1650M blend, and PMMA) after thermal pressing and the spacing between the tops of the neighboring features was reduced (Table 6-2). Therefore, the area fraction of the tops that can be wet by the liquid relative to the projected planar surface area increased, thus decreasing the heterogeneity of the surface pattern. Sessile drop water contact angles were measured in two directions: parallel to and perpendicular to the features based on the water expansion direction. After the undercut shape is formed on the Sharklet pattern for the same material, the difference between the water sessile drop contact angles measured in the two directions (parallel and perpendicular) decreased significantly for all three materials. It should be noted that for G1650M and PS/G1650M blend, the undercut +3SK2x2 topographies showed no heterogeneity in terms of the water sessile drop contact angle data (Table 6-2). As analyzed in Chapter 3, the normal and undercut +3SK2x2 Sharklet textured surfaces on the G1650M and PS/G1650M blend may all fall into the Cassie-Baxter wetting regime.

Based on the measured sizes of the topographical features for the normal and undercut patterns, the $ERI_{//}$ values can be calculated from Equation 6-1, and are shown in Table 6-2. The relative reduction of spore attachment density was then estimated, based on Long's work [27] using Equation 6-7. The $ERI_{//}$ values increase for the undercut topographical patterns relative to the normal features for all three materials. As shown in Table 6-2, the estimated reduction in the spore attachment density on the two

types of Sharklet textured surfaces, relative to the corresponding smooth surfaces was slightly greater on the undercut surface for G1650M and PS/G1650M blend, and was more improved on the undercut surface for PMMA, when compared with the normal Sharklet surface.

The wetting regime was determined by the lower (θ_{LC}) and upper (θ_{UC}) critical contact angle calculated with Equation 6-2 and 6-3, based on the geometry of the surface topographical features. As shown in Table 6-3, normal and undercut Sharklet textured surfaces on G1650M and PS/G1650M blend fall in the Cassie-Baxter regime. For PMMA, the two types of topographical surfaces were both in the Wenzel regime. The sessile drop water contact angle for PMMA with the two types of topographical patterns are all higher than that of the smooth surface of PMMA. This phenomenon may be caused by the nano-sized convex surfaces on the side walls of the protruding features on the Sharklet PMMA film. For the undercut +3SK2x2 PMMA surface, the water contact angle in perpendicular direction is less than that for the normal +3SK2x2 PMMA film (mean value 125^{o} vs. 133^{o}). Zheng [201] demonstrated that contact angle is reversely proportional to the area fraction of the solid in contact with a liquid (f) for C-B wetting regime. The decrease in contact angle for the undercut PMMA surface (relative to the normal Sharklet surface) shows that the wetting regime should be in C-B state, although the calculated lower and upper critical contact angles predicted it to be the Wenzel's wetting regime. Because the thermodynamically favored wetting regime is the Wenzel state for the two Sharklet patterns on PMMA, the high apparent water contact angles are certainly transient states and susceptible to disturbances such as shaking and ultrasonic treatments.

The $ERI_{//}^{*}$ values can also be evaluated with Equations 6-1, 6-4, 6-5 and 6-6. The contact angle data in the parallel direction were used to estimate the $ERI_{//}^{*}$ values and percent reduction (see Table 6-4). The estimated percent reduction based on water contact angle measurement and $ERI_{//}^{*}$ shows higher resistance against spore attachment on the undercut Sharklet patterns than on the normal Sharklet pattern replicated on G1650M and PS/G1650M. There is no difference in the estimated percent reduction of spore attachment density for normal and undercut Sharklet textured PMMA films.

Underwater Stability of the Undercut Surfaces

When a surface with nano/microengineered topographical features is immersed in water, an issue of concern is whether the surface can hold the composite liquid-vapor-solid contact lines underwater. The ability to keep the composite contact interface intact can help minimize the contact area between the fouling species and the surface in water, therefore deferring or preventing the biofouling process [202]. Marmur [203] used thermodynamic reasoning to show the feasibility of the underwater superhydrophobicity. On the assumption of no liquid penetration through the tops of the features, he found that the following condition must be satisfied,

$$r > r_{min} \equiv -\frac{1}{cos\theta} + f_o\left(1 + \frac{1}{cos\theta}\right) \quad (6\text{-}8)$$

where r is the surface roughness ratio, r_{min} is the minimum required value of the surface roughness ratio, f_o is the area fraction of the projected solid top that is wet by the liquid without penetration through the protruding features, and θ is the intrinsic contact angle (Young's contact angle on the smooth material). As $r>1$, Equation 6-8 constrains θ to be greater than $\pi/2$ [203], meaning the starting material must be hydrophobic. PMMA is a

hydrophilic material and therefore it will not show stable underwater superhydrophobicity.

The hydrostatic stability can be expressed as the critical pressure that the composite surface can withstand before water penetrates into the vicinities among the surface topographical features. The equilibrium of the composite interface requires, [200, 201]

$$p_c(A_C - A) = \gamma L \cos(\frac{\pi}{2} - \theta + \psi) \quad (6\text{-}9)$$

where p_c is the critical penetration pressure, A_c is the planar area of a unit cell of the periodic surface feature, A is the area of the tops of the features in the unit cell, γ is the surface free energy of the liquid (for water γ = 72.8 mJ/m^2), L is the perimeter of the top of the surface feature, θ is the intrinsic contact angle (Young's contact angle), and ψ is the geometric angle of the surface feature (see illustrations in Figure 6-8). The critical pressure can be evaluated by

$$p_c = \frac{\gamma L \cos(\frac{\pi}{2} - \theta + \psi)}{A_C - A} \quad (6\text{-}10)$$

Theoretically the deepest position (h) on the surface that will maintain the composite interface underwater will be

$$h = \frac{p_c}{\rho g} \quad (6\text{-}11)$$

Here, ρ is the density of the liquid (the density of water is 1000 kg/m^3) and g is the gravitational acceleration (9.8 m/s^2).

The surface roughness ratio for the untreated and thermal-pressed +3SK2x2 surfaces (G1650M, PS/G1650M blend and PMMA) are all about 2.5. In the case of the Sharklet pattern, the unit cell is shown in Figure 6-8. The surface pattern is anisotropic

and therefore the perimeter of the top of the features is calculated for the features in the unit cell and the average critical pressure is estimated based on the geometry of the unit cell. As shown in Table 6-5, r_{min} values for the two microengineered surfaces on G1650M are 2.9 and 2.8, respectively. Therefore, the two surfaces cannot hold the water-air-solid interfaces underwater, even though they have a relatively high penetration pressure (15 and 29 kPa, respectively). PS/G1650M blend will maintain a stable composite interface underwater, withstanding water pressure as high as 24 and 39 kPa for the normal Sharklet textured surface and the undercut +3SK2x2 surface, respectively. Thermodynamically the untreated and thermal-pressed +3SK2x2 PMMA surface cannot hold the composite interface underwater. However, with the undercut topographical features the surface can be covered with a 12-cm height of water layer and still keep the composite interface (see Table 6-5).

The work by Tuteja *et al.* [199, 200] showed that under-cut surface micro features could facilitate stable water-vapor-solid interfaces. Undercut surface nano- or micro-topographical features with proper chemical surface modification on the polymeric materials may therefore help maintain stable underwater superhydrophobicity and improve long-term performance for antifouling applications.

Conclusion

In this work, it was demonstrated that a thermal pressing technique can be carefully employed to obtain flattened-top (under-cut) microstructures on the polymeric substrate. The feature dimensions clearly showed the flattened tops of the Sharklet AF^{TM} patterns. The water contact angles showed less heterogeneity on this surface compared with the untreated topographical surfaces. The increased area fraction of the feature top suggests a more stable water-air-solid composite interface.

The resulting surfaces are expected to show higher biofouling resistance to marine microorganisms.

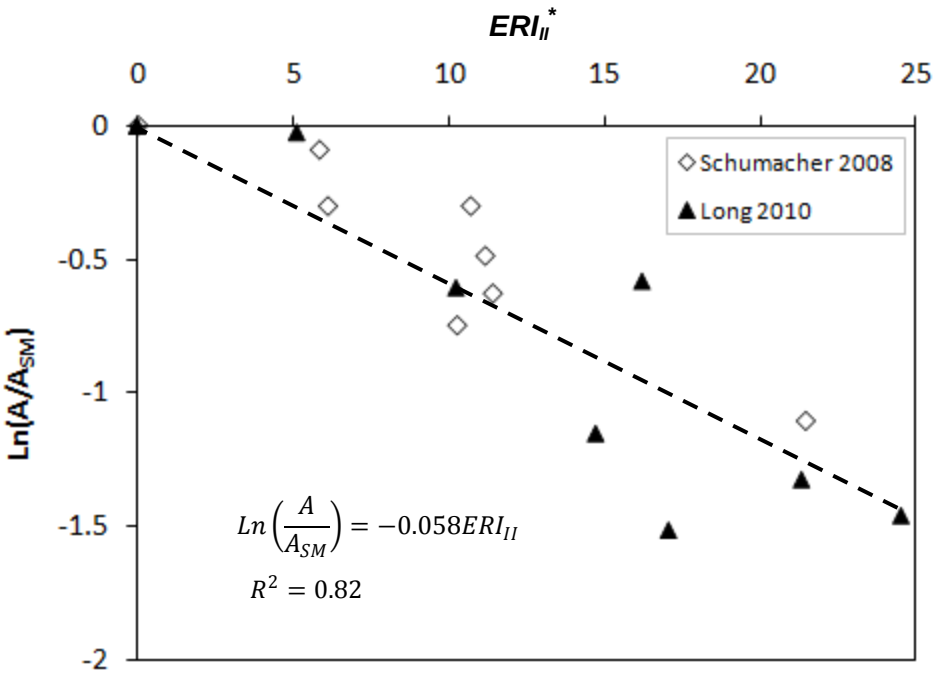

Figure 6-1. Correlation of spore attachment density and ERI_{II}^{*}. Spore attachment data and water contact angle measurements are adapted from the work of Schumacher *et al.* [19] and Long *et al.* [27], respectively.

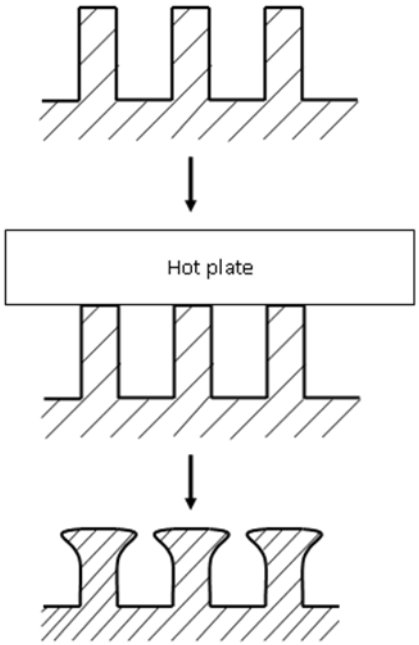

Figure 6-2. Schematic illustration of processing method for fabricating undercut surface topographies.

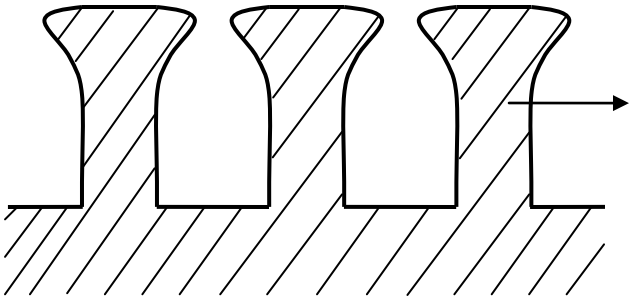

Side view

(A)

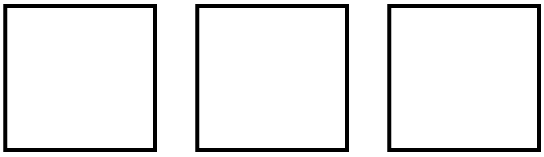

Top-down view 1

(B)

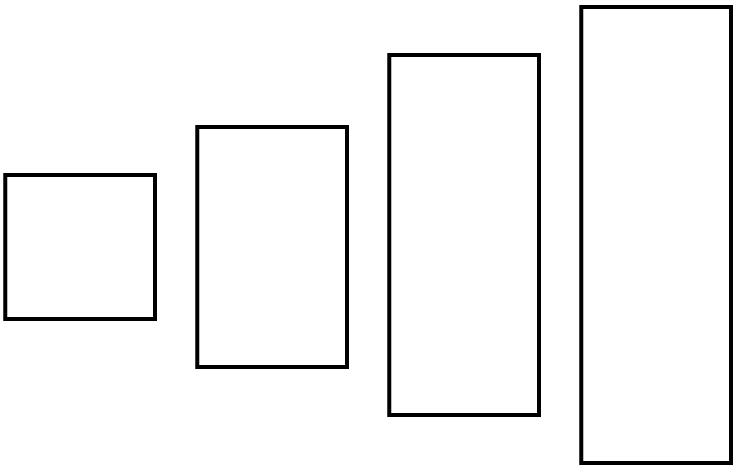

Top-down view 2

(C)

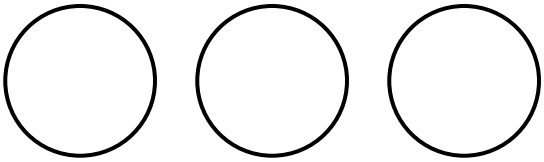

Top-down view 3

(D)

Figure 6-3. Some examples of cross-sectional view (A) and top-down view (B-D) of the undercut surface topography.

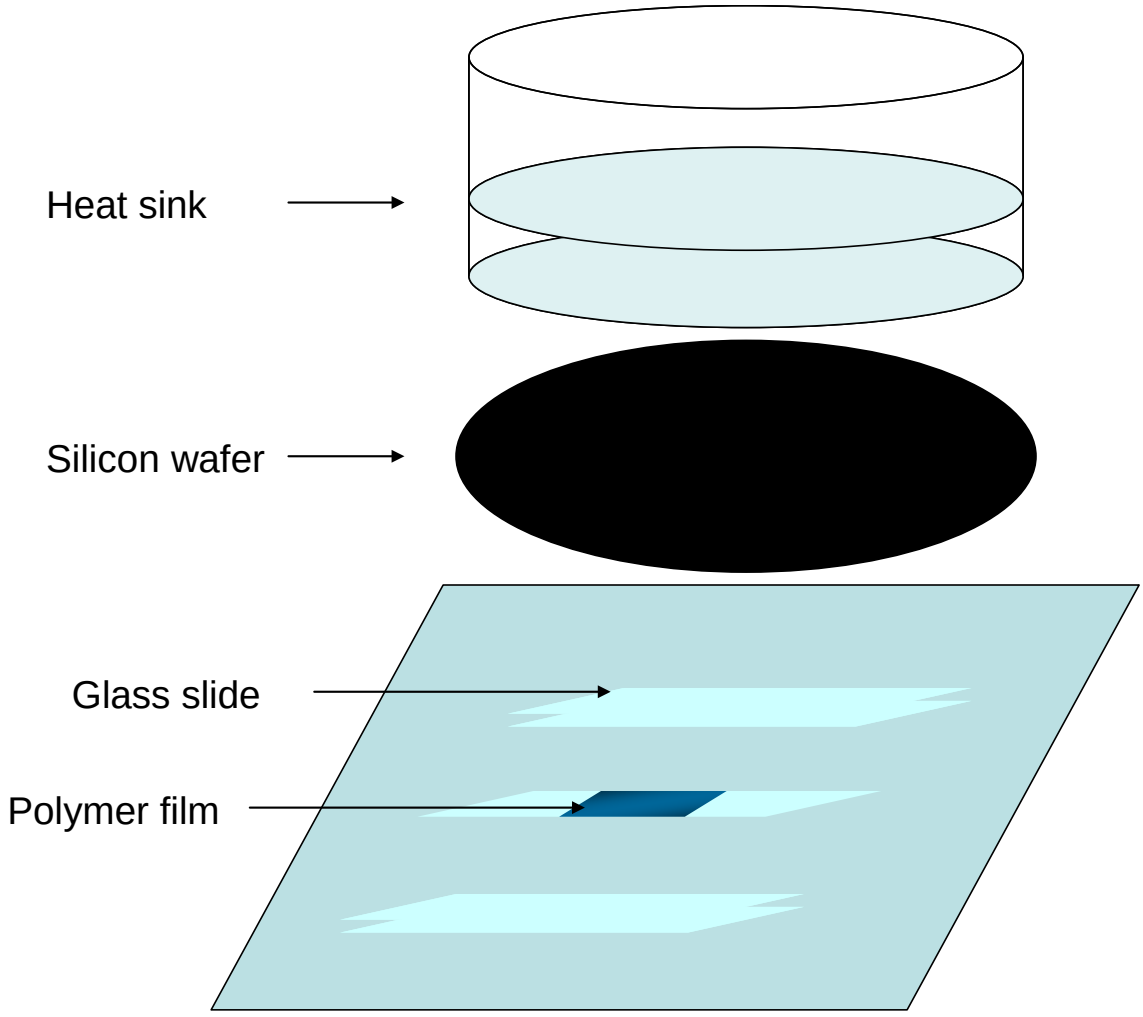

Figure 6-4. Experimental setup for processing polymer films to obtain undercut surface topographical features

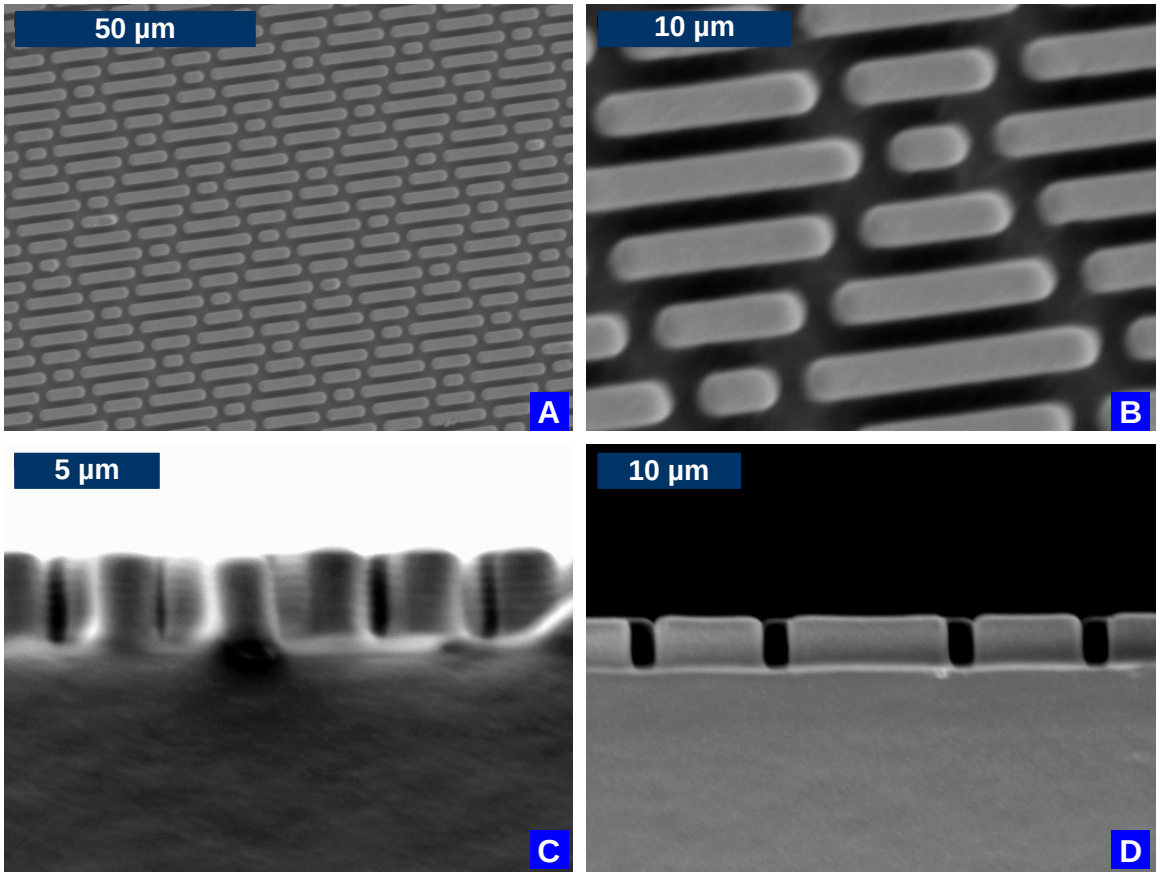

Figure 6-5. SEM images of Kraton G1650M undercut +3SK2x2 film: (A) top-down view at 1000x magnification; (B) top-down view at 3000x magnification; (C) Cross-sectional view; (D) cross-sectional view

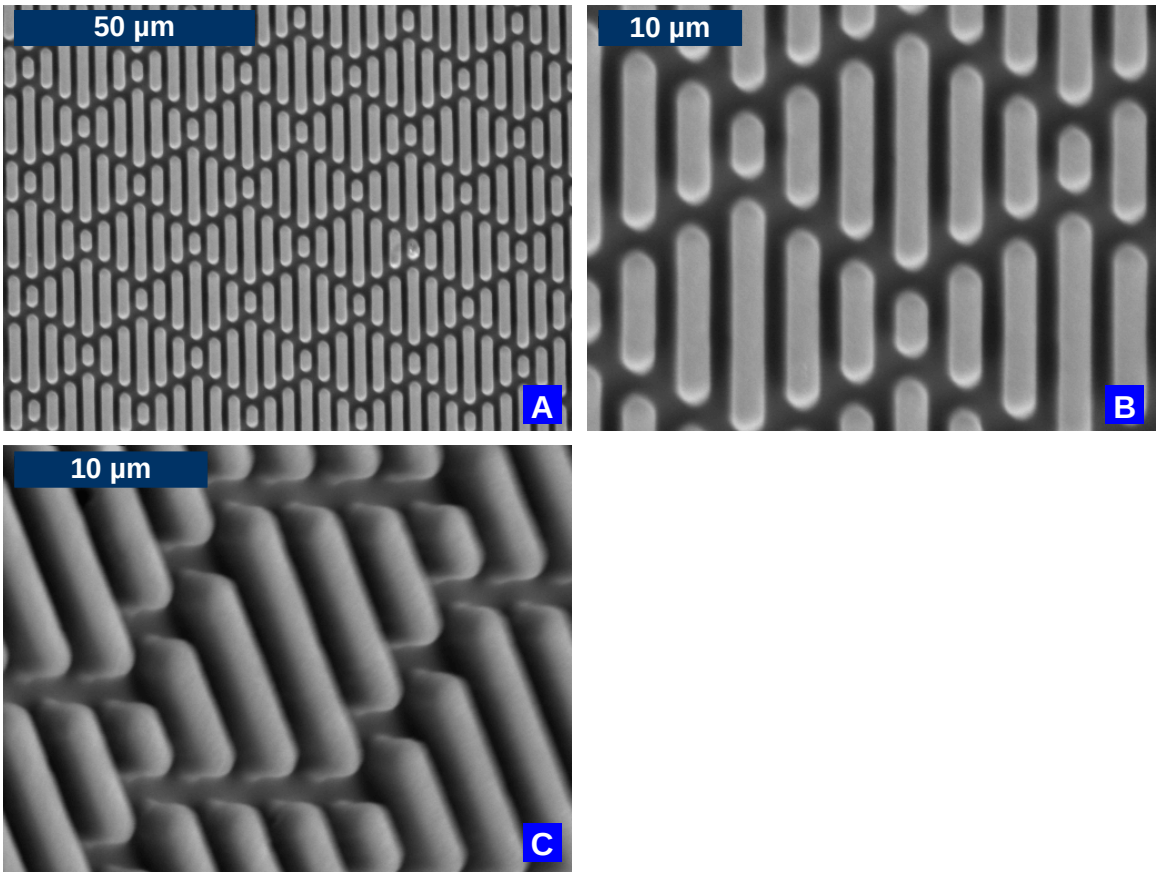

Figure 6-6. SEM images of the PS/G1650M undercut Sharklet +3SK2X2 film: (A) top-down view at 1000x magnification; (B) top-down view at 3000x magnification; (C) 40^{o} tilted view.

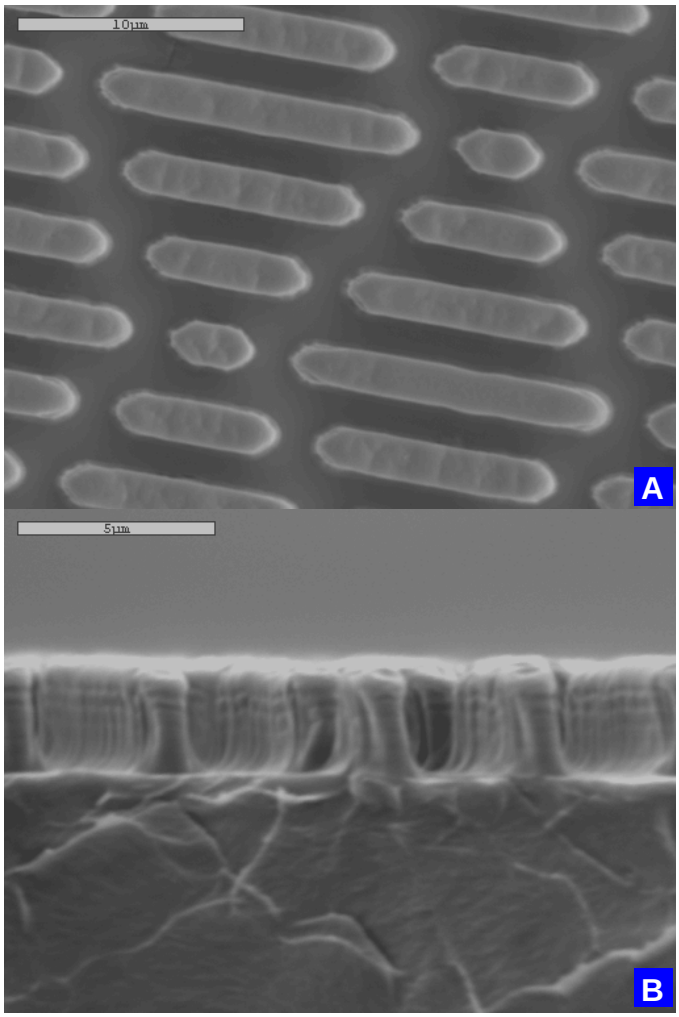

Figure 6-7. SEM images of the under-cut PMMA Sharklet +3SK2X2 film, (A) top-down view, (B) cross-sectional view.

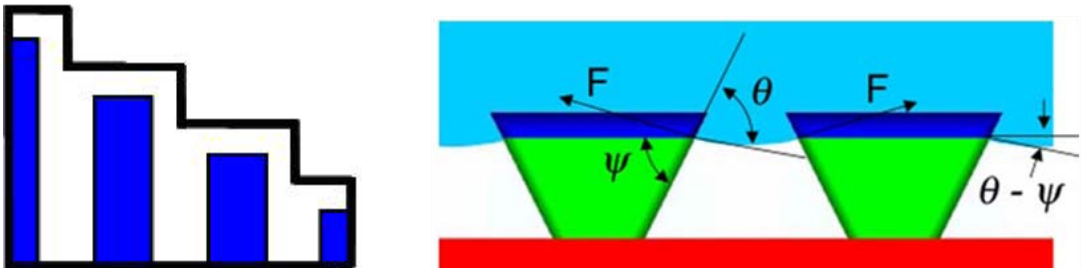

(A) (B)

Figure 6-8. (A) a unit cell of the surface features of the Sharklet pattern (top-down view), the blue area represents the tops of the surface features and the area in the thick black lines is the planar area of the unit cell (A_c). (B) Schematic illustration of the undercut surface features can increase the critical pressure exerted on the top of the features [200].

Table 6-1. Softening and melting ranges of some common thermoplastic polymers

Polymer	Softening range, ^{o}C	Melting range, ^{o}C
Polyethylene (PE)	65-110	95-135
Polypropylene (PP)	120-130	140-170
Polymethylmethacrylate (PMMA)	105-125	220-240
Polystyrene (PS)	85-100	190-260
Polyvinyl chloride (PVC)	65-150	100-260
Polycarbonate (PC)	84-140	230-280
Polyethylene terephthalate (PET)	120-150	240-260

Table 6-2. Measured geometry of the Sharklet surface features and the correlation of *Ulva* spore attachment reduction.

Material	Feature	Feature size, µm			ERI_{II}	% reduction*
		Width	Height	Spacing		
G1650M	+3SK2X2	2.1	3.0	1.9	17.9	72
	Under-cut +3SK2X2	2.3	2.9	1.6	19.4	75
PS/G1650M	+3SK2X2	2.1	3.0	1.9	17.9	72
	Under-cut +3SK2X2	2.3	2.9	1.6	19.4	75
PMMA	+3SK2X2	2.0	3.0	2.0	17.7	72
	Under-cut +3SK2X2	2.2	3.0	1.8	21.6	79

* % reduction is relative to the smooth surface of the same material predicted by Equation 6-7.

Table 6-3. Sessile drop water contact angle (CA) measurement and the wetting regime for the topographical surfaces.

Material	Feature		CA (^{o})	θ_{LC} (^{o})	θ_{UC} (^{o})	Regime
G1650M	Smooth		103 ± 6			
	+3SK2x2	parallel	139 ± 2	74	106	C-B
		perpendicular	147 ± 1			
	Under-cut	parallel	147 ± 3	76	104	C-B
	+3SK2x2	perpendicular	149 ± 2			
PS/G1650M	Smooth		112 ± 2			
	+3SK2x2	parallel	144 ± 5	74	106	C-B
		perpendicular	152 ± 3			
	Under-cut	parallel	146 ± 3	76	104	C-B
	+3SK2x2	perpendicular	147 ± 2			
PMMA	Smooth		76 ± 2			
	+3SK2x2	parallel	86 ± 1	74	106	Wenzel
		perpendicular	133 ± 2			
	Under-cut	parallel	84 ± 4	75	105	Wenzel
	+3SK2x2	perpendicular	125 ± 6			

Parallel: indicating the spreading direction of water droplet is in parallel to the longitudinal direction of the surface features
Perpendicular: indicating the spreading direction of water droplet is in perpendicular to the longitudinal direction of the surface features.

Table 6-4. Estimation of the ERI_{II}^* values and %Reduction of the attachment density of spores based on the correlation in this study.

Material	Feature	r	f	ERI_{II}^*	% Reduction
G1650M	+3SK2X2	2.5	0.32	32	84
	Under-cut +3SK2X2	2.5	0.21	48	94
PS/G1650M	+3SK2X2	2.5	0.30	33	85
	Under-cut +3SK2X2	2.5	0.27	37	88
PMMA	+3SK2X2	2.5	0.86	12	49
	Under-cut +3SK2X2	2.5	0.89	11	48

%Reduction is estimated by Equation 6-6.

Table 6-5. Estimated penetration pressure for the various surface topographies.

Material	Feature	ψ (^{o})	f_o	r_{min}	p_c, kPa	h, m
G1650M	+3SK2X2	90	0.44	2.9	15	1.5
	Under-cut +3SK2X2	80	0.49	2.8	29	3.0
PS/G1650M	+3SK2X2	90	0.44	1.9	24	2.5
	Under-cut +3SK2X2	80	0.49	1.8	39	4.0
PMMA	+3SK2X2	90	0.43	□	□	□
	Under-cut +3SK2X2	75	0.46	□	1.2	0.12

CHAPTER 7
CONCLUSIONS AND FUTURE WORK

Conclusions

In this work, the fabrication techniques of micro-engineered topographical polymer films were explored. The fabricated polymeric substrates were tested against adhesion of marine microorganisms and bacteria. New surfaces with designed properties (chemical, mechanical, topography) could be inspired from these bioresponse results.

Fabrication of Micro-engineered Polymeric Films

A solution casting method was chosen as the fabrication process under current laboratory conditions. A difficulty of this process was the demolding of the fabricated polymer films without damaging the micro-sized features. A simple wet process was developed to covalently graft a release agent onto the surface of a silicon mold. A fabrication process for polymer films was developed so that micro-engineered topographical features could be replicated onto various polymeric materials. Quality control of the resulting polymer films was simplified as the fidelity (> 99%)of the micro-features and integrity of the whole film was ensured.

Marine Antifouling Assay

The polymeric films created with specified feature dimensions, mechanical properties, surface energies and chemical compositions were tested with an *Ulva linza* zoospore assay. All the polymeric films were attached to the glass slides by an epoxy glue, which was found to be strongly attractive to the spores. The data analyses and interpretation were based on the assumption that the influence of the epoxy glue on the spores was the same among all the samples. The Sharklet AF^{TM} pattern was effective against spore attachment with some exceptions. The principal component analysis

(PCA) revealed that two groups of surface parameters may be most important. New correlations were obtained between the reduction of spore attachment and the surface parameters including the engineered roughness index, mechanical property and surface energy. PCA analysis provided potential direction of the improvement on the surface parameters for spore attachment studies, although the spore attachment assay results need to be interpreted with caution.

Bacteria Biofilm Assay

The experimental protocol for the biofilm formation assay with *S. aureus* as test bacterium was established. Based on BioTimer results, there was no difference in the colony forming units attached on the smooth polymer films with various mechanical properties, and the same result was found for the Sharklet AF^{TM} patterns. However, BioTimer assay showed that there were more metabolically active cells from the bacterial microcolonies that formed on the Sharklet patterns than on the smooth surfaces. SEM imaging showed that biofilms formed on the smooth surfaces while no biofilms formed on the Sharklet patterns. After a high-dose antibiotic treatment for 12 hr, less metabolic activities were determined by the BioTimer assay on the Sharklet textured surfaces than on the smooth surfaces, indicating that more cells on the Sharklet surfaces may be killed than on the smooth. Therefore a formation model was proposed for the development of bacterial microcolonies on the smooth and the micro-engineered surfaces. New treatment strategies for the surface attached bacterial microcolonies were also proposed based on this study.

New Undercut Surface Features

Proper processing conditions to fabricate the under-cut micro features on various thermoplastic materials were explored. The feature dimensions clearly revealed the

flattened tops of the Sharklet AF^{TM} patterns. The dimensions of the undercut features are expected to stabilize the water-vapor-solid interface, supporting higher stability of underwater superhydrophobicity for PS/G1650M blend. The resulting undercut surfaces are predicted to show a higher biofouling resistance against marine microorganisms based on predictions from two models.

Future Work

Marine Bioresponse Assays on the Polymeric Films

A new batch of micro-engineered polymeric films was prepared without using any extra adhesives. The glass slides were enclosed with the test polymer by a thermal pressing method, e.g. G1657M was used to enclose the glass slides if the test engineered films were fabricated from G1657M. The free-standing micro-engineered films were then attached to the enclosed glass slides with the help of its toluene solution. After removing the residue solvent, the samples were checked and sent to the University of Birmingham (UK) for spore attachment assay on June 18, 2010. The samples are currently undergoing tests and characterizations. We expect to obtain the results in August 2010.

The undercut surface features on polymer films were successfully processed, and the dimensions showed higher stability for resistance of water penetration when underwater. As discussed in Chapter 6, even small changes in the contact angle could induce large variations in the engineering roughness index, and thus the bioresponse is believed to change accordingly. This hypothesis therefore needs to be tested using the newly fabricated undercut features.

In vivo Study of the Efficacy of the Micro-engineered Polymer Films

Based on the protocol established for the biofilm formation assay, biofilm/microbial colonies can be formed and recovered from the polymeric substrates. To further investigate the efficacy of micro-topographical surface structrues against biofilm formation, we propose to implant the 8-mm punches from the smooth and Sharklet AF^{TM} after a 7-day *S. aureus*/TSB culture period. The paired samples (smooth and topography) will be implanted subcutaneously. The animal conditions, including body temperature, body mass, activity and wound healing, will be monitored during the test period. After a specified period of time, the samples will be retrieved from the implanted sites and the residual bacteria on the samples will be measured with a BioTimer assay.

To evaluate the effectiveness of the proposed treatment strategy, a procedure for preparing an animal model could be: (1) the paired samples (the smooth and topographical surfaces) are cultured to develop bacterial microcolonies on the surface in a 3-day to 7-day culture period; (2) 8-mm discs are punched out from the bacteria-covered samples and implanted into the bodies of the test animals (either rat or rabbit). One group of animals are implanted with the smooth samples and another group of animals are implanted with the topographical smaples. (3) the two groups of animals are subdivided into four groups, and are treated with or without antibiotics. Two more groups of animals implanted with just sterilized samples will be used as controls (see Table 7-1).

Table 7-1. *In vivo* test groups to evaluate the effectiveness of the proposed treatment strategy. Groups 1, 2 and 3 consist of the same amount of animals.

group	1 (*S. aureus* covered)		2 (*S. aureus* covered)		3 (sterilized surfaces)	
	Smooth	Sharklet	Smooth	Sharklet	Smooth	Sharklet
Treatment	No	No	antibiotics	antibiotics	No	No
Observation	Body mass, temperature, activity, mortality, healing rate, bacterial cell counts after retrieving of the samples					

LIST OF REFERENCES

1. Schultz MP. Turbulent boundary layers on surfaces covered with filamentous algae. Journal of Fluids Engineering 2000;122:357-363.

2. Townsin RL. The ship hull fouling penalty. Biofouling 2003;19(1 supp 1):9 - 15.

3. Callow ME, Callow JA. Marine biofouling: a sticky problem. Biologist 2002;49(1):10-14.

4. Bax N, Williamson A, Aguero M, Gonzalez E, Geeves W. Marine invasive alien species: a threat to global biodiversity. Marine Policy 2003;27(4):313-323.

5. Mermel L. Correction: Catheter-related bloodstream infections. Ann Intern Med 2000;133(5):395.

6. Mermel LA. Prevention of intravascular catheter-related infections. Ann Intern Med 2000;132(5):391-402.

7. Shorr AF. Epidemiology of *Staphylococcal* resistance. Clinical Infectious Diseases 2007;45:S171–176.

8. Wahl M. Marine epibiosis. I. fouling and antifouling: some basic aspects. Marine Ecology Progress Series 1989;58:175-189.

9. Fan X, Lin L, Messersmith PB. Cell fouling resistance of polymer brushes grafted from Ti substrates by surface-initiated polymerization: effect of ethylene glycol side chain length. Biomacromolecules 2006;7(8):2443-2448.

10. Kingshott P, Wei J, Bagge-Ravn D, Gadegaard N, Gram L. Covalent attachment of poly(ethylene glycol) to surfaces, critical for reducing bacterial adhesion. Langmuir 2003;19:6912-6921.

11. Chen S, Jiang S. A new avenue to nonfouling materials. Advanced Materials 2008;20:335-338.

12. Todd JS, Zimmerman RC, Crews P, Alberte RS. The antifouling activity of natural and synthetic phenolic acid sulphate esters. Phytochemistry 1993;34:401-404.

13. Scardino A, De Nys R, Ison O, O'Connor W, Steinberg P. Microtopography and antifouling properties of the shell surface of the bivalve molluscs Mytilus galloprovincialis and Pinctada imbricata. Biofouling 2003;19:221-230.

14. Scardino AJ, de Nys R. Fouling deterrence on the bivalve shell mytilus galloprovincialis: a physical phenomenon? Biofouling 2004;20(4-5):249-257.

15. Lang AW, Motta P, Hidalgo P, Westcott M. Bristled shark skin: a microgeometry for boundary layer control? Bioinspir Biomim 2008;3:046005.

16. Brennan AB, Baney RH, Estes TG, Feinberg AW, Wilson LH, Schumacher JF, inventors; University of Florida Research Foundation, Inc., assignee. Surface topography for non-toxic bioadhesion control. USA Patent No. US 7,143,709 B2, 2006.

17. Carman M, Estes T, Feinberg A, Schumacher J, Wilkerson W, Wilson L, et al. Engineered antifouling microtopographiescorrelating wettability with cell attachment. Biofouling 2006;22:11-21.

18. Schumacher JF, Aldred N, Finlay JA, Callow ME, Callow JA, Clare AS, et al. Species-specific engineered antifouling topographies: correlations between the settlement of algal zoospores and barnacle cyprids. Biofouling 2007;23(1):1-11.

19. Schumacher JF, Carman ML, Estes TG, Feinberg AW, Wilson LH, Callow ME, et al. Engineered antifouling microtopographies – effect of feature size, geometry, and roughness on settlement of zoospores of the green alga *Ulva*. Biofouling 2007;23(1):55-62.

20. Schumacher JF, Long CJ, Callow ME, Finlay JA, Callow JA, Brennan AB. Engineered nanoforce gradients for inhibition of settlement (attachment) of swimming algal spores. Langmuir 2008;24(9):4931-4937.

21. Chung KK, Schumacher JF, Sampson EM, Burne RA, Antonelli PJ, Brennan AB. Impact of engineered surface microtopography on biofilm formation of *Staphylococcus aureus*. Biointerphases 2007;2(2):89-94.

22. Schumacher JF. Control of Marine biofouling and medical biofilm formation with engineered topography. Gainesville: University of Florida; 2007.

23. Callow ME, Callow JA, Ista LK, Coleman SE, Nolasco AC, Lopez GP. Use of self-assembled monolayers of different wettabilities to study surface selection and primary adhesion processes of green algal (*Enteromorpha*) zoospores. Applied and Environmental Microbiology 2000;66(8):3249-3254.

24. Ista LK, Callow ME, Finlay JA, Coleman SE, Nolasco AC, Simons RH, et al. Effect of substratum surface chemistry and surface energy on attachment of marine bacteria and algal spores. Applied and Environmental Microbiology 2004;70(7):4151-4157.

25. Schilp S, Kueller A, Rosenhahn A, Grunze M, Pettitt ME, Callow ME, et al. Settlement and adhesion of algal cells to hexa(ethylene glycol)-containing self-assembled monolayers with systematically changed wetting properties. Biointerphases 2007;2(4):143-150.

26. Chaudhury MK, Finlay JA, Chung JY, Callow ME, Callow JA. The influence of elastic modulus and thickness on the release of the soft-fouling green alga *Ulva linza* (syn. *Enteromorpha linza*) from poly(dimethylsiloxane) (PDMS) model networks. Biofouling 2005;21(1):41-48.

27. Long CJ, Schumacher JF, Robinson P, Finlay JA, Callow ME, Callow JA, et al. Prediction of biological cell response on engineered topographies using engineered roughness index. Biofouling 2010;26(4):411-419.

28. Bridgett MJ, Davies MC, Denyer SP. Control of *Staphylococcal* adhesion to polystyrene surfaces by polymer surface modification with surfactants. Biomaterials 1992;13(7):411-416.

29. Glantz P-OJ, Arnebrant T, Nylander T, Baier RE. Bioadhesion: a phenomenon with multiple dimensions. Acta Odontologica Scandinavica 1999;57(5):238-241.

30. Harkes G, Feijen J, Dankert J. Adhesion of *Escherichia coli* on to a series of poly(methacrylates) differing in charge and hydrophobicity. Biomaterials 1991;12(9):853-860.

31. Speranza G, Gottardi G, Pederzolli C, Lunelli L, Canteri R, Pasquardini L, et al. Role of chemical interactions in bacterial adhesion to polymer surfaces. Biomaterials 2004;25(11):2029-2037.

32. Truong VK, Rundell S, Lapovok R, Estrin Y, Wang JY, Berndt CC, et al. Effect of ultrafine-grained titanium surfaces on adhesion of bacteria Applied Microbiology and Biotechnology 2009;83(5):925-937.

33. Whitehead KA, Colligon J, Verran J. Retention of microbial cells in substratum surface features of micrometer and sub-micrometer dimensions. Colloid Surf B-Biointerfaces 2005;41(2-3):129-138.

34. Flemming H-C. Biofouling in water systems - cases, causes and countermeasures. Applied Microbiology and Biotechnology 2002;59:629-640.

35. Socransky SS, Haffajee AD. Dental biofilms: difficult therapeutic targets. Periodontology 2000 2002;28(1):12-55.

36. Donlan RM, Costerton JW. Biofilms: survival mechanisms of clinically relevant microorganisms. Clinical Microbiology Reviews 2002;15(2):167-193.

37. Parsek MR, Singh PK. Bacterial biofilms: an emerging link to disease pathogenesis. Annual Review of Microbiology 2003;57(1):677-701.

38. Armor AF, inventor; Electric Power Research Institute, assignee. Two method for controlling macrofouling by mollusks by using heat. United States Patent No. 5,240,674, 1993 Aug 31, 1993.

39. Koch K, Bhushan B, Barthlott W. Diversity of structure, morphology and wetting of plant surfaces. Soft Matter 2008;4:1943-1963.

40. Nosonovsky M, Bhushan B. Multiscale effects and capillary interactions in functional biomimetic surfaces for energy conversion and green engineering. Philosophical Transactions of the Royal Society A 2009;367:1511-1539.

41. Anderson C, Atlar M, Callow M, Candries M, Milne A, Townsin RL. The development of foul-release coatings for seagoing vessels. Journal of Marine Design and Operations 2003;B4:11-23.

42. Chambers LD, Stokes KR, Walsh FC, Wood RJK. Modern approaches to marine antifouling coatings. Surface and Coatings Technology 2006;201(6):3642-3652.

43. Scotto V, Lai ME. The ennoblement of stainless steels in seawater: a likely explanation coming from the field. Corrosion Science 1998;40(6):1007-1018.

44. Sheng X, Ting Y-P, Pehkonen SO. The influence of sulphate-reducing bacteria biofilm on the corrosion of stainless steel AISI 316. Corrosion Science 2007;49(5):2159-2176.

45. Evans SM, Leksono T, McKinnell PD. Tributyltin pollution: A diminishing problem following legislation limiting the use of TBT-based anti-fouling paints. Marine Pollution Bulletin 1995;30:14-21.

46. Strand J, Jacobsen JA. Accumulation and trophic transfer of organotins in a marine food web from the Danish coastal waters. Science of the Total Environment 2005;350:72-85.

47. Callow M, Willingham G. Degradation of antifouling biocides. Biofouling 1996;10:239-249.

48. Hoipkemeier-Wilson L, Schumacher JF, Carman ML, Gibson AL, Feinberg AW, Callow ME, et al. Antifouling potential of lubricious, micro-engineered, PDMS elastomers against zoospores of the green fouling alga *Ulva* (*Enteromorpha*). Biofouling 2004;20(1):53-63.

49. Greer SP, Iken KB, McClintock JB, Amsler CD. Individual and coupled effects of echinoderm extracts and surface hydrophobicity on spore settlement and germination in the brown alga *Hincksia irregularis*. Biofouling 2003;19(5):315-326.

50. Rasmussen K, Ostgaard K. Adhesion of the marine fouling diatom Amphora coffeaeformis to non-solid gel surfaces. Biofouling 2001;17(2):103-115.

51. Finlay JA, Callow ME, Ista LK, Lopez GP, Callow JA. The influence of surface wettability on the adhesion strength of settled spores of the green alga

Enteromorpha and the diatom *Amphora*. Integrative and Comparative Biology 2002 December 1, 2002;42(6):1116-1122.

52. Ista LK, Callow ME, Finlay JA, Coleman SE, Nolasco AC, Simons RH, et al. Effect of substratum surface chemistry and surface energy on attachment of marine bacteria and algal spores. Applied and Environmental Microbiology 2004;70(7):4151-4157.

53. Schilp S, Rosenhahn A, Pettitt ME, Bowen J, Callow ME, Callow JA, et al. Physicochemical properties of (ethylene glycol)-containing self-assembled monolayers relevant for protein and algal cell resistance. Langmuir 2009;25(17):10077-10082.

54. Finlay JA, Krishnan S, Callow ME, Callow JA, Dong R, Asgill N, et al. Settlement of *ulva* zoospores on patterned fluorinated and PEGylated monolayer surfaces. . Langmuir 2007;24:503-510.

55. Chaudhury MK, Daniel S, Callow ME, Callow JA, Finlay JA. Settlement behavior of swimming algal spores on gradient surfaces. Biointerphases 2006;1(1):18-21.

56. Ederth T, Nygren P, Pettitt ME, Ostblom M, Du CX, Broo K, et al. Anomalous settlement behavior of *Ulva linza* zoospores on cationic oligopeptide surfaces. Biofouling 2008;24(4):303-312.

57. Rosenhahn A, Finlay JA, Pettit ME, Ward A, Wirges W, Gerhard R, et al. Zeta potential of motile spores of the green alga *Ulva* linza and the influence of electrostatic interactions on spore settlement and adhesion strength. Biointerphases 2009;4(1):7-11.

58. Kendall K. The adhesion and surface energy of elastic solids. Journal of Physics D: Applied Physics 1971;4:1186-1195.

59. Brady RFJ. A fracture mechanical analysis of fouling release from nontoxic antifouling coatings. Progress in Organic Coatings 2001;43:188-192.

60. Brady RFJ, Singer IL. Mechanical factors favoring release from fouling release coatings. Biofouling 2000;15(1-3):73-81.

61. Sun Y, Guo S, Kavanagh CJ, Swain GW. Surface elastic mudulus of barnacle adhesive and release characteristics from silicone surfaces. Biofouling 2004;20:279-289.

62. Andersson M, Berntsson K, Jonsson P, Gatenholm P. Microtextured surfaces: towards macrofouling resistant coatings. Biofouling 1999;14(2):167-178.

63. Petronis Å an, Berntsson K, Gold J, Gatenholm P. Design and microstructuring of PDMS surfaces for improved marine biofouling resistance. Journal of Biomaterials Science -- Polymer Edition 2000;11(10):1051-1072.

64. Berntsson KM, Jonsson PR, Lejhall M, Gatenholm P. Analysis of behavioural rejection of micro-textured surfaces and implications for recruitment by the barnacle Balanus improvisus. J Exp Mar Biol Ecol 2000;251(1):59-83.

65. Callow ME, Jennings AR, Brennan AB, Seegert CE, Gibson A, Wilson L, et al. Microtopographic cues for settlement of zoospores of the green fouling alga *Enteromorpha*. Biofouling 2002;18(3):237-245.

66. Cheng G, Zhang Z, Chen S, Bryers JD, Jiang S. Inhibition of bacterial adhesion and biofilm formation on zwitterionic surfaces. Biomaterials 2007;28(29):4192-4199.

67. Zhang Z, Chao T, Chen S, Jiang S. Superlow fouling sulfobetaine and carboxybetaine polymers on glass slides. Langmuir 2006;22(24):10072-10077.

68. Zhang Z, Finlay JA, Wang L, Gao Y, Callow JA, Callow ME, et al. Polysulfobetaine-grafted surfaces as environmentally benign ultralow fouling marine coatings. Langmuir 2009;25(23):13516-13521.

69. Krishnan S, Ayothi R, Hexemer A, Finlay JA, Sohn KE, Perry R, et al. Anti-biofouling properties of comblike block copolymers with amphiphilic side chains. Langmuir 2006;22(11):5075-5086.

70. Archambault JG, Brash JL. Protein repellent polyurethane-urea surfaces by chemical grafting of hydroxyl-terminated poly(ethylene oxide): effects of protein size and charge. Colloids and Surfaces B: Biointerfaces 2004;33:111-120.

71. Desai NP, Hubbell JA. Solution technique to incorporate polyethylene oxide and other water-soluble polymers into surfaces of polymeric biomaterials. Biomaterials 1991;12(2):144-153.

72. Statz A, Finlay J, Dalsin J, Callow M, Callow JA, Messersmith PB. Algal antifouling and fouling-release properties of metal surfaces coated with a polymer inspired by marine mussels. Biofouling 2006;22:391-399.

73. Yarbrough JC, Rolland JP, DeSimone JM, Callow ME, Finlay JA, Callow JA. Contact angle analysis, surface dynamics, and biofouling characteristics of cross-linkable, random perfluoropolyether-based graft terpolymers. Macromolecules 2006;39(7):2521-2528.

74. Ekin A, Webster DC, Daniels JW, Stafslien SJ, Casse F, Callow JA, et al. Synthesis, formulation, and characterization of siloxane-polyurethane coatings for underwater marine applications using combinatorial high-throughput experimentation. JCT Research 2007;4(4):435(417).

75. Konradi R, Pidhatika B, Muhlebach A, Textor M. Poly-2-methyl-2-oxazoline: a peptide-like polymer for protein-repellent surfaces. Langmuir 2008;24(3):613-616.

76. McMaster D, Bennett S, Tang Y, Finlay J, Kowalke G, Nedved B, et al. Antifouling character of 'active' hybrid xerogel coatings with sequestered catalysts for the activation of hydrogen peroxide. Biofouling 2009;25(1):21-33.

77. Wheeler GL, Tait K, Taylor A, Brownlee C, Joint I. Acyl-homoserine lactones modulate the settlement rate of zoospores of the marine alga *Ulva* intestinalis via a novel chemokinetic mechanism. Plant, Cell and Environment 2006;29:608-618.

78. Geiger T, Delavy P, Hany R, Schleuniger J, Zinn M. Encapulated zosteric acid embedded in poly[3-hydroxyalkanoate] coatings - protection against biofouling. Polymer Bulletin 2004;52:65-72.

79. Newby B-mZ, Cutright E, Barrios CA, Xu Q. Zosteric acid - an effective antifoulant for reducing fresh water bacterial attachment on coatings. JCT Research 2006;3(1):69-76.

80. Xu Q, Barrios CA, Cutright T, Newby B-mZ. Assessment of antifouling effectiveness of two natural product antifoulants by attachment study with freshwater bacteria. Environmental Science and Pollution Research 2005;12(5):278-284.

81. Stanley MS, Callow ME, Perry R, Alberte RS, Smith R, Callow JA. Inhibition of fungal spore adhesion by zosteric acid as the basis for a novel, nontoxic crop protection technology. Phytopathology 2002;92(4):378-383.

82. Harder T, Lau SCK, Tam W-Y, Qian P-Y. A bacterial culture-independent method to investigate chemically mediated control of bacterial epibiosis in marine invertebrates by using TRFLP analysis and natural bacterial populations. FEMS Microbiology Ecology 2004;47:93-99.

83. Bhosale SH, Nagle VL, Jagtap TG. Antifouling potential of some marine organisms from India against species of Bacillus and *Pseudomonas*. Marine Biotechnology 2002;4:111-118.

84. Lam C, Grage A, Schulz D, Schulte A, Harder T. Extracts of North Sea macroalgae reveal specific activity patterns against attachment and proliferation of benthic diatoms: a laboratory study. Biofouling 2008;24(1):59-66.

85. Wilsanand V, Wagh A, Bapuji M. Antifouling activities of octocorals on some marine microfoulers. Microbios 2001;104(409):131-140.

86. Haslbeck EG, Kavanagh CJ, Shin HW, Banta WC, Song P, Loeb GI. Minimum effective release rate of antifoulants .2. Measurement of the effect of TBT and zosteric acid on hard fouling. Biofouling 1996;10(1-3):175-186.

87. Baum C, Meyer W, Stelzer R, Fleischer L-G, Siebers D. Average nanorough skin surface of the pilot whale (*Globicephala melas*, *Delphinidae*): considerations on

the self-cleaning abilities based on nanoroughness. Marine Biology 2002;140:653-657.

88. Bers AV, Wahl M. The influence of natural surface microtopographies on fouling. Biofouling 2004 Feb;20(1):43-51.

89. Guenther J, Nys RD. Surface microtopographies of tropical sea stars: lack of an efficient physical defence mechanism against fouling. Biofouling 2007;23(6):419-429.

90. Klevens RM, Edwards JR, Richards CL, Horan TC, Gaynes RP, Pollock DA, et al. Estimating health care-associated infections and deaths in US hospitals, 2002. Public Health Reports 2007;122:160-166.

91. Reed D, Kemmerly SA. Infection control and prevention: a review of hospital-acquired infections and the economic implications. The Ochsner Journal 2009;9(1):27-31.

92. Tsibouklis J, Stone M, Thorpe AA, Graham P, Peters V, Heerlien R, et al. Preventing bacterial adhesion onto surfaces: the low-surface-energy approach. Biomaterials 1999;20(13):1229-1235.

93. Costerton JW, Lewandowski Z, Caldwell DE, Korber DR, Lappin-Scott HM. Microbial biofilms. Annual Review of Microbiology 1995;49:711-745.

94. Sauer K. The genomics and proteomics of biofilm formation. Genome Biology 2003;4(6):219.

95. An YH, Friedman RJ. Concise review of mechanisms of bacterial adhesion to biomaterial surfaces. Journal of Biomedical Materials Research Part B - Applied Biomaterials 1998;43:338–348.

96. Poortinga AT, Bos R, Norde W, Busscher HJ. Electric double layer interactions in bacterial adhesion to surfaces. Surface Science Reports 2002;47(1):1-32.

97. Davies DG, Geesey GG. Regulation of the Alginate Biosynthesis Gene algC in *Pseudomonas aeruginosa* during Biofilm Development in Continuous Culture. Applied and Environmental Microbiology 1995;61(3):860-867.

98. Sutherland IW. Biofilm exopolysaccharides: a strong and sticky framework. Microbiology 2001;147:3-9.

99. Eiff CV, Kohnen W, Becker K, Jansen B. Modern strategies in the prevention of implant-associated infections. The International Journal of Artificial Organs 2005;28(11):1146-1156.

100. Spellberg B, Guidos R, Gilbert D, Bradley J, Boucher HW, Scheld WM, et al. The epidemic of antibiotic-resistant infections: a call to action for the medical

community from the Infectious Diseases Society of America. Clinical Infectious Diseases 2008;46:155–164.

101. Palmer J, Flint S, Brooks J. Bacterial cell attachment, the beginning of a biofilm. Journal of Industrial Microbiology and Biotechnology 2007;34:577-588.

102. Kung C. A possible unifying principle for mechanosensation. Nature 2005;436(7051):647-654.

103. Martinac B. Mechanosensitive channels in prokaryotes. Cellular Physiology and Biochemistry 2001;11:61-76.

104. Martinac B, Buechner M, Delcour AH, Adler J, Kung C. Pressure-sensitive ion channel in *E. coli*. Proc Natl Acad Sci USA 1987;84:2297–2301.

105. Martinac B, Kloda A. Evolutionary origins of mechanosensitive ion channels. Progress in Biophysics & Molecular Biology 2003;82:11-24.

106. Discher DE, Janmey P, Wang Y-l. Tissue cells feel and respond to the stiffness of their substrate. 2005. p. 1139-1143.

107. Thompson MT, Berg MC, Tobias IS, Rubner MF, Van Vliet KJ. Tuning compliance of nanoscale polyelectrolyte multilayers to modulate cell adhesion. Biomaterials 2005;26(34):6836-6845.

108. Pelling AE, Sehati S, Gralla EB, Valentine JS, Gimzewski JK. Local nanomechanical motion of the cell wall of *Saccharomyces cerevisiae*. Science 2004;305:1147-1150.

109. Pelling AE, Veraitch FS, Chu CP-K, Nicholls BM, Hemsley AL, Mason C, et al. Mapping correlated membrane pulsations and fluctuations in human cells. Journal of Molecular Recognition 2007;20(6):467-475.

110. Lichter JA, Thompson MT, Delgadillo M, Nishikawa T, Rubner MF, Van Vliet KJ. Substrata mechanical stiffness can regulate adhesion of viable bacteria. Biomacromolecules 2008;9(6):1571-1578.

111. Miller MB, Bassler BL. Quorum sensing in bacteria. Annual Review of Microbiology 2001;55(1):165-199.

112. Sifri CD. Quorum sensing: Bacteria talk sense. Clinical Infectious Diseases 2008;47(8):1070-1076.

113. Federle MJ, Bassler BL. Interspecies communication in bacteria. The Journal of Clinical Investigation 2003;112:1291-1299.

114. Hughes DT, Sperandio V. Inter-kingdom signaling: communication between bacteria and their hosts. Nature Reviews Microbiology 2008;6:111-120.

115. Davies DG, Parsek MR, Pearson JP, Iglewski BH, Costerton JW, Greenberg EP. The involvement of cell-to-cell signals in the development of a bacterial biofilm. Science 1998;280:295-198.

116. Hentzer M, Givskov M. Pharmacological inhibition of quorum sensing for the treatment of chronic bacterial infections. The Journal of Clinical Investigation 2003;112:1300-1307.

117. Yarwood JM, Bartels DJ, Volper EM, Greenberg1 EP. Quorum sensing in *Staphylococcus aureus* biofilms. Journal of Baeteriology 2004;186(6):1838-1850.

118. von Eiff C, Kohnen W, Becker K, Jansen B. Modern strategies in the prevention of implant-associated infections. The International Journal of Artificial Organs 2005;28(11):1146-1156.

119. Lindsay D, Holy Av. Bacterial biofilms within the clinical setting: what healthcare professionals should know. Journal of Hospital Infection 2006;64:313-325.

120. Du H, Chandaroy P, Hui SW. Grafted poly-(ethylene glycol) on lipid surfaces inhibits protein adsorption and cell adhesion. Biochimica et Biophysica Acta - Biomembranes 1997;1326(2):236-248.

121. Cunliffe D, Smart CA, Alexander C, Vulfson EN. Bacterial adhesion at synthetic surfaces. Appl Environ Microbiol 1999;65(11):4995-5002.

122. Statz A, Finlay J, Dalsin J, Callow M, Callow JA, Messeremith PB. Algal antifouling and fouling-release properties of metal surfaces coated with a polymer inspired by marine mussels. Biofouling 2006;22(6):391-399.

123. Satomi T, Nagasaki Y, Kobayashi H, Otsuka H, Kataoka K. Density control of poly(ethylene glycol) layer to regulate cellular attachment. Langmuir 2007;23:6698-6703.

124. Haldar J, An D, Cienfuegos LAd, Chen J, Klibanov AM. Polymeric coatings that inactivate both influenza virus and pathogenic bacteria. Proceedings of the National Academy of Sciences of the United States of America 2006;103(47):17667-17671.

125. Park D, Wang J, Klibanov AM. One-step, painting-like coating procedures to make surfaces highly and permanently bactericidal. Biotechnology Progress 2006;22(2):584-589.

126. Cheng G, Zhang Z, Chen S, Bryers JD, Jiang S. Inhibition of bacterial adhesion and biofilm formation on zwitterionic surfaces. Biomaterials 2007;28(4192-4199).

127. Martin CA, Hoven AD, Cook AM. Therapeutic frontiers: preventing and treating infectious diseases by inhibiting bacterial quorum sensing. European Journal of Clinical Microbiology & Infectious Diseases 2008;27(8):635-642.

128. Hoipkemeier-Wilson L, Schumacher J, Carman M, Gibson A, Feinberg A, Callow M, et al. Antifouling potential of lubricious, micro-engineered, PDMS elastomers against zoospores of the green fouling alga *Ulva* (*Enteromorpha*). Biofouling 2004;20:53-63.

129. Campo Ad, Arzt E. Fabrication Approaches for Generating Complex Micro- and Nanopatterns on Polymeric Surfaces. Chemical Review 2008;108:911-945.

130. Srinivasan U, Houston MR, Howe RT, Maboudian R. Alkyltrichlorosilane-based self-assembled monolayer films for stiction reduction in silicon micromachines. Journal of Microelectromechanical Systems 1998;7(2):252-260.

131. Zhuang YX, Hansen O, Knieling T, Wang C, Rombach P, Lang W, et al. Thermal stability of vapor phase deposited self-assembled monolayers for MEMS anti-stiction. Journal of Micromechanics and Microengineering 2006;16:2259-2264.

132. Adarnczyk NM, Dameron AA, George SM. Molecular layer deposition of poly(p-phenylene terephthalamide) films using terephthaloyl chloride and p-phenylenediamine. Langmuir 2008;24(5):2081-2089.

133. Mate CM, Yen BK, Miller DC, Toney MF, Scarpulla M, Frommer JE. New methodologies for measuring film thickness, coverage, and topography. IEEE Transactions on Magnetics 2000;36(1):110-114.

134. Muir BW, Nelson A, Fairbrother A, Fong C, Hartley PG, James M, et al. A comparative X-ray and neutron reflectometry study of plasma polymer films containing reactive amines. Plasma Processes and Polymers 2007;4(4):433-444.

135. Nelson A, Muir BW, Oldham J, Fong C, McLean KM, Hartley PG, et al. X-ray and neutron reflectometry study of glow-discharge plasma polymer films. Langmuir 2006;22(1):453-458.

136. Toney MF, Mate CM, Leach KA, Pocker D. Thickness measurements of thin perfluoropolyether polymer films on silicon and amorphous-hydrogenated carbon with X-ray reflectivity, ESCA and optical ellipsometry. Journal of Colloid and Interface Science 2000;225(1):219-226.

137. Toney MF, Mate CM, Pocker D. Calibrating ESCA and ellipsometry measurements of perfluoropolyether lubricant thickness. IEEE Transactions on Magnetics 1998;34(4):1774-1776.

138. Werzer O, Matoy K, Strohriegl P, Resel R. Temperature treatment of semiconducting polymers: An X-ray reflectivity study. Thin Solid Films 2007;515(14):5601-5605.

139. Styrkas DA, Keddie JL, Lu JR, Su TJ, Zhdan PA. Structure of self-assembled layers on silicon: Combined use of spectroscopic variable angle ellipsometry,

neutron reflection, and atomic force microscopy. Journal of Applied Physics 1999;85(2):868-875.

140. Ton-That C, Shard AG, Bradley RH. Thickness of Spin-Cast Polymer Thin Films Determined by Angle-Resolved XPS and AFM Tip-Scratch Methods. Langmuir 2000;16(5):2281-2284.

141. Hartley PG, Thissen H, Vaithianathan T, Griesser HJ. A Surface Masking Technique for the Determination of Plasma Polymer Film Thickness by AFM. Plasmas and Polymers 2000;5(1):47-60.

142. Feng W, Zhu S, Ishihara K, Brash JL. Protein resistant surfaces: Comparison of acrylate graft polymers bearing oligo-ethylene oxide and phosphorylcholine side chains. Biointerphases 2006;1(1):50-61.

143. Cheng Y-T, Rodak DE. Is the lotus leaf superhydrophobic? Applied Physics Letters 2005;86(14):144101.

144. Wenzel RN. Resistance of solid surfaces to wetting by water. Industrial & Engineering Chemistry 1936;28:988-994.

145. Cassie ABD, Baxter S. Wettability of porous surfaces. Transactions of the Faraday Society 1944;40:546-551.

146. Marmur A. From Hygrophilic to Superhygrophobic: Theoretical Conditions for Making High-Contact-Angle Surfaces from Low-Contact-Angle Materials. Langmuir 2008;24(14):7573-7579.

147. Nosonovsky M. Multiscale roughness and stability of superhydrophobic biomimetic interfaces. Langmuir 2007;23:3157-3161.

148. Zhuang YX, Hansen O, Knieling T, Wang C, Rombach P, Lang W, et al. Thermal stability of vapor phase deposited self-assembled monolayers for MEMS anti-stiction. Journal of Micromechanics and Microengineering 2006;16(11):2259-2264.

149. Lee MJ, Lee NY, Lim JR, Kim JB, Kim M, Baik HK, et al. Antiadhesion surface treatments of molds for high-resolution unconventional lithography. Advanced Materials 2006;18:3115-3119.

150. Graf N, Yegen E, Lippitz A, Treu D, Wirth T, Unger WES. Optimization of cleaning and amino- silanization protocols for Si wafers to be used as platforms for biochip microarrays by surface analysis (XPS, ToF-SIMS and NEXAFS spectroscopy). Surface and Interface Analysis 2008;40(3-4):180-183.

151. Kowalczyk D, Slomkowski S, Chehimi MM, Delamar M. Adsorption of aminopropyltriethoxy silane on quartz: an XPS and contact angle measurements study. International Journal of Adhesion and Adhesives 1996;16(4):227-232.

152. Sui G, Wang J, Lee C-C, Lu W, Lee SP, Jeffrey V. Leyton, et al. Solution-Phase Surface Modification in Intact Poly(dimethylsiloxane) Microfluidic Channels. Analytical Chemistry 2006;78:5543-5551.

153. Faibish RS, Yoshida W, Cohen Y. Contac angle studay on polymer-grafted silicon wafers. Journal of Colloid and Interface Science 2002;256:341-350.

154. Marmur A. Thermodynamic aspects of contact angle hysteresis. Advances in Colloid and Interface Science 1994;50:121-141.

155. Yasuda T, Okuno T, Yasuda H. Contact Angle of Water on Polymer Surfaces. Langmuir 1994;10(7):2435-2439.

156. Tao Y, Lu ZH, Graham MJ, Tay SP. X-ray photoelectron spectroscopy and x-ray absorption near-edge spectroscopy study of SiO_2/Si(100). Journal of Vacuum Science & Technology B 1994;12(4):2500-2503

157. Alexander MR, Short RD, Jones FR, Michaeli W, Blomfield CJ. A study of HMDSO/O2 plasma deposits using a high-sensitivity and -energy resolution XPS instrument: curve fitting of the Si 2p core level. Applied Surface Science 1999;137(1-4):179-183.

158. Roualdes S, Berjoan R, Durand J. 29Si NMR and Si2p XPS correlation in polysiloxane membranes prepared by plasma enhanced chemical vapor deposition. Separation and Purification Technology 2001;25(1-3):391-397.

159. O'Hare L-A, Hynes A, Alexander MR. A methodology for curve-fitting of the XPS Si 2p core level from thin siloxane coatings. Surface and Interface Analysis 2007;39(12-13):926-936.

160. Long CJ, Schumacher JF, Brennan AB. Potential for tunable static and dynamic contact angle anisotropy on gradient microscale patterned topographies. Langmuir 2009;25(22):12982-12989.

161. Quéré D. Rough ideas on wetting. Physica A: Statistical Mechanics and its Applications 2002;313(1-2):32-46.

162. Shimizu RN, Demarquette NR. Evaluation of surface energy of solid polymers using different models. Journal of Applied Polymer Science 2000;76(12):1831-1845.

163. Brown L, Koerner T, Horton JH, Oleschuk RD. Fabrication and characterization of poly(methylmethacrylate) microfluidic devices bonded using surface modifications and solvents. Lab on a Chip 2006;6(1):66-73.

164. Di Cinto RA, De Carolis G. Biofouling and corrosion. Corrosion Prevention and Control 1993;40(5):104-107.

165. Umemura K, Yamada T, Maeda Y, Kobayashi K, Kuroda R, Mayama S. Regulated growth of diatom cells on self-assembled monolayers. Journal of Nanobiotechnology 2007;5(2).

166. Baier RE. Substrata influences on adhesion of microorganisms and their resultant new surface properties. New York: Wiley Interscience, 1980.

167. Gindl M, Sinn G, Gindl W, Reiterer A, Tschegg S. A comparison of different methods to calculate the surface free energy of wood using contact angle measurements. Colloids and Surfaces A: Physicochemical and Engineering Aspects 2001;181:279-287.

168. Owens DK, Wendt RC. Estimation of surface free energy of polymers. Journal of Applied Polymer Science 1969;13(8):1741-1747.

169. Callow ME, Callow JA. Primary adhesion of *Enteromorpha* (*Chlorophyta*, *Ulva*les) propagules: quantitative settlement studies and video microscopy. Journal of Phycology 1997;33(6):938-947.

170. Callow ME, Callow JA, Pickett-Heaps JD, Wetherbee R. Primary adhesion of *Enteromorpha* (*Chlorophyta*, *Ulvales*) *propagules*: quantitative settlement studies and video microscopy. Journal of Phycology 1997;33(6):938-947.

171. Callow ME, Jennings AR, Brennan AB, Seegert CE, Gibson AL, Wilson LH, et al. Microtopographic cues for settlement of zoospores of the green fouling alga *Enteromorpha*. Biofouling 2002;18:237-245.

172. Chan Y. Phthalic Anhydride. 1991 [cited 2010 March 19th]; Available from: http://www.osha.gov/dts/sltc/methods/organic/org090/org090.html

173. Wilson LH. Bioresponse to Polymmeric Substrates: Effect of Surface Energy, Modulus, Topography, and Surface Graft Copolymers. Gainesville: University of Florida; 2005.

174. Liu Y, Strauss J, Camesano TA. Thermodynamic investigation of Staphylococcus epidermidis interactions with protein-coated substrata. Langmuir 2007;23:7134-7142.

175. Feinberg AW, Gibson AL, Wilkerson WR, Seegert CA, Wilson LH, Zhao LC, et al. In synthesis and properties of silicones and silicone-modified materials. In: Clarson SJ, Fitzgerald JJ, Owen MJ, Smith SD, Van Dyke ME, editors. ACS Symposium Series 838; 2003; Washington DC, USA: American Chemical Society; 2003. p. 196-211.

176. Perutz S, Wang J, Kramer EJ, Ober CK, Ellis K. Synthesis and surface energy measurement of semi-fluorinated, low-energy surfaces. Macromolecules 1998;31:4272-4276.

177. Creton C, Kramer EJ, Hui CY, Brown HR. Failure mechanisms of polymer interfaces reinforced with block copolymers. Macromolecules 1992;25(12):3075-3088.

178. Tanaka K, Takahara A, Kajiyama T. Film thickness dependence of the surface of immiscible polystyrene/poly(methyl mechacrylate) blends. Macromolecules 1996;29:3232-3239.

179. Klevens RM, Edwards JR, Richards CL, Horan TC, Gaynes RP, Pollock DA, et al. Estimating Health Care-Associated Infections and Deaths in U.S. Hospitals, 2002. Public Health Reports 2007;122(2):160-166.

180. Hidron AI, Edwards JR, Patel J, Horan TC, Sievert DM, Pollock DA, et al. Antimicrobial-resistant pathogens associated with healthcare-associated infections: annual summary of data reported to the National Healthcare Safety Network at the Centers for Disease Control and Prevention, 2006–2007. Infection Control and Hospital Epidemiology 2008;29(11):996-1011.

181. Shorr AF. Epidemiology of Staphylococcal resistance. Clinical Infectious Diseases 2007;45:S171-S176.

182. Costerton JW, Stewart PS, Greenberg EP. Bacterial biofilms: a common cause of persistent infections. Science 1999;284:1318-1322.

183. Romero R, Schaudinn C, Kusanovic JP, Gorur A, Gotsch F, Webster P, et al. Detection of a microbial biofilm in intraamniotic infection. American Journal of Obstetrics and Gynecology 200;198(1):135.e1.

184. Pantanella F, Valenti P, Frioni A, Natalizi T, Coltella L, Berlutti F. BioTimer Assay, a new method for counting Staphylococcus spp. in biofilm without sample manipulation applied to evaluate antibiotic susceptibility of biofilm Journal of Microbiological Methods 2008;75(3):478-484.

185. Pantanella F, Valenti P, Frioni A, Natalizi T, Coltella L, Berlutti F. BioTimer assay, a new method for counting Staphylococcus spp. in biofilm without sample manipulation applied to evaluate antibiotic susceptibility of biofilm. Journal of Microbiological Methods 2008;75:478-484.

186. Kaps M, Lamberson WR. Biostatistics for animal science. Second ed. Cambridge: CAB International, 2009. p. 245-246.

187. Sternberg C, Christensen BB, Johansen T, Toftgaard Nielsen A, Andersen JB, Givskov M, et al. Distribution of bacterial growth activity in flow-chamber biofilms. Applied and Environmental Microbiology 1999;65(9):4108-4117.

188. Rani SA, Pitts B, Beyenal H, Veluchamy RA, Lewandowski Z, Davison WM, et al. Spatial patterns of DNA replication, protein synthesis, and oxygen concentration

within bacterial biofilms reveal diverse physiological states. Journal of Bacteriology 2007;189(11):4223-4233.

189. Yarwood JM, Bartels DJ, Volper EM, Greenberg EP. Quorum sensing in *Staphylococcus aureus* biofilms. Journal of Bacteriology. 2004;186(6):1838-1850.

190. Amorena B, Gracia E, Monzon M, Leiva J, Oteiza C, Perez M, et al. Antibiotic susceptibility assay for *Staphylococcus aureus* in biofilms developed *in vitro*. Journal of Antimicrobial Chemotherapy 1999;44(1):43-55.

191. Dunne WM, Jr., Mason EO, Jr., Kaplan SL. Diffusion of rifampin and vancomycin through a *Staphylococcus epidermidis* biofilm. Antimicrobial Agents and Chemotherary 1993;37(12):2522-2526.

192. Stewart PS, Davison WM, Steenbergen JN. Daptomycin rapidly penetrates a *Staphylococcus epidermidis* biofilm. Antimicrobial Agents and Chemotherapy 2009;53(8):3505-3507.

193. Smith K, Perez A, Ramage G, Gemmell CG, Lang S. Comparison of biofilm-associated cell survival following *in vitro* exposure of meticillin-resistant *Staphylococcus aureus* biofilms to the antibiotics clindamycin, daptomycin, linezolid, tigecycline and vancomycin. International Journal of Antimicrobial Agents 2009;33(4):374-378.

194. Fux CA, Wilson S, Stoodley P. Detachment characteristics and oxacillin resistance of Staphyloccocus aureus biofilm emboli in an *in vitro* catheter infection model. Journal of Bacteriology 2004;186(14):4486-4491.

195. Lewis K. Persister cells, dormancy and infectious disease. Nature Reviews Microbiology 2007;5(1):48-56.

196. Singh R, Ray P, Das A, Sharma M. Role of persisters and small-colony variants in antibiotic resistance of planktonic and biofilm-associated *Staphylococcus aureus*: an *in vitro* study. Journal of Medical Microbiology 2009;58:1067-1073.

197. Hume EBH, Baveja J, Muir B, Schubert TL, Kumar N, Kjelleberg S, et al. The control of *Staphylococcus epidermidis* biofilm formation and *in vivo* infection rates by covalently bound furanones. Biomaterials 2004;25(20):5023-5030.

198. Tsao CW, Hromada L, Liu J, Kumar P, DeVoe DL. Low temperature bonding of PMMA and COC microfluidic substrates using UV/ozone surface treatment. Lab on a Chip 2007;7:499-505.

199. Tuteja A, Choi W, Ma M, Mabry JM, Mazzella SA, Rutledge GC, et al. Designing superoleophobic surfaces. Science 2007;318:1618-1622.

200. Tuteja A, Choi W, Mabry JM, McKinley GH, Cohen RE. Robust omniphobic surfaces. Proceedings of the National Academy of Sciences 2008;105(47):18200-18205.

201. Zheng Q-S, Yu Y, Zhao Z-H. Effects of hydraulic pressure on the stability and transition of wetting modes of superhydrophobic surfaces. Langmuir 2005;21:12207-12212.

202. Marmur A. Super-hydrophobicity fundamentals: implications to biofouling prevention. Biofouling 2006;22(2):107-115.

203. Marmur A. Underwater Superhydrophobicity: theoretical feasibility. Langmuir 2006;22(4):1400-1402.

BIOGRAPHICAL SKETCH

Liwen Jin (Kevin), son of Zhongjiang Jin and Yun Zhou, was born in Yili, Xinjiang, China. He was raised there until thirteen years old, when he moved with his family to Bole city, Xinjiang.

Liwen finished his high school study from the Forth High School of Bole City and passed the entrance examination of college. He was then admitted to Petroleum University (East China), majoring in Applied Chemistry. During the four-year college life, not only did he receive scholarship every semester, but he also took part in various campus activities including physical exercises, English-learning group, ball-room dancing, and research.

After graduating from the university, Liwen has been working for several organizations, mainly focusing on research and consulting in the area of chemical engineering. He found that he was eager to absorb more knowledge in this area. In 2001, he was admitted to the Department of Chemical Engineering at Clemson University, SC, USA. He finished his master's degree over there and worked for a local company as a research intern.

In 2006, Liwen joined Dr Baney research group in the Department of Materials Science and Engineering at the University of Florida. Under the guidance of Dr Baney and Dr Brennan, he has been working on antifouling of both marine microorganisms and bacteria using micro-engineered polymeric materials. Liwen will receive his PhD degree in August 2010.